Title
Reprogramming of Glutamate Metabolism and Redox Homeostasis in De Novo MYC-Driven Liver Tumors

Author
Anderton, Brittany Nicole

Publication Date
2015

Peer reviewed|Thesis/dissertation

Reprogramming of Glutamate Metabolism and Redox Homeostasis in De Novo MYC-Driven Liver Tumors

by

Brittany N. Anderton

DISSERTATION

Submitted in partial satisfaction of the requirements for the degree of

DOCTOR OF PHILOSOPHY

in

Biomedical Sciences

in the

GRADUATE DIVISION

of the

UNIVERSITY OF CALIFORNIA, SAN FRANCISCO

DEDICATION

This work is dedicated to my parents for their unending support, and to Dr. Candy DeBerry, who first introduced me to the world of research.

ACKNOWLEDGEMENTS

First and foremost, I would like to thank my thesis advisor, Andrei Goga, for his continued support and guidance during my time in the Goga Lab. Andrei strives to create a working environment that is driven by curiosity, creativity and passion, and it has been a rewarding experience to be able to lead my own research project and career development with his support from day one. Andrei treats all members of his lab as peers rather than employees; in effect, we are free to follow our passions and craft our own research projects according to our personal interests and desires. This freedom has led me to become a confident and independent scientist.

I thank my thesis committee, Eric Verdin, Jay Debnath, and Suneil Koliwad, for their incredibly valuable guidance throughout my thesis training. The project that ultimately became my thesis is entirely different from the one that I presented at my first committee meeting; my committee has been flexible and supportive throughout the entirety of my training and has guided me to create a body of work that I am very proud to present here.

A huge thank you goes to members of the Goga Lab, old and new. I was fortunate to join the lab while many of the original members were still there. Noelle Huskey Mullin and Lionel Lim served as graduate student role models, confidantes, and basketball teammates. Asha Balakrishnan and Dai Horiuchi served as my early lab mentors. Specifically, Asha was my liver tumor model and metabolism guru and without her hard work in establishing our transgenic lines and performing the profiling and miRNA studies, this thesis wouldn't exist. Dai provided endless guidance on sound research and technical strategies; mentorship on paper writing; and friendship over beers and science policy issues.

Thank you to Alicia Zhou for helping me through the final push of graduate school. I learned more in the final two years of my thesis than in the first three and a half, and much of it is owed to her tireless mentorship in all things. Thank you to Roman Camarda, who joined the lab in my later years and has brought contagious enthusiasm to the Goga Lab. I have valued our many discussions on everything from music and tattoos to philosophical ideologies about art to how cool and exciting intermediary metabolism can be. Thanks to Kim Evason for her extensive knowledge of pathology and her willingness to share it; also thanks to Kim for sharing her shockingly dry humor. Thank you to Sanjeev Balakrishnan for providing vast quantities of *in silico* analyses for my paper and thesis. Sanjeev is always receptive of requests for new analyses and new figures, even when he is juggling five projects at once. His efforts elevated my thesis project from pretty interesting to very exciting. I thank Dan Nomura and Rebecca Kohnz for their assistance and expertise on all things metabolism and metabolic flux. Thank you to Mercedes Joaquin for her crucial maintenance of our mouse colony. Finally, I thank former Goga Lab members for their various assistances throughout the years: Antonio Sorrentino, Linda Starnes, Len Kusdra, Klaus Kruttwig, Henok Eyob, and Meng Li; and current lab members for their continued friendship and support: Julia Rohrberg, Olga Momcilovic, Macrina Francisco, Joy Gittins, Andrew Beardsley, Kai Kessenbrock, Devon Lawson and Susan Zhang.

Thank you to Mike Bishop, Aaron Tward, and current and former Bishop Lab members for your insights during our weekly lab meetings. Thanks to all the labs involved in Anti-Cancer Club, which I have found to be one of the best research-in-progress series at UCSF.

Thank you to Lisa Magargal, Monique Piazza, Demian Sainz, and all other members of the Biomedical Sciences administrative staff for your tireless support over the years. It has been comforting to know that there is a group of people dedicated to making our time here as students run as smoothly as

possible, and your hard work shows. Furthermore, thank you to the administration and staff of UCSF in general for making this university such a rewarding place to work.

Thank you to members of the Science and Health Education Partnership, Women in Life Sciences and the Science Policy Group for your camaraderie over the past several years. My time spent in volunteer or leadership roles in each group has greatly shaped my skills and career aspirations, while also providing much needed reprieve from the daily grind of lab life.

Now to move beyond UCSF – thank you to all of the amazing people I have met during my six years in San Francisco who I am fortunate to call my friends. There are too many to name, but you come from classmates, Craigslist, Davis crew, track, and beyond. You have made every moment outside of class and lab as fun as possible, and you have enriched my life with your varied career interests, life experiences, and love for random and fun themed parties and outdoor activities. Thank you to Robert and Yuko McDaniels and the MacCanDo team for taking me in as family and allowing me to coach and enrich the lives of young people through track. Having track practice to look forward to often helped get me through long days in lab.

Thank you to the Oksenberg-Markley clan for taking me in so readily and including me in all family activities from very early on. Special thanks to Donna and Jorge for allowing Nir and I to treat your house like a spa retreat whenever we needed a break from the stress of being graduate students. Thank you to my aunts and uncles Vi and Scott Piatek and Lisa and Joe Truppi for your many efforts to visit me in San Francisco and your gracious hosting when I visited while in graduate school.

To my parents, Tom and Janice Anderton, thank you for everything you have done for me throughout my life. Thank you for instilling in me a strong work ethic and for supporting me at every stage of my education and career. I look forward to finally being able to host you the next time you come out to visit me. To Ashley Valentino and Courtney Anderton, thank you for the millions of giggles that make me so grateful to have sisters. Thank you for your interest in my research and your readiness to visit my workplace, don a lab coat, and hang out with me while I finish up that "one last thing I need to do" before we can go explore California.

Finally, thank you to Nir Oksenberg for all of your support during my graduate training. I am so lucky to have a partner with whom I can commiserate about science one moment then forget about it all and go on an adventure with the next. You inspire me to enjoy every day and to not waste my time stressing about things I can't control. Most importantly, you kept me happy and sane throughout grad school. Thanks also to Moe the Dog, for entering our lives at a perfect time and for being a fantastic companion and stress reliever. I look forward to reuniting our little family in Davis and seeing what the future holds.

The LT2-MYC mouse model was developed by Dean Felsher in the laboratory of Mike Bishop at UC San Francisco. The gene expression and biochemical profiling described in Chapter 1 were performed by Asha Balakrishnan. Bioinformatics analyses of the gene expression and metabolite datasets were performed by Sanjeev Balakrishnan. Mass spectrometry for the glutamine flux experiment described in Chapter 2 was performed by Rebecca Kohnz in the laboratory of Dan Nomura at UC Berkeley, and the data were analyzed by Sanjeev Balakrishnan. The mouse model used in the glutamine flux experiment was developed by Aaron Tward in the laboratory of Mike Bishop at UC San Francisco. The liver tumor cell line used in Chapter 3 was developed by David Bellovin in the laboratory of Dean

Felsher at Stanford University. Luciferase reporter assay and LNA inhibitor experiments described in Chapter 3 were performed by Asha Balakrishnan. The human HCC metabolite datasets described in Chapter 3 were produced in and shared by the laboratories of Guowang Xu at the Chinese Academy of Sciences, Dalian and Xin Wei Wang at NCI. The human HCC gene expression and metabolite datasets presented in Chapter 3 were analyzed by Sanjeev Balakrishnan. Isoprostane analysis was performed as a core service in the laboratory of Holly Van Remmen at UTHSCSA. Histological analysis of fat accumulation and Ki67 staining in tumor tissues (Chapter 4) was performed by Kim Evason. The contents of this thesis are modified and reproduced from a manuscript currently under review at *Cell Metabolism*. The co-authors for this manuscript are Asha Balakrishnan, Sanjeev Balakrishnan, Rebecca Kohnz, Lionel Lim, Kimberley Evason, Klaus Kruttwig, Qiang Huang, Guowang Xu, Daniel Nomura, and Andrei Goga.

ABSTRACT

Reprogramming of Glutamate Metabolism and Redox Homeostasis in De Novo MYC-Driven Liver Tumors

Brittany Anderton

MYC overexpressing cells frequently exhibit increased dependence on uptake of glutamine and its conversion to glutamate. However, whether MYC shapes downstream glutamate utilization decisions *in vivo* is poorly understood. We employed integrated gene expression and metabolite profiling analyses to identify novel metabolic pathways that are altered in primary MYC-driven liver cancers. We identified six metabolic pathways deregulated in MYC-driven liver tumors, including glutathione metabolism. In primary, MYC-driven tumors, glutamine-derived carbons preferentially enter central carbon metabolism and proliferative metabolic pathways and have diminished incorporation into glutathione and its precursor metabolite. We find that protein expression of the rate-limiting enzyme of glutathione synthesis, GCLC, is suppressed in a MYC-dependent manner. We further show that GCLC is targeted by a MYC-induced microRNA, miR-18a. MiR-18a expression is elevated in human hepatocellular carcinoma (HCC) and correlates with altered glutathione pathway gene expression. Further, poorly differentiated human HCCs have low tumor glutathione levels. MYC-driven liver tumors compensate for loss of glutathione by upregulating several antioxidant regeneration pathways. However, MYC-driven liver tumors exhibit increased sensitivity to exogenous oxidative stress, as demonstrated by tumor-specific fat accumulation and cell death following treatment with the potent oxidant diquat. Thus, despite sufficient antioxidant capacity at baseline, MYC-driven liver tumors are sensitive to exogenous oxidative stress. In total, we show that MYC regulates glutamate utilization by

attenuating glutathione production via miR-18a, leading to preferential shunting of glutamate toward proliferative metabolism in tumors and altering redox homeostasis mechanisms.

TABLE OF CONTENTS

LIST OF TABLES

Number *Page*

LIST OF FIGURES

Number *Page*

Chapter 1

INTRODUCTION

1.1 MYC BIOLOGY

The c-MYC (MYC) proto-oncogene is a pleiotropic transcription factor that is deregulated in some of the most aggressive human malignancies (Ben-Porath et al., 2008). MYC belongs to the basic helix-loop-helix leucine zipper (bHLH/LZ) protein family. The bHLH domain enables MYC binding to DNA, while the LZ domain enables dimerization between MYC and its canonical interaction partner MAX, another bHLH transcription factor. The two domains, bHLH and LZ, are located adjacent to each other near the carboxyl-terminal end of MYC. MYC-MAX heterodimerization is necessary for MYC localization to its target consensus DNA sequence CACGTG, which is known as the enhancer box (E-box) (Dang, 2012). Although E-box binding is important for MYC-dependent transcriptional regulation, E-box-independent transcriptional functions of MYC have also been proposed (Uribesalgo et al., 2011). MAX is expressed ubiquitously in cells but also heterodimerizes with the MXD family of proteins, which act as transcriptional repressors (Conacci-Sorrell et al., 2014). Thus, the activity of MYC/MAX heterodimers relies not only on the precise regulation of MYC protein expression but also on the availability of MAX for MYC-specific binding (Cascoń and Robledo, 2012). There is likely an intricate balance between MYC and MXD proteins in normal cells. MYC is essential for normal cell cycle progression and mammalian development; germ-line deletion of the MYC gene results in embryonic lethality due to

developmental defects in multiple organ systems (Davis et al., 1993). Additionally, MYC-dependent signaling is crucial for cell cycle progression from G1 to S phase in both normal and tumor cells (Meyer and Penn, 2008).

The MYC gene is located at chromosome 8q24 in humans (Takahashi et al., 1991). MYC is estimated to be aberrantly expressed or activated in up to 50% of all human cancers, including lymphomas, neuroblastomas, melanomas, breast, ovarian, prostate, and liver cancers. In human cancer, MYC is most often deregulated through chromosomal translocation, gene amplification, and post-translational modifications, which can lead to elevated MYC protein expression and activity (Conacci-Sorrell et al., 2014). Elevated MYC expression has been correlated with reduced disease-free survival in a number of human cancers (Ben-Porath et al., 2008; Horiuchi et al., 2014). As a transcription factor, MYC can effect both up- and downregulation of hundreds of coding and noncoding genes (Chang et al., 2008). Current studies suggest that acute MYC activation in mammalian cells or tissues can lead to expression changes of approximately 300-400 coding genes and about a dozen miRNA genes (Bui and Mendell, 2010; Chandriani et al., 2009). These genes are involved in numerous processes, including the cell cycle, proliferation, differentiation, metabolism, and cell death. Additionally, there is recent evidence that MYC acts as an enhancer or amplifier of existing gene expression by "scanning" along DNA for activated transcription sites (Lin et al., 2012; Nie et al., 2012). Regardless of the exact mechanisms of its activity, it is evident that MYC orchestrates an optimal cellular context whereby tumor cell proliferation is enhanced while cell death mechanisms are disabled. Not surprisingly, MYC is indispensable for the growth of many tumor types (Dang, 2012). Because there are currently no effective targeted therapies for cancers with high MYC expression, it remains important to understand the underlying biology behind MYC.

1.2 MYC AND METABOLISM

Metabolic reprogramming, the co-opting of biochemical pathways to provide substrates and energy for enhanced cell proliferation, is now considered a bona fide hallmark of cancer (Hanahan and Weinberg, 2011). Not surprisingly, altered metabolism is consistently observed in MYC-driven tumor growth and maintenance (Dang, 2012; Li and Simon, 2013) (**Figure 1**). MYC orchestrates tumor cell dependence on bioenergetic sources such as glucose and glutamine for biomass accumulation (Dang, 2012, 2013; Horiuchi et al., 2014; Li and Simon, 2013). Accordingly, glucose and glutamine deprivation in MYC-overexpressing cells leads to apoptosis (Shim et al., 1998; Yuneva et al., 2007). There is currently great interest in targeting MYC-dependent metabolic pathways for tumor therapy (Dang, 2012; Li and Simon, 2013).

MYC regulates many points in glycolysis through transcriptional regulation of glycolytic genes. For example, MYC regulates the GLUT1 transporter (Osthus et al., 2000) and glycolytic enzymes such as lactate dehydrogenase A (LDHA) (Le et al., 2010) and the M2 isoform of muscle pyruvate kinase (PKM2) (David et al., 2010). Notably, expression of PKM2 in cancer cells enhances proliferative metabolism by causing a backflow of metabolites into anabolic pathways such as the serine biosynthesis pathway (Vander Heiden et al., 2011).

Like its involvement in glycolysis, MYC also regulates glutaminolysis at multiple nodes. Many MYC-overexpressing cell lines are addicted to exogenous glutamine (Yuneva et al., 2007; Wise et al., 2008) and primary MYC-driven murine lung and liver tumors display markers of increased glutamine

metabolism such as increased expression of glutaminase (GLS), the enzyme that catalyzes the conversion of glutamine to glutamate (Yuneva et al., 2012). MYC increases Slc1a5 transporter expression to facilitate glutamine uptake (Le et al., 2012; Yuneva et al., 2012). MYC-dependent suppression of miR-23a/b leads to upregulation of glutaminase (Gao et al., 2009). GLS inhibition in cell lines can cause MYC-dependent cell death or reduced proliferation (Le et al., 2012; Yuneva et al., 2012). Taken together, glutamine metabolism is important for MYC-driven tumor growth and maintenance.

Although glucose and glutamine metabolism are the most notable metabolic pathways altered by MYC, several others have been shown to be important for MYC-driven tumor progression and maintenance. For example, MYC stimulates ribosomal and mitochondrial biogenesis to help provide building blocks and fuel for proliferating cells (Li et al., 2005; van Riggelen et al., 2010). Specifically, MYC regulates chromatin remodeling and recruitment of RNA polymerase I cofactors to stimulate transcription of ribosomal DNA (rDNA) genes (Arabi et al., 2005; Grandori et al., 2005; Shiue et al., 2009). MYC also regulates RNA polymerase II-dependent transcription of ribosomal structural protein genes in both human and mouse cells (Kim et al., 2000; Wu et al., 2008) as well as factors for ribosomal RNA processing and subunit export (Maggi et al., 2008; Zeller et al., 2001). Further, MYC regulates the expression of translation initiation factors that are important for protein expression (De Benedetti and Graff, 2004). Regarding mitochondrial biogenesis, MYC has been shown to regulate mitochondrial mass in primary hepatocytes as well as induce expression of genes involved in mitochondria structure and function in a model of MYC-driven B cell lymphoma (Li et al., 2005).

MYC also alters serine, glycine, and proline metabolism in some cell types. Transcript expression of phosphoglycerate dehydrogenase (PHGDH), the first enzyme of serine biosynthesis, is dramatically elevated in MYC-driven murine liver tumors and returns to baseline when MYC is withdrawn in established tumors (Vazquez et al., 2011). Serine hydroxymethyltransferase (SHMT), another key enzyme in the serine biosynthesis pathway, is a MYC target and is able to partially rescue growth in MYC-deficient cells (Nikiforov et al., 2002). MYC-dependent upregulation of the proline biosynthesis enzymes pyrroline-5-carboxylate synthase (P5CS) and pyrroline-5-carboxylate reductase 1 (PYCR1) increases the biosynthesis of proline from glutamine (Liu et al., 2012b). Further, MYC overexpressing cells appear to be dependent on proline, as MYC suppresses expression of the first enzyme of proline catabolism, proline oxidase (POX), and elevated activity of POX can inhibit MYC-mediated cancer cell proliferation and survival (Liu et al., 2012b).

MYC can also co-opt metabolic regulators. A kinome siRNA screen performed in an osteosarcoma cell line with conditional MYC activity identified AMPK-related kinase 5 (ARK5) or AMPK itself as synthetic lethal partners of MYC, whereby inhibition of ARK5 or AMPK induced cell death in a MYC-dependent manner. ARK5 expression was confirmed to be necessary for MYC-driven liver cancer progression, and ARK5 was shown to enhance MYC-driven tumor growth and maintenance by restraining mTOR-mediated translation while maintaining electron transport chain component expression and activity (Liu et al., 2012a). Finally, MYC and the NAD-dependent deacetylase SIRT1 form a positive feedback loop in multiple cancer cell lines. This connects MYC activity to the metabolic state of cells, since SIRT1 serves as a metabolic sensor and coordinates intracellular energetics with transcriptional regulation (Menssen et al., 2012). Taken together, these studies

highlight the importance of several metabolic pathways to MYC-driven tumor growth and maintenance.

1.3 MYC AND microRNAS

MicroRNAs (miRNAs) are a family of endogenous, single stranded, small noncoding RNAs that are typically 20-23 nucleotides long. MiRNAs are key post-transcriptional regulators of gene expression in many species (Bartel, 2004; He and Hannon, 2004). They were first discovered in the nematode worm *Caenorhabditis elegans*, when *lin-4* and *let-7* were identified as two noncoding genes that control larval development (Ambros, 1989; Lee et al., 1993; Reinhart et al., 2000). It was later confirmed that *let-7* is evolutionarily conserved across metazoans from molluscs to humans (Pasquinelli et al., 2000). Like the *let-7* family, many other miRNA families are highly conserved across species. Recent estimates suggest that there are up to 2000 functional miRNAs in humans, which are predicted to regulate 60% of all protein coding genes (Friedman et al., 2009; Lewis et al., 2005). The highly regulated expression of miRNAs is thought to allow fine-tuning of diverse cellular processes including differentiation, development, cell proliferation, and apoptosis (He and Hannon, 2004; Krol et al., 2010).

MiRNA biogenesis

In brief, miRNA biogenesis occurs in four main steps: transcription, nuclear processing, nuclear export, and cytoplasmic processing (Kim, 2005). Transcription of miRNAs occurs via RNA polymerase II and is regulated similarly to that of protein-coding genes. Nascent miRNA transcripts

(termed primary miRNAs or pri-miRNAs) contain a hairpin structure where the mature miRNA sequence is found (Cai et al., 2004; Lee et al., 2004). Following transcription, pri-miRNAs are processed in the nucleus by the "microprocessor complex" comprised of the RNA binding protein DGCR8 and the RNase III endonuclease Drosha. DGCR8 recognizes and binds target sequences flanking the hairpin structure and guides Drosha to the correct sites of cleavage. Cleavage of the hairpins from pri-miRNAs produces precursor miRNAs (pre-miRNAs) (Gregory et al., 2006). Pre-miRNAs are then exported from the nucleus via Exportin-5. Once in the cytoplasm, pre-miRNAs are cleaved by a second RNase III endonuclease, Dicer. This cleavage produces ~22 nucleotide long double stranded RNA duplexes that contain the mature miRNA and its complementary strand, known as miRNA* (Lund and Dahlberg, 2006; Winter et al., 2009).

The mature miRNA strand is then loaded into the RNA-induced silencing complex (RISC) via guidance from the ribonucleoprotein (RNP) complex comprised of Dicer, TRBP, and Argonaute-2, while the complementary miRNA* strand is generally thought to be rapidly degraded upon its exclusion from the RISC (Hammond et al., 2001; Mourelatos et al., 2002). Once loaded into RISC, mature miRNAs generally recognize and bind the 3' untranslated regions (3' UTRs) of target mRNAs via a 5-8 nucleotide sequence at the 5' end of the miRNA known as a seed sequence (Lewis et al., 2005). Depending upon the degree of complementarity between the miRNA seed sequence and the miRNA 3'UTR, miRNA binding can effect either mRNA degradation through RISC-mediated cleavage or translational repression via deadenylation of the mRNA poly(A) tail (Behm-Ansmant et al., 2006; Grishok et al., 2001; Orban and Izaurralde, 2005; Parker and Sheth, 2007).

MYC and miRNA processing enzymes

MYC regulates multiple elements of miRNA processing. For example, MYC induces transcriptional upregulation of RNA binding proteins such as Lin28, Lin28b, and HNRNPA1 (Chang et al., 2009; David et al., 2010). MYC also transcriptionally regulates the expression of Drosha and thus modulates pri-miRNA processing (Wang et al., 2013). Conversely, alterations in miRNA biogenesis may affect MYC-driven tumorigenesis in a cell- and tissue- specific manner. For example, Dicer was shown to be a haploinsufficient tumor suppressor in a mouse model of soft tissue sarcoma (Kumar et al., 2009). Similarly, diminished Dicer expression correlates with poor prognosis in human lung cancer and chronic lymphocytic leukemia patients (Karube et al., 2005; Zhu et al., 2012). However, haploinsufficiency or deletion of *Dicer1* failed to promote malignancy in a mouse model of MYC-driven B-cell lymphoma (Arrate et al., 2010). Thus, aberrant expression of miRNA biogenesis enzymes likely promotes MYC-driven tumor growth and maintenance in a tissue-restricted manner. Further investigations into the role of miRNA processing in MYC-driven tumorigenesis are warranted.

MYC-regulated miRNAs in vitro *and* in vivo

Induction of miRNAs is a bona fide method by which MYC indirectly represses protein-coding genes. Accordingly, MYC has been shown to increase expression of many miRNAs with diverse targets. The best-known miRNA target of MYC is the miR-17-92 cluster, which is activated by E-box binding in its first intron (He et al., 2005; Jackstadt and Hermeking, 2015). This polycistronic cluster encodes miR-17, miR-18a, miR-19a, miR-20a, miR-19b-1, and miR-92a-1 (He et al., 2005; O'Donnell et al., 2005). The miR-17-92 cluster has two paralogous clusters: the miR-106b-25 and

miR-106a-363 clusters, both of which have MYC binding sites near their transcription start sites (Kumar et al., 2013; Tanzer and Stadler, 2004). The 15 miRNAs of this family are frequently activated in solid tumors and B-cell lymphomas (He et al., 2005; Jackstadt and Hermeking, 2015; Volinia et al., 2006). The miR-17-92 cluster has been demonstrated as a bona fide oncogene and an essential mediator of MYC-induced lymphomagenesis in a mouse model of MYC-driven B-cell lymphoma (Mu et al., 2009; Sandhu et al., 2013). Additionally, elevated miR-17-92 expression enhances tumorigenesis in mouse models of retinoblastoma, colorectal cancer, and medulloblastoma (Conkrite et al., 2011; Dews et al., 2006; Uziel et al., 2009). The miR-17-92 miRNAs target many transcripts and have demonstrated roles in cellular processes including cell proliferation, apoptosis, angiogenesis, and metabolism. Specifically regarding metabolism, the miR-19 family has been shown to target PTEN, leading to PI3K pathway activation and upregulation of glycolysis (DeBerardinis et al., 2008; Mu et al., 2009). Surprisingly, miR-17 and miR-20 have been shown to inhibit tumor cell invasion and metastasis in a model of breast cancer (Yu et al., 2010). Thus, although the miR-17-92 cluster is a critical component of MYC-mediated tumorigenesis, it likely has tissue- and tumor stage-specific functions (Jackstadt and Hermeking, 2015).

In addition to the miR-17-92 cluster, many other miRNAs are induced by MYC activation. These include miR-22, miR-378, and miR-9 (Jackstadt and Hermeking, 2015). MiR-22 regulates TET-family dependent chromatin remodeling and was shown to be important for breast cancer stemness (i.e., maintenance of stem-cell like properties) and metastasis (Song et al., 2013). MiR-378 cooperates with activated Ras or HER2 to promote cellular transformation and relieves cyclin D1 repression by targeting TOB2 (Feng et al., 2011). MiR-9 is activated by both MYC and N-MYC and plays a role in

cancer metastasis by regulating E-cadherin (Ma et al., 2010). Additionally, miR-9 can promote tumor angiogenesis by activating the JAK-STAT pathway (Zhuang et al., 2012).

MYC not only activates miRNAs but can also repress them. In fact, some evidence suggests that MYC activation leads to widespread miRNA repression (Chang et al., 2008). Most notably, MYC represses p53-dependent miRNAs. For example, MYC represses the canonical p53-regulated miR-34a by binding near its promoter (Chang et al., 2008). MiR-34a regulates genes involved in the cell cycle and apoptosis (Chang et al., 2007; Raver-Shapira et al., 2007; Tarasov et al., 2007), stemness (Siemens et al., 2013), senescence (Christoffersen et al., 2010), and mesenchymal-epithelial transition (Siemens et al., 2011). MiR-34a antagonism is effective for promoting growth of colon, prostate, and lung cancer (Jackstadt and Hermeking, 2015). However, miR-34a rescue had antiapoptotic effects in MYC-overexpressing lymphoma cells while miR-34a inhibition sensitized the same cells to apoptosis (Sotillo et al., 2011). Thus, the output of miR-34a is likely determined by cellular context and fine-tuning of its intracellular levels. Finally, MYC regulates the miR-15a/16-1 cluster by recruiting HDAC3 to the promoter region of its host gene, *DLEU2* (Zhang et al., 2012a). MiR-15a/16-1 are activated by p53 via multiple mechanisms involving both transcription and miRNA processing (Fabbri et al., 2011; Suzuki et al., 2009). Repression of these tumor suppressor miRNAs by MYC inhibits their apoptotic and cell cycle regulatory functions (Cimmino et al., 2005; Liu et al., 2008). Thus, downregulation of miRNAs is one way that MYC antagonizes p53 function.

Beyond p53-dependent miRNAs, MYC can repress let-7, leading to upregulation of the oncogene RAS, a small GTP binding protein, or HMGA2, a chromatin architectural factor (Yong and Dutta,

2007). MYC represses miR-23a/b to relieve glutaminase (GLS) repression and drive glutaminolysis (Gao et al., 2009). MYC also represses miR-29 in lymphoma via coordination with histone deacetylase 3 (HDAC3) and EZH2, a member of the Polycomb-group family of proteins important for sustained transcriptional repression; in turn, MYC upregulates EZH2 by targeting miR-26a and EZH2 sustains MYC expression by targeting miR-494 in a complex positive feedback loop (Sander et al., 2008; Zhang et al., 2012b). MiR-29b is repressed by MYC as well as the transcription regulators NF-kB and Hedgehog in cholangiocarcinoma cells (Mott et al., 2010).

MiRNAs that regulate MYC

MYC itself can be regulated by miRNAs. For example, let-7 is predicted to target the MYC 3' UTR, and ectopic let-7 expression leads to MYC protein and mRNA depletion and reduced proliferation in Burkitt lymphoma cells (Sampson et al., 2007). MiR-196b and miR-184 both target MYC and BCL2 for concomitant regulation of proliferation and survival (Abe et al., 2013; Zhen et al., 2013). MiR-449c targets MYC and suppresses invasion and migration of non-small cell lung cancer cells (Miao et al., 2013). Two p53-activated miRNAs, miR-145 and miR-34a, target MYC, adding another layer of complexity to the antagonism between MYC and p53 in tumorigenesis (Sachdeva et al., 2009; Yamamura et al., 2012a, 2012b). Finally, miR-24 can target MYC via noncanonical "seedless" binding and degradation that is aided by the ribosomal protein L11 (Challagundla et al., 2011; Lal et al., 2009). In summary, the interplay between MYC and miRNAs leads to complex regulatory circuits that contribute to cancer cell progression and tumor maintenance (Jackstadt and Hermeking, 2015).

1.4 OXIDATIVE STRESS AND CANCER

Reactive oxygen species (ROS) are defined as oxygen-containing molecules with reactive properties. ROS include free radicals such as the superoxide and hydroxyl radicals, as well as non-radical molecules such as hydrogen peroxide (H_2O_2). ROS are primarily derived from oxygen-dependent metabolic reactions that occur in the mitochondria, peroxisomes and the endoplasmic reticulum, with the mitochondria being the major source of these molecules (Finkel, 2012; Handy and Loscalzo, 2012). Within these cellular compartments, ROS can be produced via both enzymatic and non-enzymatic reactions. For example, the mitochondrial electron transport chain is a non-enzymatic source of ROS (Gorrini et al., 2013a). Modulation of intracellular ROS levels is important for normal cellular homeostasis (Janssen-Heininger et al., 2008; Sena and Chandel, 2012). For example, H_2O_2 can serve as a signal for cellular proliferation, differentiation and migration at intermediate levels (Rhee, 2006). However, too much ROS can damage intracellular biomolecules including lipids, DNA and proteins (Gorrini et al., 2013a).

The role of oxidative stress and ROS in cancer is a controversial subject. A growing body of evidence suggests that ROS can either aid or hinder tumor progression, depending upon their level and the stage of tumor growth (Gorrini et al., 2013a). For example, ROS have been shown to activate MAPK, ERK, and JNK, and can elevate cyclin D1 expression (Martindale and Holbrook, 2002; Ranjan et al., 2006). Additionally, ROS can inactivate the tumor suppressor PTEN (Leslie et al., 2003). Conversely, common cancer therapies such as chemotherapeutic drugs and ionizing radiation are effective in part by inducing high levels of ROS in tissues (Conklin, 2004; Yoshida et al., 2012). Regardless of the effects of elevated ROS on tumor cell survival, it is generally agreed that

tumor cells exhibit aberrant antioxidant systems that aid their survival in environments with fluctuating oxygen and nutrient availability, both of which affect tissue redox state (Gorrini et al., 2013a). These altered antioxidant systems may render subsets of tumor cells insensitive to chemotherapy and radiation (Diehn et al., 2009; Jones and Thompson, 2009). Thus, a better understanding of the role of ROS in tumor initiation, progression, and maintenance is clearly warranted.

Cells have evolved innate systems to combat oxidative stress and to prevent or mitigate oxidative damage to intracellular macromolecules (**Figure 2**). There are three major transcriptional regulators of antioxidant response genes in cells: NRF2, FOXO, and p53. Although NRF2 is considered to be the "master regulator" of antioxidant response, all three of these transcription factors have both distinct and overlapping targets and can support complementary antioxidant pathways. The major antioxidants produced by cells are glutathione (GSH) and NADPH. These antioxidants work in concert with dietary antioxidants, such as Vitamin C, and tissue-specific redox systems to maintain redox homeostasis (Gorrini et al., 2013a). GSH is the most abundant non-enzymatic antioxidant molecule in the cell (Meister, 1991). It is synthesized by the successive reactions of glutamate-cysteine ligase (GCLC, catalytic subunit/GCLM, modifier subunit) and GSH synthetase (GSS) (Lu, 2013).

Several studies indicate that various oncogenic pathways, including KRAS, MYC, PI3K-AKT, and DJ1/PARK7 can promote NRF2 stability and activation (Clements et al., 2006; DeNicola et al., 2011; Mitsuishi et al., 2012). Further, mutations in NRF2 and its regulator KEAP1 that result in

NRF2 activation have been identified in human cancers. These mutations have been found primarily in squamous cell carcinomas and to a lesser extent in lung, skin, oesophageal, ovarian, and breast cancers (Hayes and McMahon, 2009; Kim et al., 2010; Shibata et al., 2008). Similarly, FOXO transcription factor function can be enhanced by or cooperate with activation of the oncogenes AKT, β-catenin and TGFβ to promote tumorigenesis (Naka et al., 2010; Sykes et al., 2011; Tenbaum et al., 2012). However, loss of the tumor suppressor RB (in the context of TSC2 loss) can lead to reduced FOXO activity (Li et al., 2010). Similarly, the tumor suppressor BRCA1, important for DNA integrity and repair, is required for NRF2-mediated antioxidant response (Bae et al., 2004; Gorrini et al., 2013b; Saha et al., 2009) while loss of the tumor suppressor Ataxia Telangiectasia Mutated (ATM), an important cell cycle checkpoint protein, correlates with increased oxidative stress in tissues (Alexander et al., 2010; Barzilai et al., 2002; Ito et al., 2004). Thus, oncogenes and tumor suppressors may not have strictly opposing roles in antioxidant regulation; instead, their functions in regulating ROS are likely context- and stage-specific. Further investigation of the interplay between oncogenes, tumor suppressors, and oxidative stress response in cancer is required.

Several metabolic pathways are regulated by and/or mediate ROS through their activity. The M2 isoform of muscle pyruvate kinase, PKM2, is redox-sensitive. Under conditions of high ROS, PKM2 is inactivated, leading to a backflow of glycolytic intermediates through the pentose-phosphate pathway and resulting in NADPH generation (Anastasiou et al., 2011). Another metabolic pathway that is important for antioxidant generation is the serine biosynthesis pathway. Serine is a precursor of glycine, which is used in glutathione synthesis (Lu, 2013). Importantly, glycine is required for cancer cell proliferation (Jain et al., 2012) while activity of PHGDH, the rate-limiting enzyme of serine biosynthesis, is essential in breast cancer and melanoma cells (Locasale et al., 2011; Possemato

et al., 2011). Glutamine is also essential for glutathione synthesis (Lu, 2013). Not surprisingly, the xCT cystine/glutamate transporter has been implicated in redox homeostasis and tumor growth (Ishimoto et al., 2011).

1.5 MYC AND HEPATOCELLULAR CARCINOMA

Hepatocellular carcinoma (HCC) is a leading cause of cancer-related death worldwide, yet there are few effective therapies (Jemal et al., 2009; Lin et al., 2010). HCC has a complex etiology, with approximately 75% of HCC is attributed to chronic HBV and HCV infections (Yang and Roberts, 2010). MYC is activated in chronic liver disease (Chan et al., 2004) and can drive human hepatocarcinogenesis (Kaposi-Novak et al., 2009). Accordingly, MYC overexpression is present in up to 70% of viral- and alcohol-related HCC (Sanyal et al., 2010; Schlaeger et al., 2008). MYC amplification in HCC is associated with aggressive disease and poor prognosis (Kawate et al., 1999; Peng et al., 1993). The HBV-associated protein HBx activates MYC, which accelerates HBx-mediated oncogenesis in transgenic mice (Balsano et al., 1991; Terradillos et al., 1997). It is thought that MYC's activation of hTERT may contribute to aggressive phenotypes in human HCC (Lin et al., 2010). Importantly, MYC-driven murine liver tumors regress when MYC is inactivated *in vivo* (Shachaf et al., 2004).

The interplay between MYC and miRNAs also appears to be a key component of liver tumor progression and maintenance (Jackstadt and Hermeking, 2015). For example, MYC represses miR-26a (Sander et al., 2008). Reintroduction of miR-26a in a MYC-driven liver tumor model could suppress

tumorigenesis and induce apoptosis in established tumors (Kota et al., 2009). Additionally, MYC represses miR-148a-5p and miR-363-3p, both of which target MYC through different mechanisms. Inhibition of either miR-148a-5p or miR-363-3p could induce liver tumorigenesis by promoting G1/S phase transition, while activation of these miRNAs could diminish tumor growth (Han et al., 2013). Our lab has previously shown that inhibition of miR-494, which is part of an oncogenic miRNA megacluster upregulated in aggressive HCC subsets, significantly diminishes growth of MYC-driven liver tumors (Lim et al., 2014). MYC likely interacts with many other miRNA and protein-coding genes in the context of human hepatocarcinogenesis. Thus, a better understanding of MYC signaling in liver tumorigenesis may contribute to the development of future therapies for HCC.

1.6 FIGURES AND TABLES

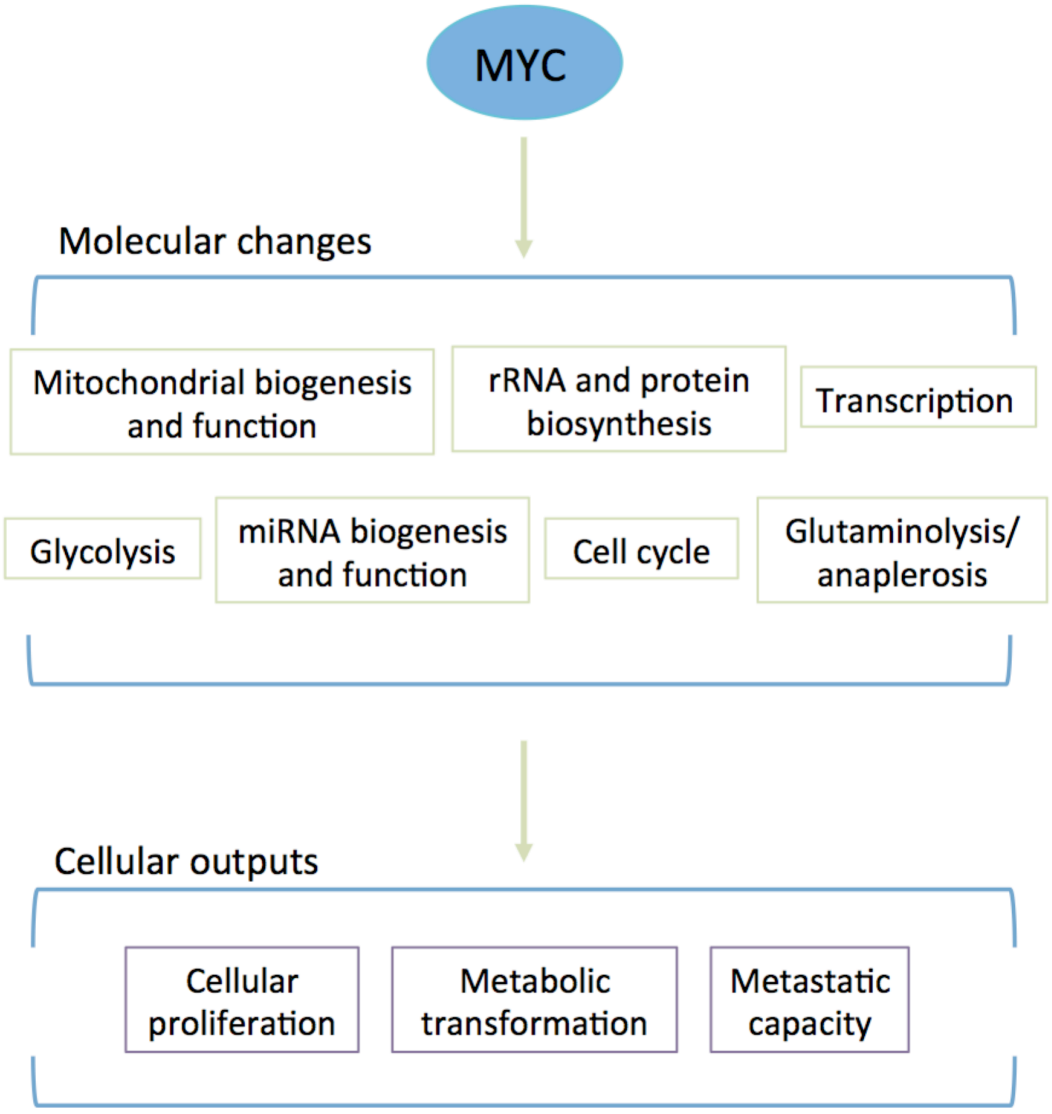

Figure 1, Summary of MYC-regulated tumor metabolism and cellular outputs. MYC transcriptionally regulates multiple metabolic pathways. The co-opting of these pathways by MYC enables enhanced cellular proliferation and tumor progression. Adapted from Miller et al., Clinical Cancer Research, 2011.

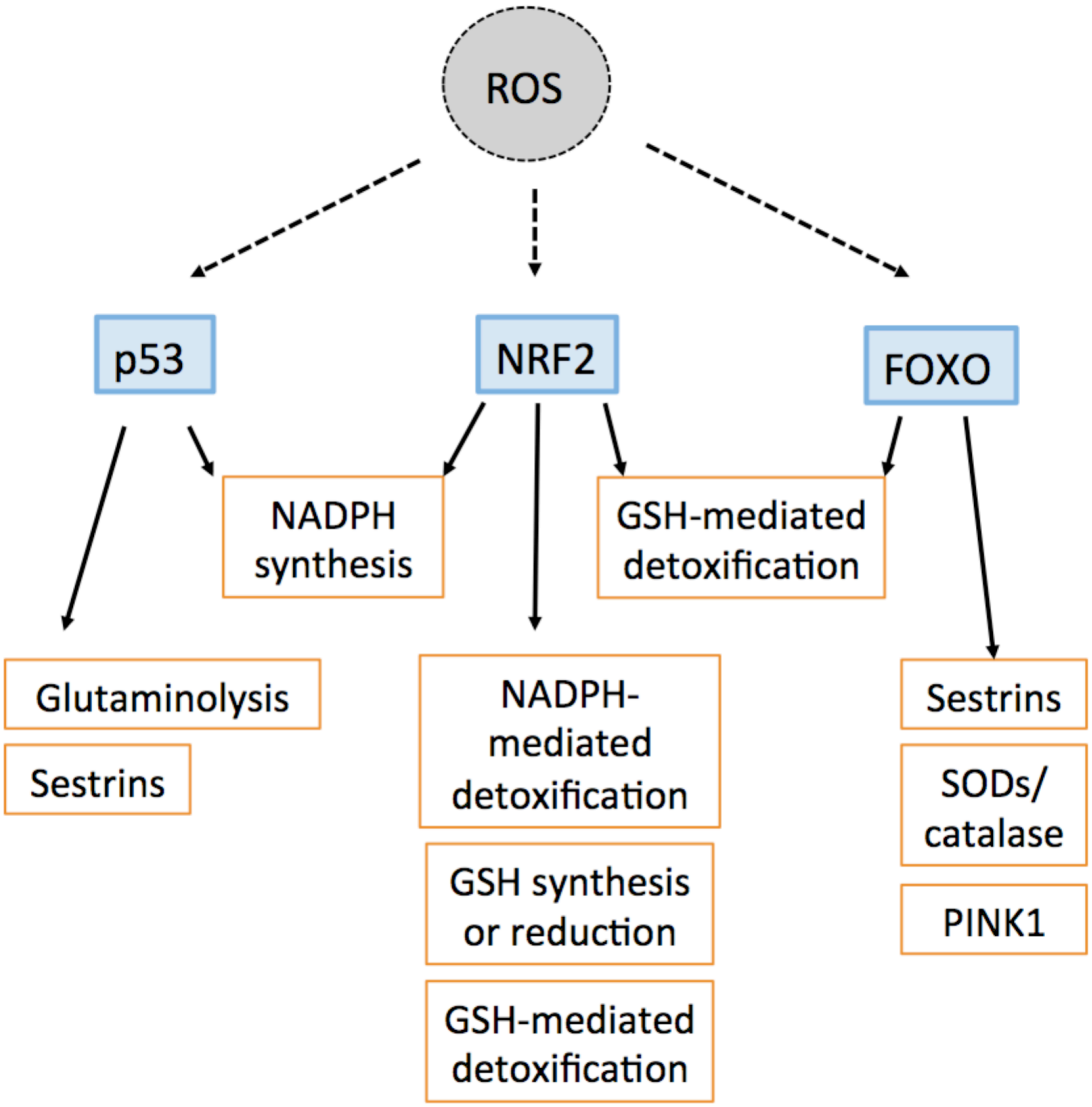
ROS
p53
NRF2
FOXO
NADPH synthesis
GSH-mediated detoxification
Glutaminolysis
Sestrins
NADPH-mediated detoxification
GSH synthesis or reduction
GSH-mediated detoxification
Sestrins
SODs/ catalase
PINK1

Figure 2, Summary of innate cellular defenses against reactive oxygen species (ROS) and oxidative stress. p53, NRF2, and FOXO transcription factors regulate complementary antioxidant pathways in response to oxidative insults. NRF2 mainly regulates glutathione and NADPH-dependent antioxidant responses, while FOXO proteins and p53 activate superoxide dismutases (SODs), catalase, PTEN-induced putative kinase 1 (PINK1), and sestrins, all of which mitigate oxidative stress. Glutaminolysis provides glutamate necessary for glutathione (GSH) synthesis. Adapted from Gorrini et al., 2013.

Chapter 2

GLUTATHIONE METABOLISM IS DEREGULATED IN A MOUSE MODEL OF MYC-DRIVEN LIVER CANCER

2.1 INTRODUCTION

The c-MYC (MYC) proto-oncogene is deregulated in many human cancers and is often associated with aggressive disease and poor prognosis. MYC is a pleiotropic transcription factor that controls expression of hundreds of both coding and noncoding genes. These genes are involved in diverse cellular functions including cell cycle, proliferation, differentiation, metabolism, and death/survival decisions. Currently, there are no targeted therapeutic strategies for cancers with deregulated MYC activity. Thus, it remains imperative to fully understand the biology of MYC activity in tumor cells in order to identify potential therapeutic targets.

Altered metabolism is a hallmark of cancer biology and has recently gained attention as a therapeutic target. Accordingly, MYC has been shown to transcriptionally regulate many metabolic genes both directly and indirectly. Two of the most notable metabolic pathways that MYC deregulates are glycolysis and glutaminolysis; MYC directly regulates glycolytic genes such as LDHA and PKM2 and indirectly regulates GLS via miR-23a/b suppression. However, because intermediary cellular metabolism is comprised of hundreds of pathways and enzymatic reactions, it is likely that there are numerous other metabolic pathways and nutrients that are critical for the survival of MYC-driven tumor cells. For example, carbon sources beyond glucose and glutamine, such as acetate and fatty

acids, may prove to be important for MYC-overexpressing cells in certain contexts. Moreover, the relevance of metabolic pathways to MYC-driven tumor growth *in vivo* has not been extensively explored.

We thus sought to identify novel metabolic pathways that are altered in MYC-driven cancer *in vivo*. We performed mRNA gene expression and mass-spectrometry-based biochemical profiling to characterize altered metabolism in the LAP-tTA x Tet-O-MYC (LT2-MYC) bitransgenic mouse, a conditional model that drives MYC expression and tumorigenesis specifically in hepatocytes (Shachaf et al., 2004). Our lab recently showed that this model has gene expression changes consistent with aggressive human liver cancers (Lim et al., 2014). Use of this model provides two major advantages over traditional, cell-based approaches: observation of oncogene-mediated metabolic reprogramming in *de novo* tumor formation, as well as the ability to discern which changes are a direct effect of oncogene signaling by taking advantage of its conditional nature (**Figure 3**). Further, because hepatocellular carcinoma (HCC) is a therapeutically challenging disease, our work contributes to a better understanding of the underlying biology in MYC-associated, aggressive subsets of HCC.

2.2 RESULTS

LT2-MYC TUMORS EXHIBIT DEREGULATED GLUTATHIONE METABOLISM

To identify novel metabolic pathways that are altered in liver tumors with high MYC expression, we performed combined mRNA expression and mass-spectrometry based biochemical profiling of primary LT2-MYC tumor samples and naïve LT2 controls. Of 333 detected polar and non-polar

metabolites with KEGG PATHWAY database identifiers (Tanabe and Kanehisa, 2012), 188 were significantly altered in LT2-MYC tumors versus controls (FDR < 0.05). Likewise, 3706 genes with KEGG identifiers exhibited significant deregulation in LT2-MYC tumors versus control liver tissue (FDR < 0.05). We performed pathway enrichment analysis on the significantly altered transcripts and metabolites identified, using all metabolic pathways defined by KEGG (**Figure 4**). We identified six KEGG pathways that were significantly altered both transcriptionally and biochemically in LT2-MYC tumors compared to control liver tissues. These pathways are: glycine, serine, and threonine metabolism; aminoacyl-tRNA biosynthesis; cysteine and methionine metabolism; ABC transporters; mineral absorption; and glutathione metabolism (**Figures 5-10; Table 1**).

Glycine, serine, and threonine metabolism

Serine and glycine are important amino acids for the biosynthesis of macromolecules including proteins, nucleic acids, and lipids (Amelio et al., 2014). Recently, the serine biosynthesis pathway has been recognized to be important for the survival of both melanoma and breast cancer cells (Locasale et al., 2011; Possemato et al., 2011). We observed a significant elevation in abundance of glycine, serine, and threonine in LT2-MYC tumors versus non-tumor control livers (**Figure 6 C and 6 D**). Further, we observed transcriptional upregulation of Phgdh, Psat1, and Psph, the rate-limiting enzymes of serine biosynthesis (Possemato et al., 2011) (**Figure 6 A and 6 B**). Glycine is produced from serine by the activity of the enzyme SHMT; accordingly, we observed elevation of Shmt2 transcript in the LT2-MYC tumors as compared to naïve control livers.

Aminoacyl-tRNA biosynthesis

We observed transcriptional upregulation of several aminoacyl-tRNA synthetases, which catalyze the aminoacylation of tRNA by their cognate amino acid (Kim et al., 2011), in LT2-MYC tumors versus non-tumor control livers. Some of the most dramatically upregulated aminoacyl-tRNA synthetases in the tumors included leucine-tRNA synthetase (Lars), isoleucyl-tRNA synthetase (Iars), glycyl-tRNA synthetase (Gars), tyrosyl-tRNA synthetase 2 (Yars2), and lysyl-tRNA synthetase (Kars); many of which are cytoplasmic aminoacyl-tRNA synthetases (**Figure 7 A and 7 B**). Interestingly, the transcript for alanyl-tRNA synthetase (Aars) was the only aminoacyl-tRNA synthetase transcript that was suppressed in the MYC-driven liver tumors according to our analysis (**Figure 7 B**).

Cysteine and methionine metabolism

Cysteine and methionine are sulfur-containing amino acids. Cysteine is synthesized from serine, while methionine is an essential amino acid and cannot be made by animals (Townsend et al., 2004). Both cysteine and methionine are elevated in LT2-MYC tumors relative to non-tumor controls (**Figure 8 C and 8 D**). Methionine is used to produce S-adenosylmethionine (SAM), a methyl group donor important for many transfer reactions including DNA methylation (Loenen, 2006). We observed increased abundance of SAM in LT2-MYC tumors compared to non-tumor control livers (**Figure 8 C and 8 C**). Further, we saw tumor-specific upregulation of the transcripts for Dnmt3a and Dnmt1, which are DNA methyltransferases thought to function in genome-wide *de novo* and maintenance methylation, respectively, during development (Jin and Robertson, 2013) (**Figure 8 A and 8 B**). Alterations in cysteine and methionine metabolism may aid MYC-dependent genome-wide gene expression changes in tumors.

ABC transporters

The ATP-binding cassette (ABC) transporters are a large family of proteins that couple ATP hydrolysis to active transport of a wide variety of substrates across extra- and intra-cellular membranes. The substrates transported by ABC proteins include ions, sugars, lipids, sterols, peptides, proteins, and drugs (Fletcher et al., 2010). We observed a dramatic upregulation of transcripts for two ABC transporters, Abcg1 and Abcc4, in LT2-MYC tumors compared to LT2 non-tumor control tissues (**Figure 9 A and 9 B**). Abcg1 is involved in macrophage cholesterol and phospholipid transport, and may regulate lipid homeostasis in other cell types (Schmitz et al., 2001). Abcc4 is thought to be an organic anion pump and may play a role in cellular detoxification (Ritter et al., 2005). The relevance of these transporters to MYC-driven tumorigenesis and tumor maintenance remain to be determined.

Mineral absorption

Minerals are a fundamental group of nutrients necessary to sustain life. For example, calcium is a critical component of bone as well as an intracellular messenger in muscle, neural networks, immune cells, and the endocrine system (Clapham, 2007). We observed an elevation of the transcript for S100G (calbindin D9K), which is a vitamin D-dependent calcium-binding protein that may increase cellular calcium absorption by buffering Ca2+ in the cytoplasm (Schwaller, 2010) (**Figure 10 A and 10 B**). In addition to calcium, iron and copper serve as cofactors for redox reactions and are also important for oxygen transport and binding. We saw a tumor-specific increase in transcript expression of Slc11a1, which is an iron and manganese transporter (Forbes and Gros, 2003); Steap2, which stimulates the cellular uptake of iron and copper *in vitro* (Ohgami et al., 2006); and Atp7a, which functions in copper transport across intra- and extra-cellular membranes (Kaler, 2014) (**Figure 10 A**

and 10 B). Many enzymes require specific metal atoms for their catalytic functions; thus the importance of minerals such as calcium, iron and copper to MYC-driven tumor development and maintenance warrants further investigation.

Glutathione metabolism

Of the six KEGG pathways identified, glutathione metabolism was the most significantly altered according to our transcriptional analysis (**Table 1**). Further, reduced (GSH) and oxidized (GSSG) glutathione were among the most dramatically depleted metabolites identified in the MYC-driven tumors. Glutathione is synthesized downstream of glutamine conversion to glutamate (Lu, 2013) and increased glutamine uptake and utilization is known to be metabolically important for MYC-overexpressing cells (Dang, 2013). Thus, we were surprised that the reduced (GSH) and oxidized (GSSG) isoforms of glutathione were consistently depleted in all tumor samples (**Figure 5 C**) and we sought to identify the significance of depleted glutathione in the MYC-driven tumors.

We independently confirmed the depletion of total glutathione (GSH + GSSG) in MYC liver tumors using an enzymatic assay (**Figure 11**). In accordance with our integrated gene expression and metabolite profiling, altered glutathione pathway transcripts (**Figure 5 A**) and metabolites (**Figure 5 C**) readily segregate LT2-MYC tumors from LT2 control livers by unsupervised hierarchical clustering. Together, these data indicate a wholesale, tumor-specific change in glutathione metabolism that is represented both transcriptionally and biochemically. Furthermore, multiple metabolites associated with the glutathione biosynthetic pathway are significantly altered (either up or down) in LT2-MYC

tumors versus control livers (**Figure 5 D and Figure 12**). Intriguingly, we saw an increased abundance of cysteine, glycine and glutamate concomitant with decreased abundance of GSH and GSSG in the MYC-driven tumors, indicative of a bottleneck at glutathione production (**Figure 12**).

MYC-DRIVEN LIVER TUMORS FAVOR CENTRAL CARBON METABOLISM OVER GLUTATHIONE SYNTHESIS

MYC reprograms glutamine metabolism by increasing expression of the Slc1a5 glutamine transporter and GLS (Gao et al., 2009; Le et al., 2012; Yuneva et al., 2012). Consistent with prior observations, we found that glutamate is elevated in LT2-MYC tumors relative to LT2 control tissue (**Figure 5 C-D**). However, total glutathione is dramatically depleted in LT2-MYC tumor tissue (**Figure 5 C-D & Figure 11**). Since glutathione is synthesized from glutamate (Lu, 2013) (**Figure 12**), we hypothesized that the depletion of glutathione in LT2-MYC tumors despite high amounts of glutamate must be due to a disruption in glutathione synthesis. Indeed, elevated levels of glutathione precursors in the LT2-MYC tumors indicate impaired glutathione production (**Figure 12**). We further hypothesized that diminished glutathione production may allow glutamate to be used preferentially in other pathways important to tumor cell metabolism, such as the TCA cycle. We therefore sought to identify changes in glutamine utilization that occur in MYC-driven liver tumors versus non-tumor liver tissues.

To determine how exogenous glutamine is used in MYC-driven tumors, we intravenously injected MYC-driven tumor-bearing mice (Tward et al., 2005) (**Figure 13**) with fully labeled (U-^{13}C)-glutamine and performed mass spectrometry-based flux analysis of liver tumors versus adjacent non-tumor liver tissue. We found decreased incorporation of glutamine-derived carbons into glutathione and its

immediate precursor, γ-glutamyl-cysteine, consistent with the observed diminished steady state abundance of GSH and GSSG (**Figure 14 A & 14 B**). In contrast, we saw increased incorporation of glutamine-derived carbons into many other metabolites, including nucleotides, amino acids, and pentose phosphate pathway and TCA cycle intermediates, in tumors as compared to adjacent non-tumor tissue (**Figure 14 A & 14 B**). We performed pathway enrichment analysis of the significantly altered metabolites using annotations from the KEGG pathway database. Our analysis revealed predominant dysregulation of "central carbon metabolism in cancer" (KEGG map05230) in MYC-driven tumors versus adjacent non-tumor tissue. Central carbon metabolism is comprised of the canonical biochemical pathways of glycolysis, the pentose phosphate pathway, and the TCA cycle (Noor et al., 2010). Accordingly, central carbon metabolism of cancer genes defined by KEGG, which include both metabolic genes as well as the oncogenes and tumor suppressors that regulate them, readily segregate LT2-MYC tumor tissue from control liver tissue by unsupervised hierarchical clustering (**Figure 15**). These results indicate both a gene expression and biochemical switch in glutamine utilization in tumor versus non-tumor tissue that favors central carbon metabolism.

Because the TCA cycle is both a key component of central carbon metabolism and an important source of biosynthetic precursors for proliferating cancer cells (DeBerardinis et al., 2007), we next asked whether enzymes that convert glutamate to α-ketoglutarate for entry into the TCA cycle exhibit altered protein expression in LT2-MYC tumors versus control liver tissue. Glutamate can be transaminated by one of several enzymes prior to entry into the TCA cycle (Son et al., 2013). We therefore examined the expression of transaminases in MYC tumors versus LT2 control tissues by Western Blot analysis. Interestingly, we found altered protein expression of four out of five canonical transaminases (GLUD1, GPT1, GPT2, and GOT2) in LT2-MYC tumors versus LT2 control liver

(**Figure 16**). Specifically, GPT2 and GOT2 are elevated in LT2-MYC tumors while GPT1 and GLUD1 are depleted. Both GPT2 and GOT2 are the mitochondrial isoforms of their respective enzymes. Thus, their elevated expression likely aids the increased flux of glutamine-derived carbons to α-ketoglutarate and the TCA cycle in a spatially restricted manner while also providing the biosynthetic substrates alanine and aspartate (**Figure 17**). Together, our results suggest that MYC-driven murine liver tumors reprogram glutamine utilization for increased anaplerotic and biosynthetic metabolism. Specifically, we show that glutamine-derived carbons are preferentially used for the TCA cycle and central carbon metabolism, at the expense of glutathione production, in MYC-driven liver tumors. This reprogramming likely increases the amount of biosynthetic substrates available for proliferating tumor cells.

2.3 DISCUSSION

Altered tumor metabolism is a bona fide hallmark of cancer. MYC is a transcription factor oncogene that has been shown to both directly and indirectly regulate metabolic enzymes and orchestrate cancer cell metabolic changes. However, little is known about the effects of MYC signaling on tumor cell metabolism *in vivo*. In this chapter, we took an unbiased approach to elucidate novel metabolic pathways deregulated by MYC *in vivo*. We identified six metabolic pathways that are significantly altered at both the metabolite and transcript level in primary MYC-driven liver cancer. At least two of these pathways, serine metabolism and ABC transporters, have been described in connection with MYC signaling previously (Nikiforov et al., 2002; Porro et al., 2011), while to our knowledge the remaining pathways have yet to be associated with MYC activation in cancer. The relevance of these pathways (aminoacyl-tRNA biosynthesis, cysteine and methionine metabolism, and mineral

absorption) to MYC-dependent tumor growth and maintenance remains to be determined.

The most striking pathway alteration we identified in our integrated approach is suppressed glutathione biosynthesis. Glutathione is a key cellular antioxidant that is synthesized downstream of glutamine conversion to glutamate (Wu et al., 2004). We find that both the reduced and oxidized forms of glutathione (GSH and GSSG, respectively) are depleted and glutamine-derived carbons are preferentially shunted away from glutathione and toward proliferative metabolism in MYC-driven liver tumors as compared to non-tumor liver tissue.

Prior studies of MYC overexpressing cell lines (Le et al., 2012; Wise et al., 2008) have identified their use of anaplerotic glutamine flux. Our work suggests that glutathione production is suppressed in MYC-driven liver tumors, leading to a shift in glutamine flux toward central carbon metabolism *in vivo*. The observed shift in glutamine utilization may support the proliferative capacity of tumor cells by enhancing glutamine-dependent anaplerotic pathways that provide biosynthetic substrates. Indeed, we see preferential incorporation of glutamine-derived carbons into multiple anabolic substrates in tumor tissues compared to adjacent non-tumor liver.

2.4 FIGURES AND TABLES

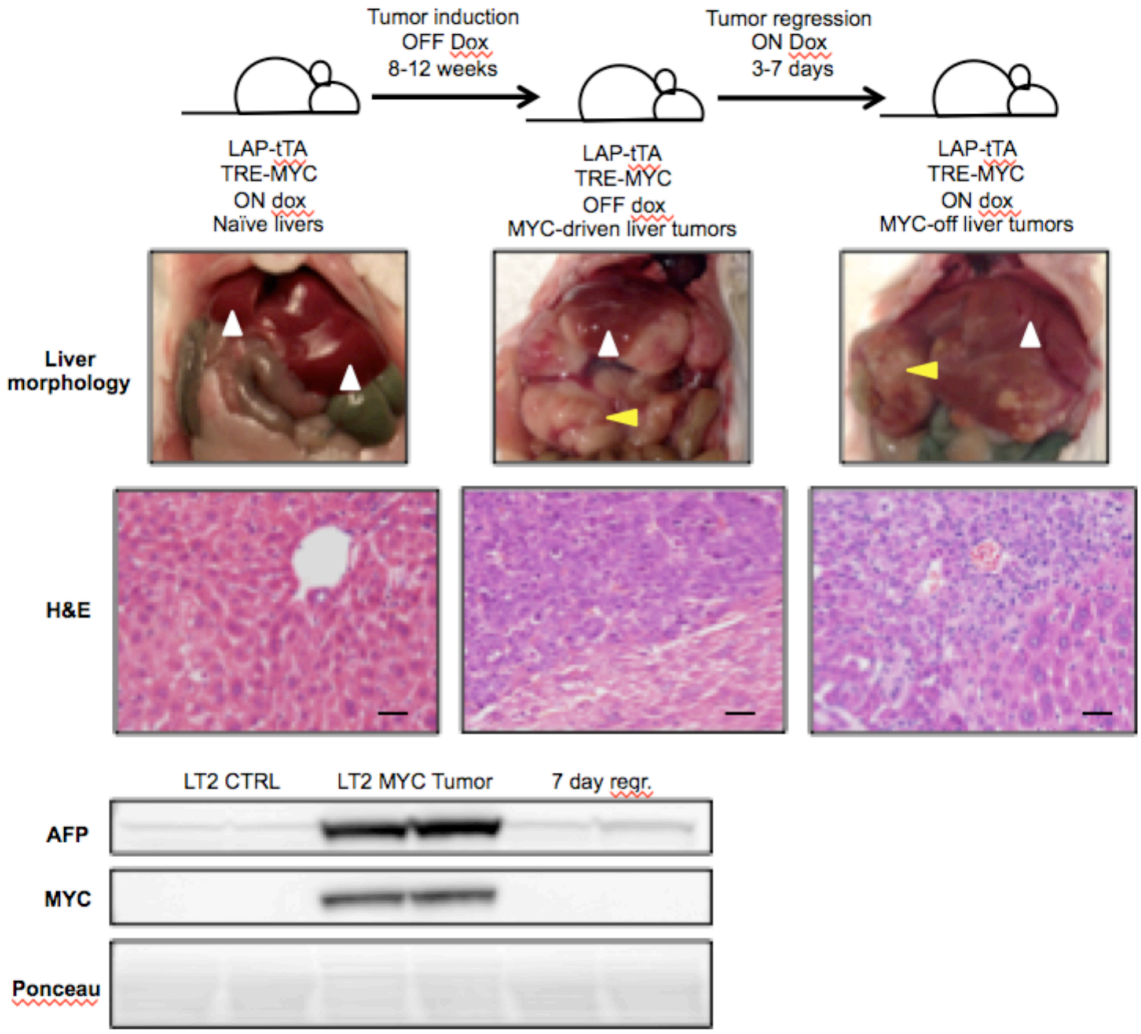

Figure 3, Summary of LT2-MYC conditional transgenic mouse model of MYC-induced hepatocarcinogenesis. Prolonged MYC overexpression induces tumor nodules that are morphologically and histologically distinct from non-tumor tissue. MYC protein expression can be turned off in established tumors and tracks with alpha-fetoprotein (AFP) expression. In tumor gross images, white arrows indicate non-tumor liver and yellow arrows indicate liver tumors. Scale bars in hematoxylin-and-eosin stained (H&E) sections represent 20μm.

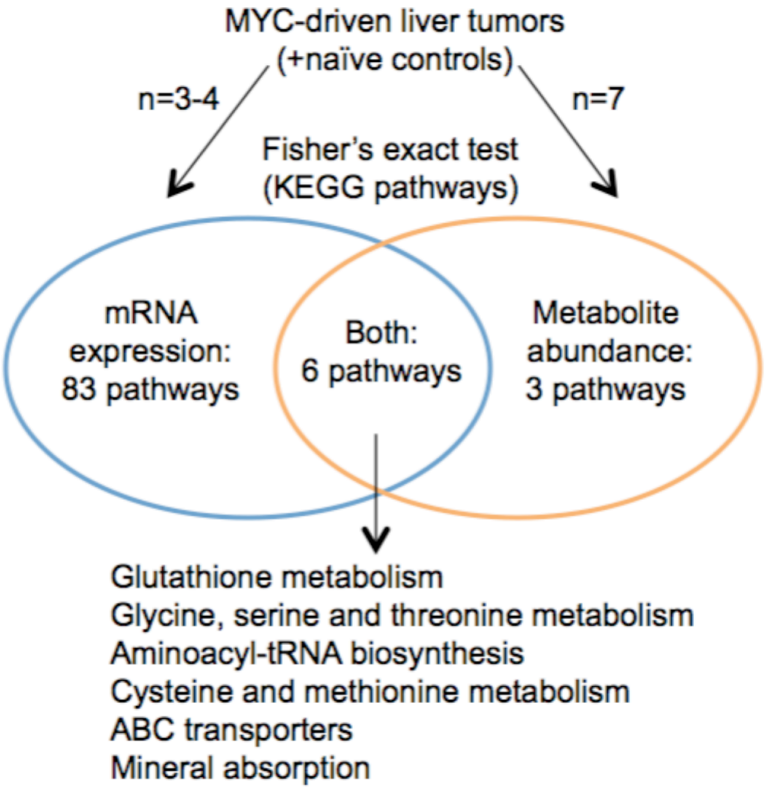

Figure 4, Schematic of integrated gene expression and metabolite profiling of MYC-driven liver tumors to identify novel MYC-regulated metabolic pathways. Transcriptional and metabolic profiling analyses were performed separately and then integrated to identify six pathways that are significantly altered in LT2-MYC tumors versus control livers (Fisher's exact test, $p < 0.05$).

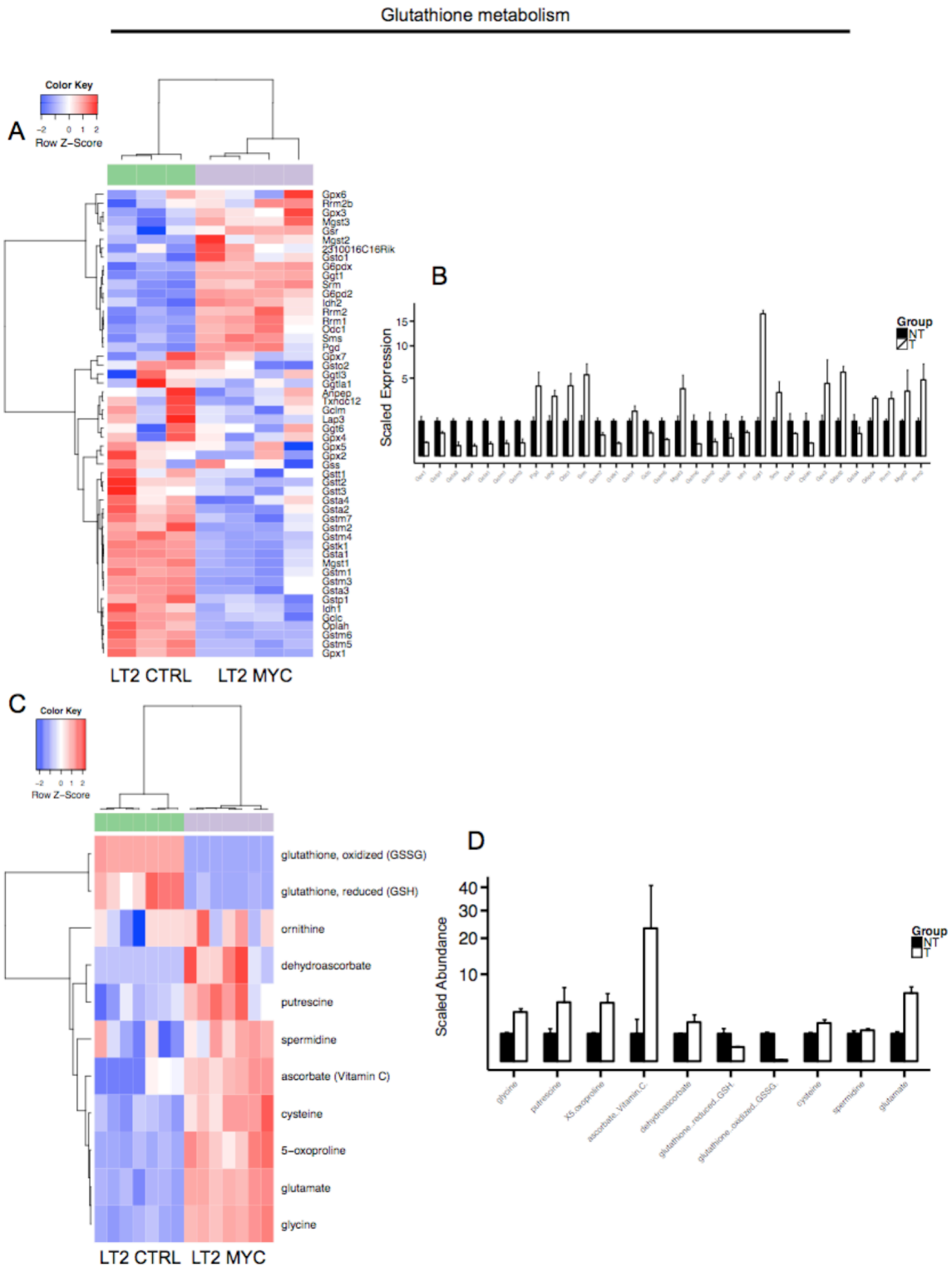
Glutathione metabolism
A
Color Key
−2 0 1 2
Row Z−Score
Gpx6
Rrm2b
Gpx3
Mgst3
Gsr
Mgst2
2310016C16Rik
Gsto1
G6pdx
Ggt1
Srm
G6pd2
Idh2
Rrm2
Rrm1
Odc1
Sms
Pgd
Gpx7
Gstc2
Ggti3
Ggtla1
Anpep
Txndc12
Gclm
Lap3
Ggt6
Gpx4
Gpx5
Gpx2
Gss
Gstt1
Gstt2
Gstt3
Gsta4
Gsta2
Gstm7
Gstm2
Gstm4
Gstk1
Gsta1
Mgst1
Gstm1
Gstm3
Gsta3
Gstp1
Idh1
Gclc
Cplah
Gstm6
Gstm5
Gpx1
LT2 CTRL
LT2 MYC
B
Scaled Expression
15
10
5
Group
NT
T
C
Color Key
−2 0 1 2
Row Z−Score
glutathione, oxidized (GSSG)
glutathione, reduced (GSH)
ornithine
dehydroascorbate
putrescine
spermidine
ascorbate (Vitamin C)
cysteine
5−oxoproline
glutamate
glycine
LT2 CTRL
LT2 MYC
D
Scaled Abundance
40
30
20
10
Group
NT
T
glycine
putrescine
X5.oxoproline
ascorbate..Vitamin.C.
dehydroascorbate
glutathione..reduced..GSH.
glutathione..oxidized..GSSG.
cysteine
spermidine
glutamate

Figure 5, Glutathione metabolism is significantly altered both transcriptionally and biochemically in MYC-driven liver tumors. A, Glutathione pathway transcripts segregate LT2-MYC tumors from control livers by unsupervised hierarchical clustering (n=3-4 per group). B, Barplot summarizing differential expression of glutathione pathway transcripts. Barplot shows only transcripts that are significantly different between LT2-MYC tumors and control livers (Data represented as mean ± SEM; $p < 0.05$). C, Glutathione pathway metabolites segregate LT2-MYC tumors from control livers by unsupervised hierarchical clustering (n=7 per group). D, Barplot summarizing differential expression of glutathione pathway metabolites. Barplot shows only metabolites that are significantly different between LT2-MYC tumors and control livers (Data represented as mean ± SEM; $p < 0.05$).

Glycine, serine, and threonine metabolism

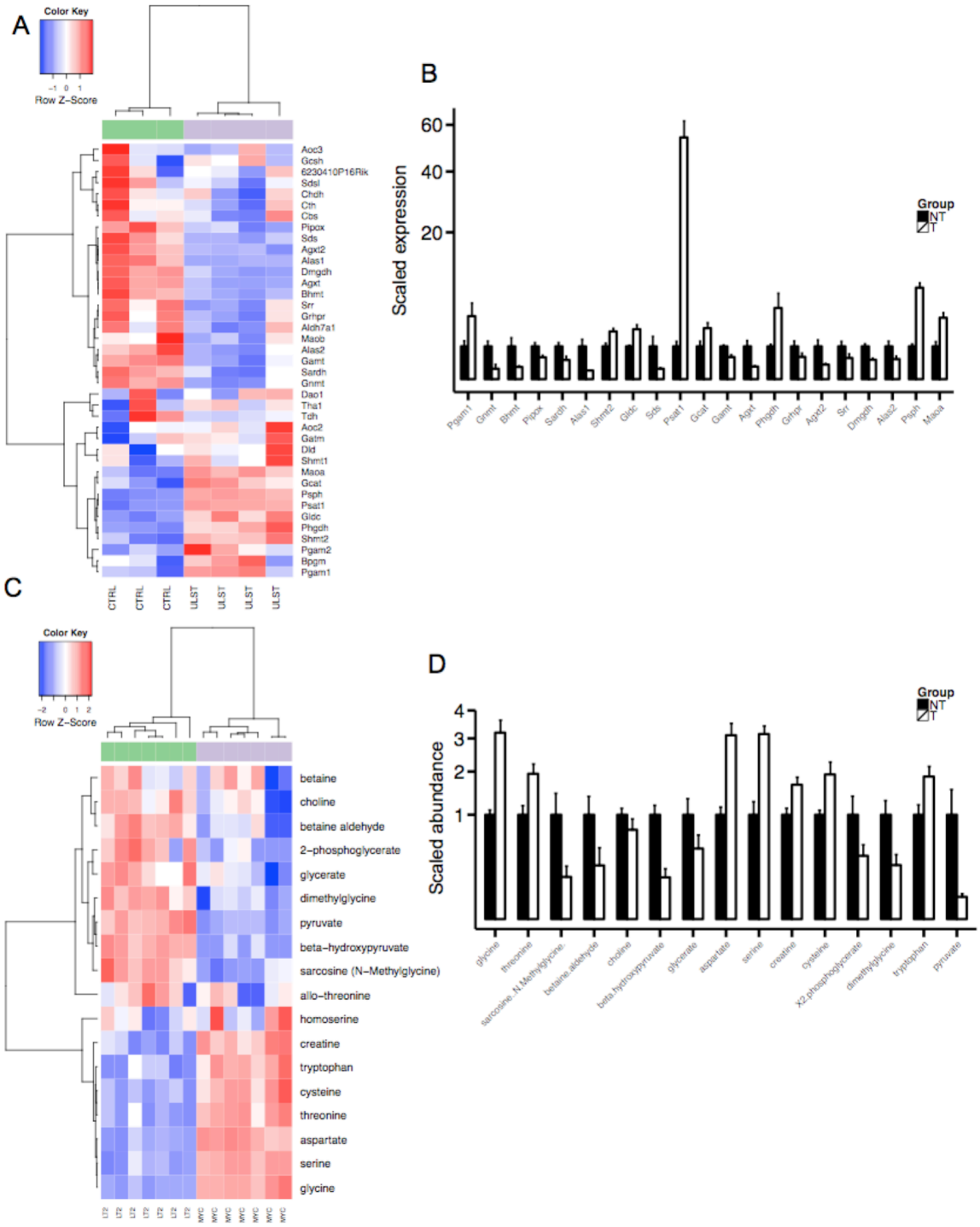

Figure 6, **Glycine, serine and threonine metabolism is significantly altered both transcriptionally and biochemically in MYC-driven liver tumors**. A, Glycine, serine and threonine pathway transcripts segregate LT2-MYC tumors from control livers by unsupervised hierarchical clustering (n=3-4 per group). B, Barplot summarizing differential expression of glycine, serine and threonine pathway transcripts. Barplot shows only transcripts that are significantly different between LT2-MYC tumors and control livers (Data represented as mean ± SEM; $p < 0.05$). C, Glycine, serine and threonine pathway metabolites segregate LT2-MYC tumors from control livers by unsupervised hierarchical clustering (n=7 per group). D, Barplot summarizing differential expression of glycine, serine and threonine pathway metabolites. Barplot shows only metabolites that are significantly different between LT2-MYC tumors and control livers (Data represented as mean ± SEM; $p < 0.05$).

Aminoacyl-tRNA biosynthesis

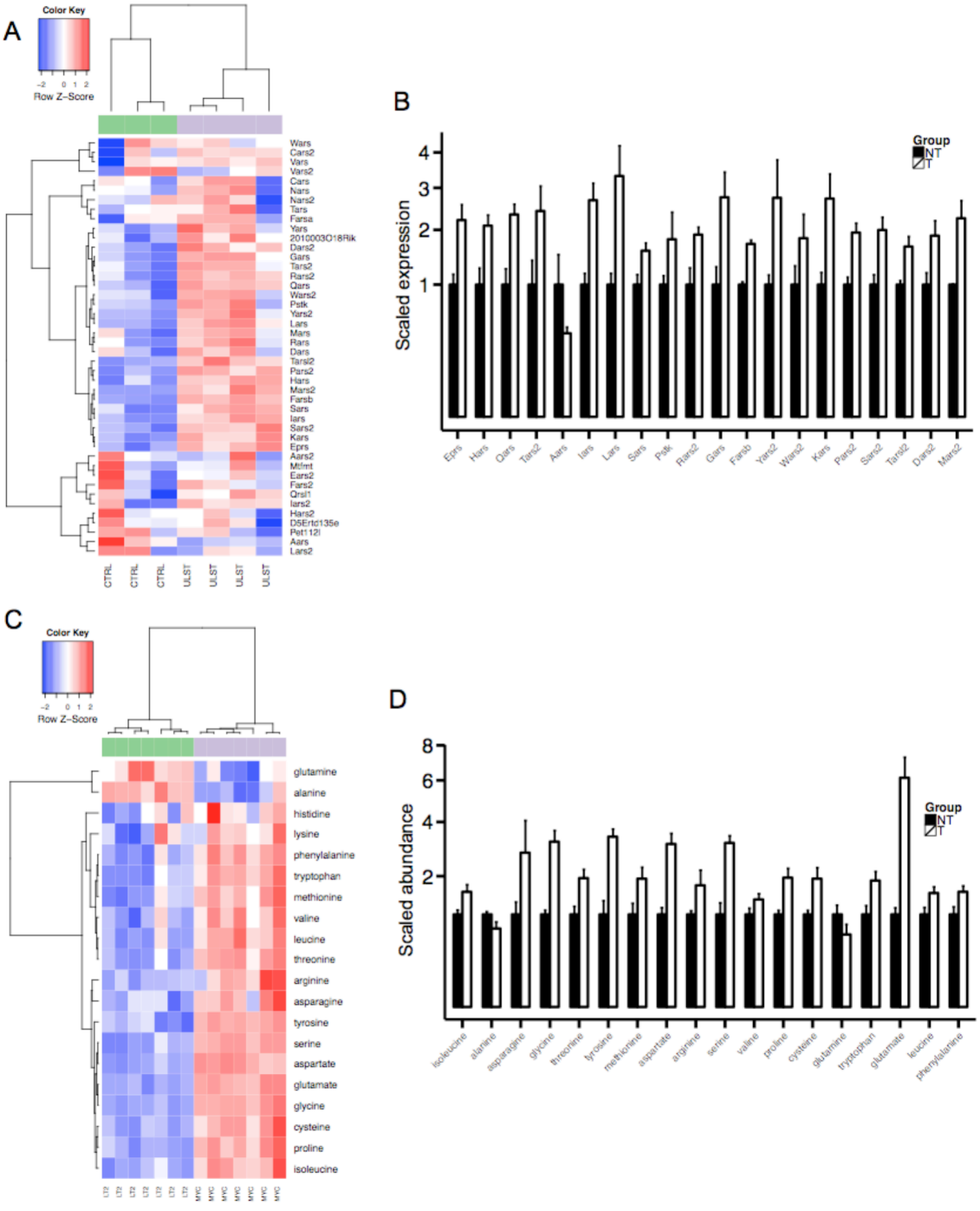

Figure 7, Aminoacyl-tRNA biosynthesis is significantly altered both transcriptionally and biochemically in MYC-driven liver tumors. A, Aminoacyl-tRNA biosynthesis pathway transcripts segregate LT2-MYC tumors from control livers by unsupervised hierarchical clustering (n=3-4 per group). B, Barplot summarizing differential expression of aminoacyl-tRNA biosynthesis pathway transcripts. Barplot shows only transcripts that are significantly different between LT2-MYC tumors and control livers (Data represented as mean ± SEM; $p < 0.05$). C, Aminoacyl-tRNA biosynthesis pathway metabolites segregate LT2-MYC tumors from control livers by unsupervised hierarchical clustering (n=7 per group). D, Barplot summarizing differential expression of aminoacyl-tRNA biosynthesis pathway metabolites. Barplot shows only metabolites that are significantly different between LT2-MYC tumors and control livers (Data represented as mean ± SEM; $p < 0.05$).

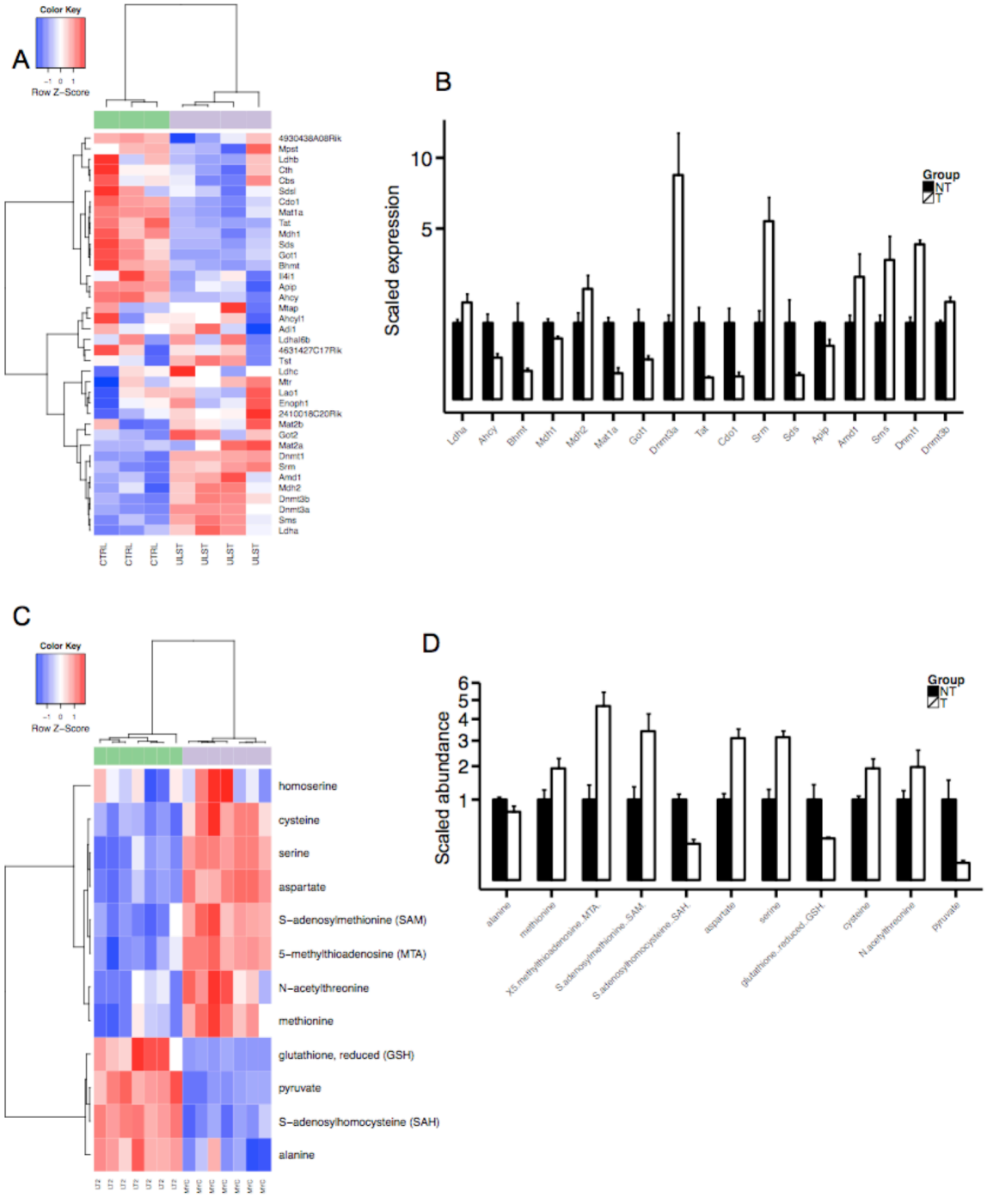
A
Color Key
Row Z-Score
4930438A08Rik
Mpst
Ldhb
Cth
Cbs
Sdsl
Cdo1
Mat1a
Tat
Mdh1
Sds
Got1
Bhmt
Ii4i1
Apip
Ahcy
Mtap
Ahcyl1
Adi1
Ldhal6b
4631427C17Rik
Tst
Ldhc
Mtr
Lao1
Enoph1
2410018C20Rik
Mat2b
Got2
Mat2a
Dnmt1
Srm
Amd1
Mdh2
Dnmt3b
Dnmt3a
Sms
Ldha
CTRL
CTRL
CTRL
ULST
ULST
ULST
ULST
B
Scaled expression
10
5
Group
NT
T
Ldha
Ahcy
Bhmt
Mdh1
Mdh2
Mat1a
Got1
Dnmt3a
Tst
Cdo1
Srm
Sds
Apip
Amd1
Sms
Dnmt1
Dnmt3b
C
Color Key
Row Z-Score
homoserine
cysteine
serine
aspartate
S-adenosylmethionine (SAM)
5-methylthioadenosine (MTA)
N-acetylthreonine
methionine
glutathione, reduced (GSH)
pyruvate
S-adenosylhomocysteine (SAH)
alanine
D
Scaled abundance
6
5
4
3
2
1
Group
NT
T
alanine
methionine
X5.methylthioadenosine..MTA.
S.adenosylmethionine..SAM.
S.adenosylhomocysteine..SAH.
aspartate
serine
glutathione..reduced..GSH.
cysteine
N.acetylthreonine
pyruvate

Figure 8, **Cysteine and methionine metabolism is significantly altered both transcriptionally and biochemically in MYC-driven liver tumors**. A, Cysteine and methionine pathway transcripts segregate LT2-MYC tumors from control livers by unsupervised hierarchical clustering (n=3-4 per group). B, Barplot summarizing differential expression of cysteine and methionine pathway transcripts. Barplot shows only transcripts that are significantly different between LT2-MYC tumors and control livers (Data represented as mean ± SEM; $p < 0.05$). C, Cysteine and methionine pathway metabolites segregate LT2-MYC tumors from control livers by unsupervised hierarchical clustering (n=7 per group). D, Barplot summarizing differential expression of cysteine and methionine pathway metabolites. Barplot shows only metabolites that are significantly different between LT2-MYC tumors and control livers (Data represented as mean ± SEM; $p < 0.05$).

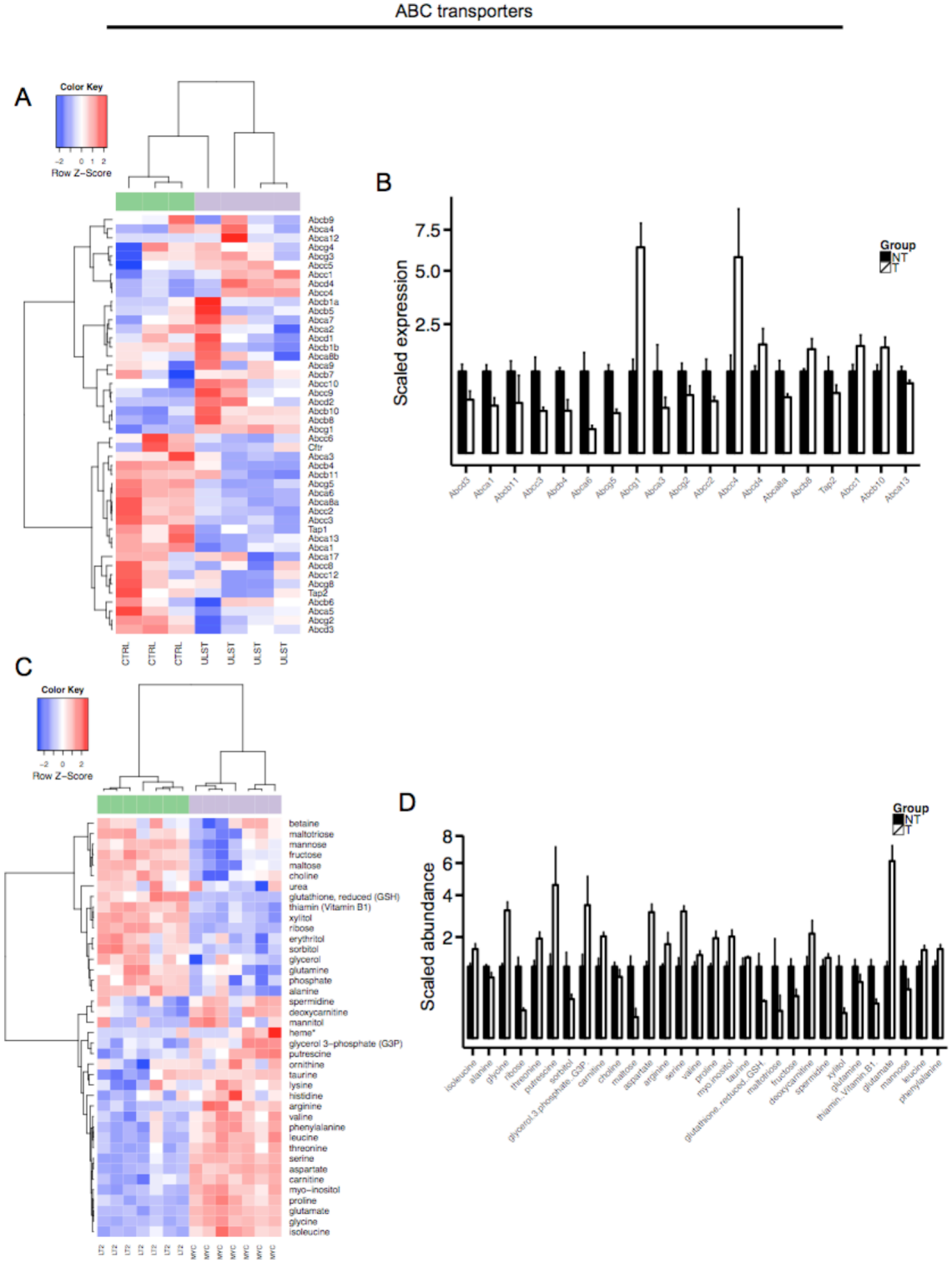
ABC transporters
A
Color Key
−2 0 1 2
Row Z−Score
Abcb9
Abca4
Abca12
Abcg4
Abcg3
Abcc5
Abcc1
Abcd4
Abcc4
Abcb1a
Abcb5
Abca7
Abca2
Abcd1
Abcb1b
Abca8b
Abca9
Abcb7
Abcc10
Abcc9
Abcd2
Abcb10
Abcb8
Abcg1
Abcc6
Cftr
Abca3
Abcb4
Abcb11
Abcg5
Abca6
Abca8a
Abcc2
Abcc3
Tap1
Abca13
Abca1
Abca17
Abcc8
Abcc12
Abcg8
Tap2
Abcb6
Abca5
Abcg2
Abcd3
CTRL CTRL CTRL ULST ULST ULST ULST
B
Scaled expression
7.5
5.0
2.5
Group
NT
T
Abcd3 Abca1 Abcb11 Abcc3 Abcb4 Abca6 Abcg5 Abcg1 Abca3 Abcg2 Abcc2 Abcc4 Abca4 Abca8a Abcb8 Tap2 Abcc1 Abcb10 Abca13
C
Color Key
−2 0 2
Row Z−Score
betaine
maltotriose
mannose
fructose
maltose
choline
urea
glutathione, reduced (GSH)
thiamin (Vitamin B1)
xylitol
ribose
erythritol
sorbitol
glycerol
glutamine
phosphate
alanine
spermidine
deoxycarnitine
mannitol
heme*
glycerol 3−phosphate (G3P)
putrescine
ornithine
taurine
lysine
histidine
arginine
valine
phenylalanine
leucine
threonine
serine
aspartate
carnitine
myo−inositol
proline
glutamate
glycine
isoleucine
L72 L73 L75 L23 L25 L21 L22 MYC MYC MYC MYC MYC MYC
D
Scaled abundance
8
6
4
2
Group
NT
T
isoleucine alanine glycine ribose threonine putrescine sorbitol glycerol.3.phosphate..G3p carnitine choline maltose aspartate arginine serine valine proline myo.inositol taurine glutathione..reduced..GSH maltotriose fructose deoxycarnitine spermidine xylitol glutamine thiamin..Vitamin.B1. glutamate mannose leucine phenylalanine

Figure 9, **ABC transporters metabolism is significantly altered both transcriptionally and biochemically in MYC-driven liver tumors**. A, ABC transporters pathway transcripts segregate LT2-MYC tumors from control livers by unsupervised hierarchical clustering (n=3-4 per group). B, Barplot summarizing differential expression of ABC transporters pathway transcripts. Barplot shows only transcripts that are significantly different between LT2-MYC tumors and control livers (Data represented as mean ± SEM; $p < 0.05$). C, ABC transporters pathway metabolites segregate LT2-MYC tumors from control livers by unsupervised hierarchical clustering (n=7 per group). D, Barplot summarizing differential expression of ABC transporters pathway metabolites. Barplot shows only metabolites that are significantly different between LT2-MYC tumors and control livers (Data represented as mean ± SEM; $p < 0.05$).

Mineral absorption

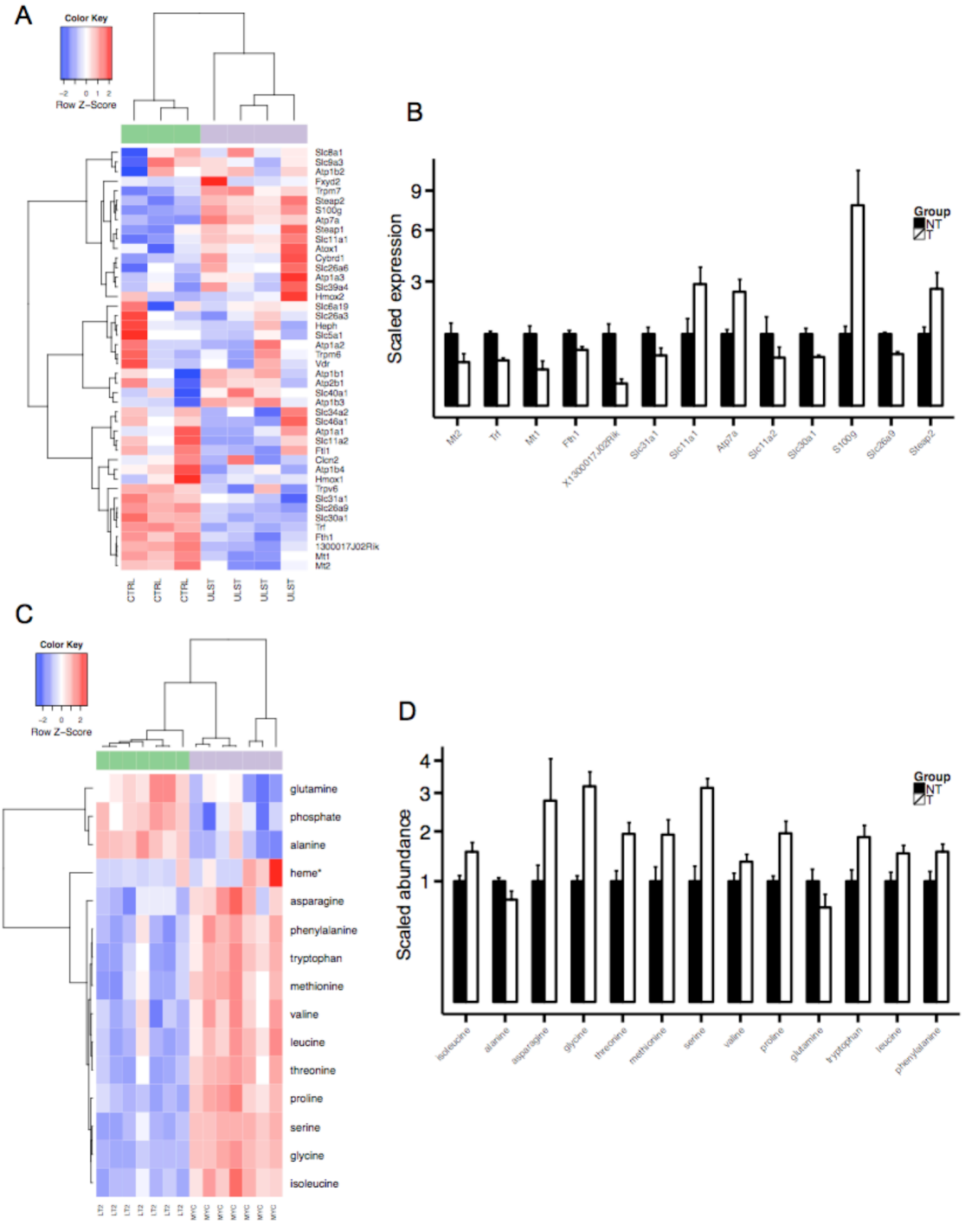

Figure 10, Mineral absorption metabolism is significantly altered both transcriptionally and biochemically in MYC-driven liver tumors. A, Mineral absorption pathway transcripts segregate LT2-MYC tumors from control livers by unsupervised hierarchical clustering (n=3-4 per group). B, Barplot summarizing differential expression of mineral absorption pathway transcripts. Barplot shows only transcripts that are significantly different between LT2-MYC tumors and control livers (Data represented as mean ± SEM; $p < 0.05$). C, Mineral absorption pathway metabolites segregate LT2-MYC tumors from control livers by unsupervised hierarchical clustering (n=7 per group). D, Barplot summarizing differential expression of mineral absorption pathway metabolites. Barplot shows only metabolites that are significantly different between LT2-MYC tumors and control livers (Data represented as mean ± SEM; $p < 0.05$).

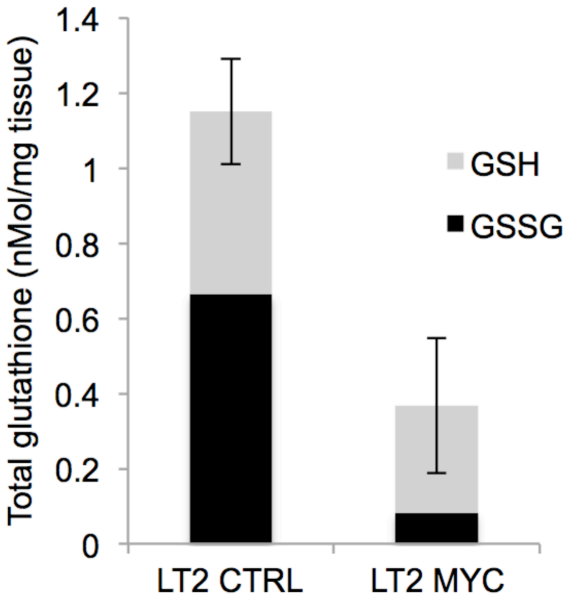

Figure 11, Total glutathione (GSH + GSSG) is depleted in LT2-MYC tumors versus control livers. Glutathione levels were measured via an enzymatic assay on frozen tissue extracts (n=5-6 each; data represented as mean ± SEM; $p < 0.01$).

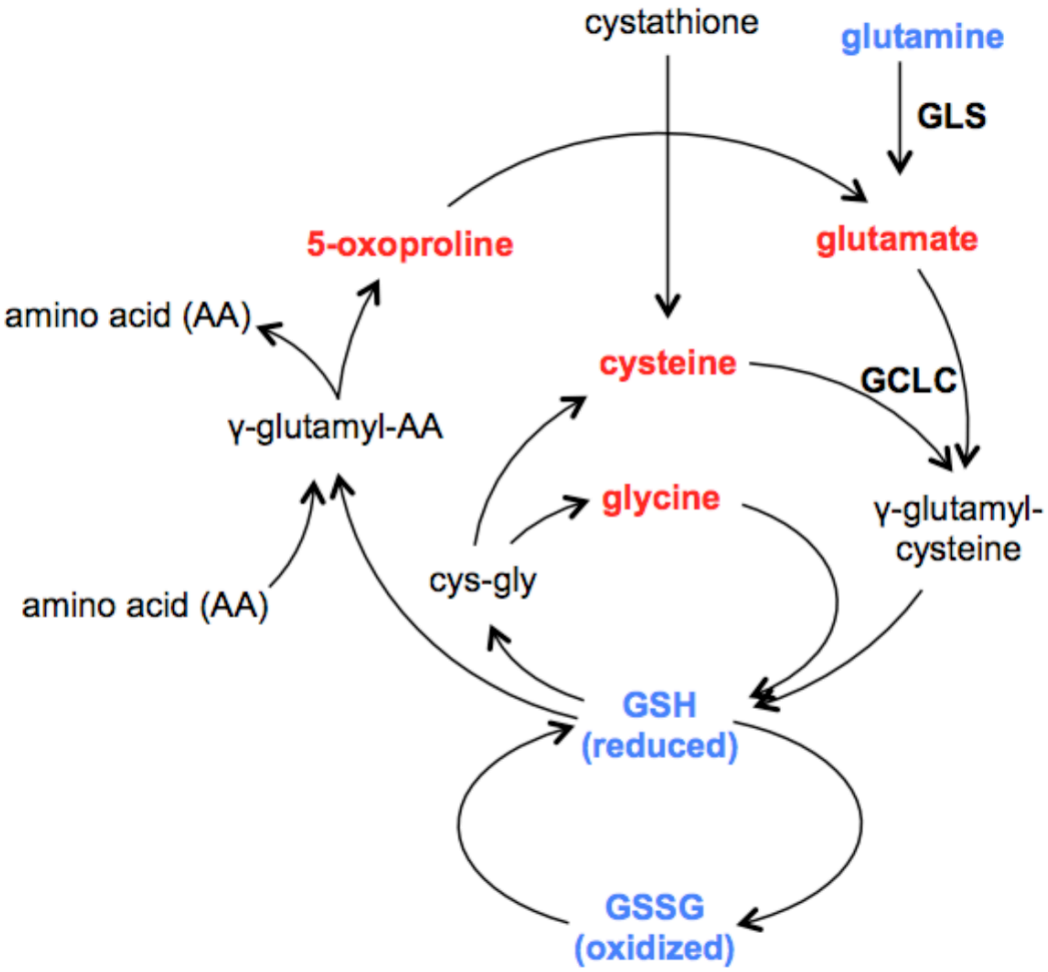

Figure 12, Multiple metabolites in the glutathione synthesis pathway are significantly altered in LT2-MYC tumors versus control livers. Red = significantly elevated; blue = significantly depleted; ($p < 0.05$).

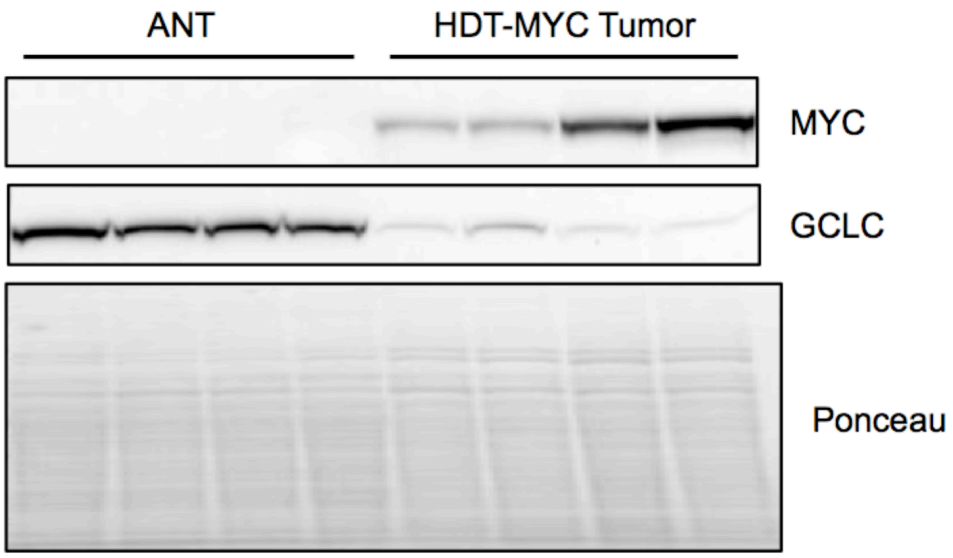

Figure 13, **MYC-driven tumors established by hydrodynamic transfection have high MYC and low GCLC protein expression.** Western Blot analysis of MYC and GCLC protein expression in MYC-driven liver tumors established by hydrodynamic transfection, as compared to adjacent non-tumor liver tissue (n=4 per group) (Tward et al., 2005).

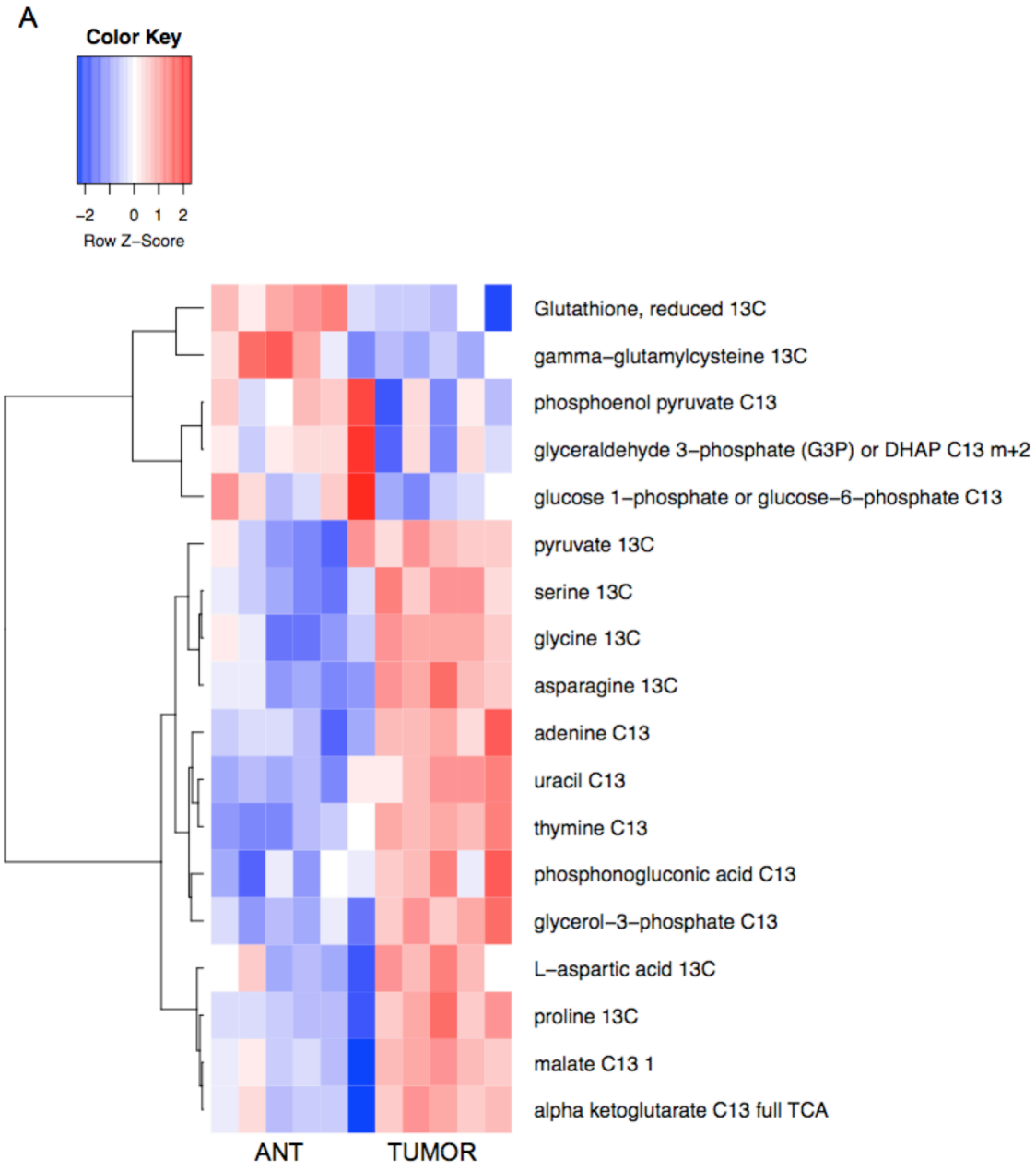
A
Color Key
−2
0
1
2
Row Z−Score
Glutathione, reduced 13C
gamma−glutamylcysteine 13C
phosphoenol pyruvate C13
glyceraldehyde 3−phosphate (G3P) or DHAP C13 m+2
glucose 1−phosphate or glucose−6−phosphate C13
pyruvate 13C
serine 13C
glycine 13C
asparagine 13C
adenine C13
uracil C13
thymine C13
phosphonogluconic acid C13
glycerol−3−phosphate C13
L−aspartic acid 13C
proline 13C
malate C13 1
alpha ketoglutarate C13 full TCA
ANT
TUMOR

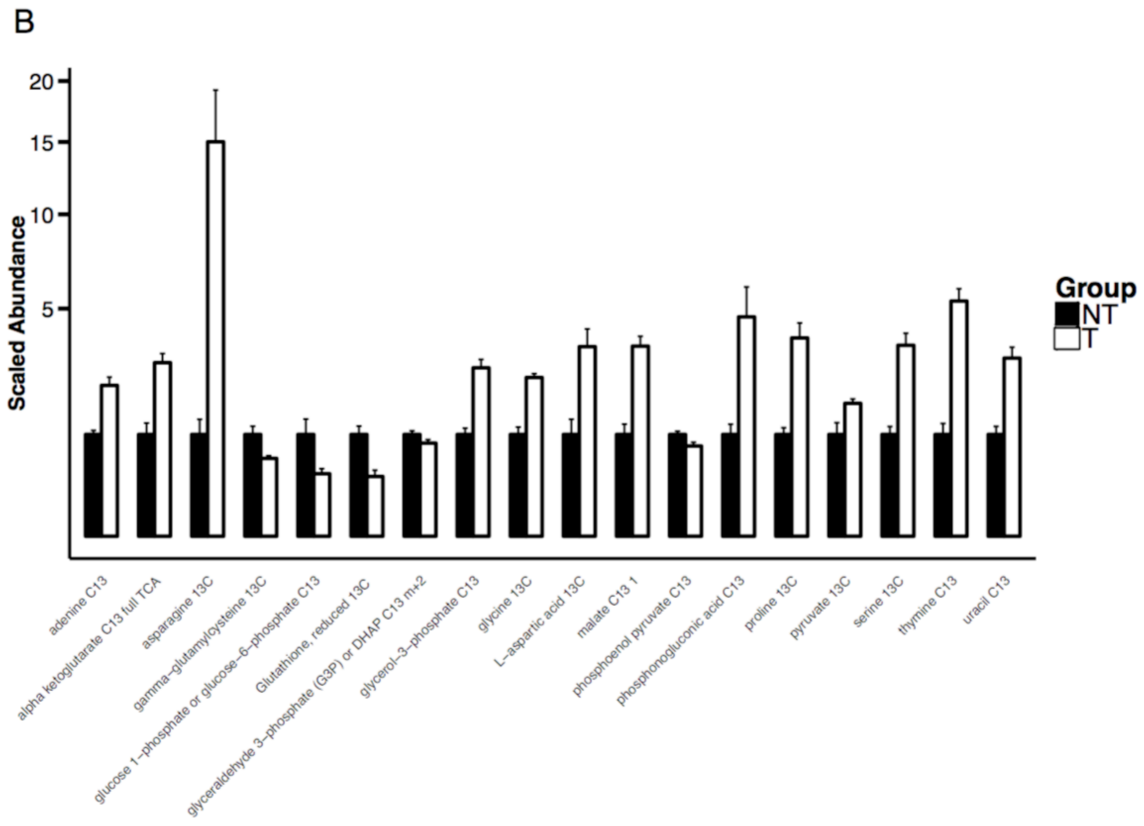

Figure 14, MYC-driven liver tumors preferentially use glutamine-derived carbons for central carbon and proliferative metabolism. A, Heatmap summarizing metabolites significantly enriched or de-enriched with U-^{13}C-glutamine-derived carbons in MYC-driven liver tumors versus adjacent non-tumor (ANT) (n=5-6; $p < 0.05$). B, Relative scaled abundances of metabolites significantly enriched or de-enriched with U-^{13}C-glutamine-derived carbons in tumor as compared to adjacent non-tumor (n=5-6; data represented as mean ± SEM; $p < 0.05$).

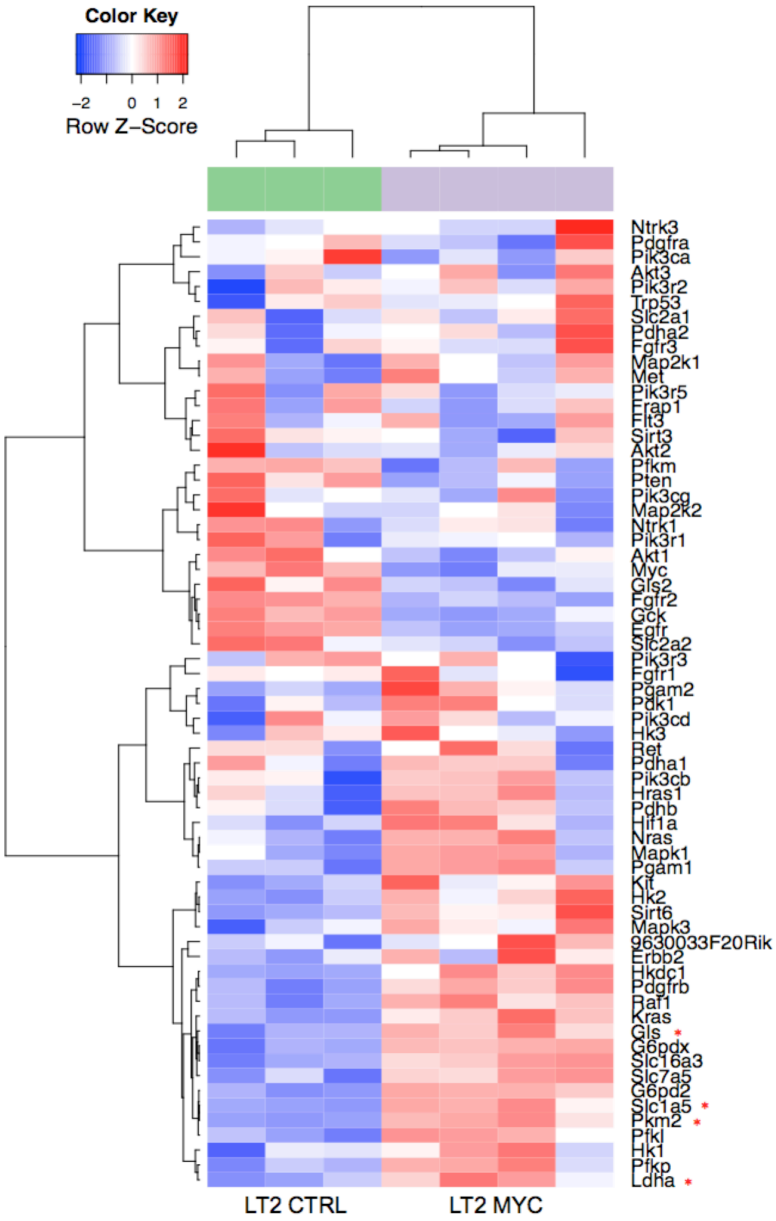

Figure 15, Expression of central carbon metabolism pathway transcripts differentiates MYC-driven liver tumor from control liver tissues. Unsupervised hierarchical clustering of KEGG-defined 'central carbon metabolism of cancer' gene expression in LT2-MYC tumors versus control liver tissue (n=3-4). Known MYC-regulated genes are marked with red asterisks.

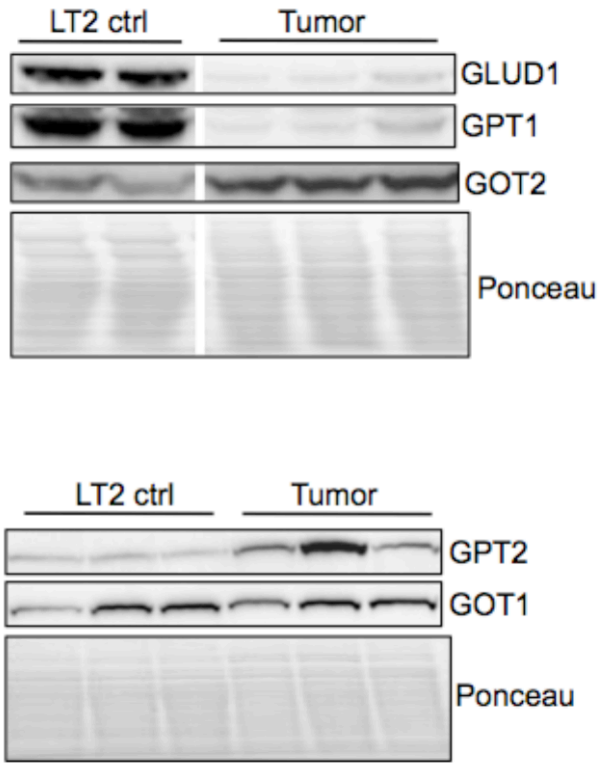

Figure 16, Transaminases exhibit tumor-specific protein expression patterns in LT2-MYC tumors. Western blot analysis of canonical transaminases in LT2-MYC tumors versus non-tumor LT2 control livers (n=2-3 each).

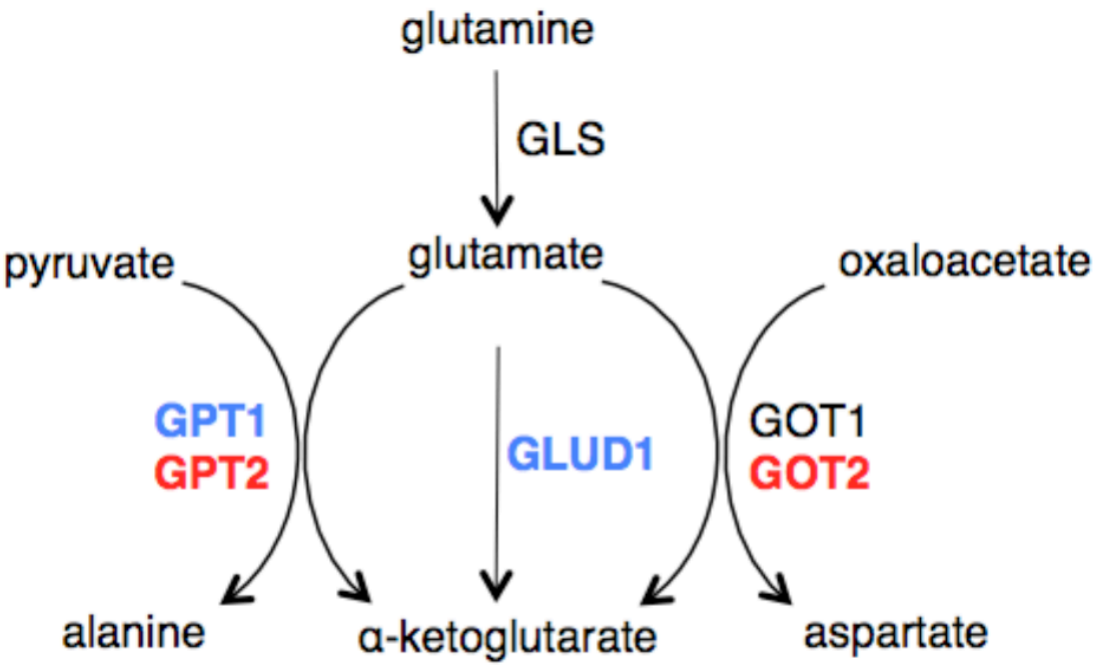

Figure 17, Schematic summary of differential expression of transaminases in MYC-driven liver tumors. Red = elevated protein expression in tumor versus control liver; blue = diminished protein expression in tumor versus control liver.

Kegg Pathway	Significantly altered mRNAs	p value	Significantly altered metabolites	p value
Glutathione metabolism	32/52 (62%)	1.05E-12	10/11 (91%)	0.0293
Glycine, serine and threonine metabolism	21/39 (54%)	2.16E-07	15/18 (83%)	0.0304
Aminoacyl-tRNA biosynthesis	20/44 (45%)	1.25E-05	18/20 (90%)	0.0029
Cysteine and methionine metabolism	17/38 (45%)	7.13E-05	11/12 (92%)	0.0186
ABC transporters	19/46 (41%)	0.0001	30/40 (75%)	0.0276
Mineral absorption	13/44 (30%)	0.0302	13/15 (87%)	0.0255

Table 1, Metabolic pathways overrepresented in mRNA and metabolite profiling of LT2-MYC tumors. Fisher's exact test ($p < 0.05$) was performed using KEGG pathway classifications on global gene expression and metabolite profiling data from LT2-MYC tumors and LT2 controls.

Chapter 3

A MYC-MIRNA AXIS REGULATES GLUTATHIONE SYNTHESIS IN MYC-DRIVEN LIVER TUMORS AND IS DEREGULATED IN HUMAN HCC

3.1 INTRODUCTION

In the previous chapter, we used an integrated approach to identify novel metabolic pathways that are altered in *de novo* MYC-driven liver tumors. We found the glutathione synthesis pathway to be dramatically downregulated in a mouse model of MYC-driven hepatocarcinogenesis. Importantly, we saw glutamine-derived carbons being used preferentially for central carbon metabolism, at the expense of glutathione synthesis, in MYC-driven liver tumors versus control liver tissues. This led us to next ask how glutathione synthesis is downregulated in MYC-driven liver tumors. Specifically, we were interested in identifying transcriptional targets of MYC that may contribute to the altered metabolic phenotype we observed.

In this chapter, we identify the mechanism by which MYC regulates glutathione synthesis. We find that the rate-limiting enzyme of glutathione synthesis, glutamate-cysteine ligase (GCLC), is indirectly regulated by MYC via MYC-dependent miR-18a. MiR-18a, part of an oncogenic miRNA cluster previously recognized to be activated by MYC, exhibits MYC-dependent expression in cultured cells and in tumor tissue, and targets the 3' UTR of GCLC in an *in vitro* assay. Further, miR-18a expression is elevated in human HCCs and inversely correlates with *GCLC* transcript. We find that in two separate cohorts of human HCC, low tumor tissue GSH abundance corresponds with an aggressive

tumor phenotype. Thus, the diminished glutathione observed in MYC-driven liver tumors appears to be clinically relevant to aggressive human HCC.

3.2 RESULTS

GCLC IS REPRESSED BY MIRNA-18A IN LT2-MYC TUMORS

In the previous chapter, we observed steady state accumulation of glutathione precursor metabolites (glycine, glutamate, and cysteine) in tumor tissues as compared to non-tumor control livers (**Figure 12**). Further, we found increased incorporation of glutamine-derived carbons into central carbon metabolites concomitant with diminished incorporation into glutathione in tumor versus adjacent non-tumor tissues (**Figure 14**). We thus reasoned that MYC-driven tumors specifically inhibit glutathione production from glutamine, leading to shunting of glutamine-derived carbons into alternative pathways. The catalytic subunit of glutamate-cysteine ligase, GCLC, is the rate-limiting enzyme of glutathione production (Sies, 1999). We therefore hypothesized that GCLC is downregulated in LT2-MYC tumors. Western blot analysis and quantitative RT-PCR (qRT-PCR) confirm that GCLC protein and mRNA (**Figure 18 A and 18 B**) are markedly diminished in LT2-MYC tumors and return to baseline after MYC is turned off in established tumors for several days (**Figure 3**). Similarly, we observed MYC-dependent changes in GCLC protein expression in a murine liver tumor cell line derived from the LT2-MYC model (Cao et al., 2011). When cells are grown in the presence of 8ng/mL doxycycline, MYC expression is rapidly inhibited (**Figure 18 C**). Using this conditional system we found that GCLC protein expression increases when MYC expression is conditionally turned off over several days (**Figure 18 C**).

MYC has been previously shown to indirectly regulate glutamine conversion to glutamate via suppression of miR-23a/b, which targets the 3' UTR of GLS (Gao et al., 2009). Since we observed MYC-dependent suppression of GCLC expression, we hypothesized that MYC may attenuate GCLC expression, at least in part, via regulation by a miRNA. Using the Targetscan database (v6.2) (Lewis et al., 2005), we identified miRNAs whose seed sequences are predicted to bind the 3' UTR of *GCLC* transcript. Interestingly, miR-18a, a known MYC-regulated miRNA that is transcribed as part of the oncogenic miR-17-92 miRNA cluster (Dews et al., 2006; He et al., 2005) had the lowest predicted Total Context Score, which correlates with high probability of targeting (**Table 2**) (Grimson et al., 2007). Additionally, of the miRNAs predicted by Targestscan to bind the 3' UTR of *GCLC*, miR-18a was one of the most highly elevated in LT2-MYC tumors as compared to non-tumor controls based on miRNA profiling (**Figure 19 A**). We confirmed that miR-18a is elevated in LT2-MYC tumors using qRT-PCR and that its expression returns to baseline when MYC expression is inhibited for 72hrs in established tumors (**Figure 19 B**). We also observed miR-18a downregulation in liver tumor cells derived from the LT2-MYC model following treatment with doxycycline to inhibit MYC expression (**Figure 19 C**). Furthermore, previous work suggests that the MYC-regulated protein HNRNPA1 (David et al., 2010) directs processing of mature miR-18a (Guil and Cáceres, 2007). Accordingly, we observe that HNRNPA1 protein is elevated in liver tumors in a MYC-dependent manner (**Figure 19 D**). Thus, both miR-18a transcription and processing may be coordinately increased in MYC-driven liver tumors. Our results confirm that miR-18a expression is elevated in a MYC-dependent manner in the LT2-MYC tumor model.

To determine whether miR-18a directly targets the *GCLC* transcript, we generated a luciferase reporter fusion containing the *GCLC* 3' UTR downstream of firefly luciferase. Reporter expression was

diminished following transfection of a miR-18a mimic in murine liver tumor cells but was unchanged when four bases of the predicted miR-18a binding site were mutated in the 3' UTR (**Figure 19 E**). We next asked whether miR-18a antagonists could regulate GCLC expression in MYC-driven tumor cells. When miR-18a is inhibited by locked-nucleic acid (LNA) antagonist in cells derived from the LT2-MYC model we observe that GCLC protein expression is increased relative to cells treated with control LNA (**Figure 19 F and 19 G**). Thus, our results demonstrate that GCLC is regulated by MYC-dependent miR-18a expression in murine liver tumor cells.

MIR-18A IS ELEVATED IN HUMAN HCC AND CORRELATES WITH ALTERED GLUTATHIONE PATHWAY GENE EXPRESSION

We next sought to determine if there is a link between miR-18a expression and altered glutathione metabolism in human liver cancers. Using a previously published dataset (Burchard et al., 2010), we confirmed that miR-18a expression is significantly elevated in human HCC (**Figure 20 A**) and inversely correlates with *GCLC* mRNA expression (**Figure 20 B**). When stratified by miR-18a expression, the top tertile of human HCC exhibits a glutathione pathway gene expression pattern that is similar to that of the MYC-driven liver tumor model (**Figure 20 C**).

MYC is associated with a variety of poorly differentiated human tumors (Ben-Porath et al., 2008). In human liver cancer, elevated tumor alpha-fetoprotein (AFP) expression is a clinical marker of poorly differentiated and aggressive disease (Yamashita et al., 2008). Accordingly, we find that MYC and AFP proteins are both expressed in MYC-driven liver tumors (**Figure 3**). We thus sought to determine if poorly differentiated human liver tumors characterized by elevated AFP expression have alterations in

glutathione abundance. Metabolite profiling of primary human HCCs has recently been reported (Budhu et al., 2013; Huang et al., 2013). Examining these datasets, we find that HCC patients with high serum AFP levels (**Figure 20 D**) or high tissue AFP expression (HpSC subtype in **Figure 20 E**) exhibit lower tumor glutathione abundance than those with low serum or tissue AFP. Additionally, tumor *AFP* transcript strongly correlates with miR-18a in human HCC (**Figure 20 F**). Taken together, our results indicate that both elevated miR-18a expression and AFP, a marker of poorly differentiated tumors, correlate with diminished glutathione production in human liver cancer.

3.3 DISCUSSION

Our integrated analysis identified the glutathione synthesis pathway as significantly deregulated in MYC-driven liver tumors. In this chapter, we found that expression of the rate-limiting enzyme of glutathione synthesis, GCLC (Wu et al., 2004), is diminished in MYC-driven liver tumors and is MYC-dependent. We have identified a novel regulatory axis whereby the MYC-induced miRNA, miR-18a (Dews et al., 2006; He et al., 2005), targets GCLC and leads to glutathione depletion (**Figure 21**). It is important to note that GCLC is also likely directly regulated. The GCLC promoter contains several potential transcriptional regulatory elements. These include an E-box, which can be targeted by MYC or NRF2, an antioxidant response transcription factor. Using cultured cells, different groups have shown opposing transcriptional effects of MYC binding to the GCLC promoter (Levy and Forman, 2010; Benassi et al., 2006). Taken together with our work, it is likely that GCLC expression is regulated by both transcriptional and miRNA-mediated regulation in a context-specific manner.

MYC regulates GLS and PKM2 via suppression of specific miRNAs (Gao et al., 2009) and regulation of RNA processing enzyme expression (David et al., 2010), respectively. Interestingly, we find that HNRNPA1, an RNA processing protein that regulates both *PKM2* (David et al., 2010) and miR-18a (Guil and Cáceres, 2007) RNAs, is upregulated in LT2-MYC tumors in a MYC-dependent manner (**Fig 19 D**). It is possible that in addition to its capacity for direct transcriptional regulation, MYC orchestrates tumor-specific metabolic aberrations through indirect, post-transcriptional means. Such multiple levels of regulation may enable MYC to fine-tune metabolic pathways to coordinate anabolic processes.

We found that miR-18a expression is elevated in human HCC and strongly correlates with altered glutathione pathway gene expression (Burchard et al., 2010). Previous work has shown that miR-18a is elevated in HCC tissues of female patients (Liu et al., 2009), and serum miR-18a levels may serve as a biomarker for HBV-related HCC (Li et al., 2012). We found that HCC patients with high serum and tissue AFP, a marker of aggressive disease, exhibit lower GSH abundance in their tumor tissues than patients with low AFP. At least two papers have previously indicated a correlation between MYC overexpression in HCC tissue and increased serum AFP (Pedica et al., 2013; Peng et al., 1993). Accordingly, we observe co-expression of MYC and AFP protein in MYC-driven liver tumors (**Figure 3**). Thus, high tumor miR-18a expression and/or high serum or tissue AFP levels may indicate tumor glutathione synthesis suppression due to MYC activation. These findings may have clinical relevance in identifying and treating aggressive tumor subsets.

3.4 FIGURES AND TABLES

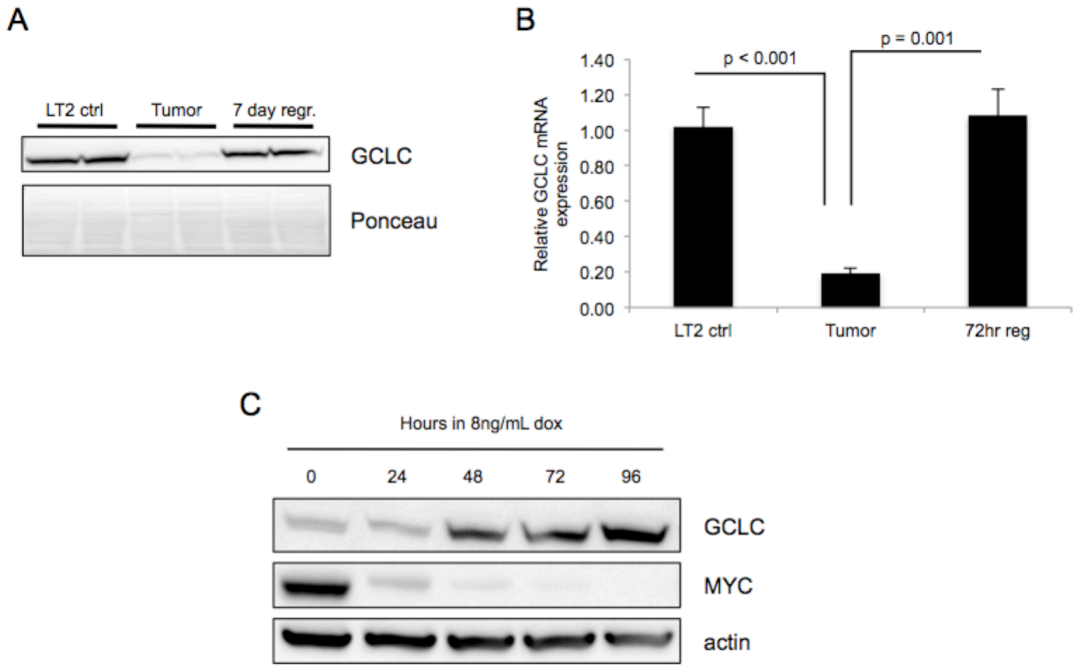

Figure 18, GCLC is downregulated in MYC-driven liver tumors and is MYC-dependent. A, Western blot analysis of GCLC in LT2-MYC tumors versus control livers and tumors regressed for 7 days (n=2 each). B, Relative expression of *GCLC* mRNA in LT2-MYC tumors, control livers, and liver tumors regressed for 72 hours (Data represented as mean ± SEM; n=4 each; p = 0.001). C, Western blot analysis of GCLC and MYC protein expression in conditional cells derived from an LT2-MYC tumor (Western Blot is a representative of a minimum of four experiments).

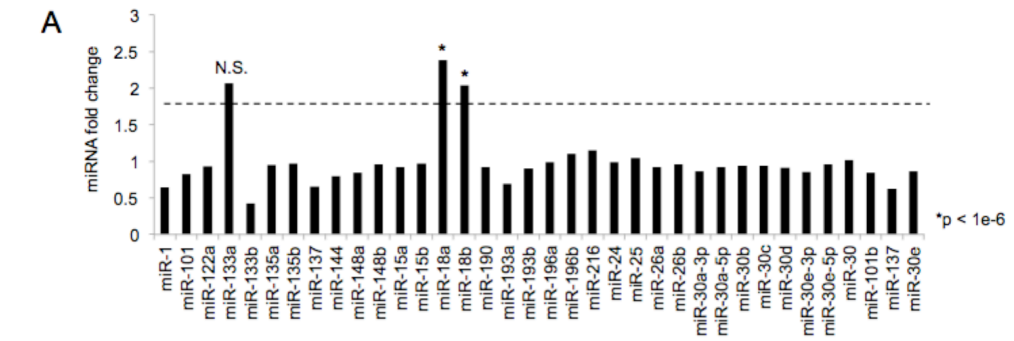
A
miRNA fold change
N.S.
*p < 1e-6
miR-1
miR-101
miR-122a
miR-133a
miR-133b
miR-135a
miR-135b
miR-137
miR-144
miR-148a
miR-148b
miR-15a
miR-15b
miR-18a
miR-18b
miR-190
miR-193a
miR-193b
miR-196a
miR-196b
miR-216
miR-24
miR-25
miR-26a
miR-26b
miR-30a-3p
miR-30a-5p
miR-30b
miR-30c
miR-30d
miR-30e-3p
miR-30e-5p
miR-30
miR-101b
miR-137
miR-30e

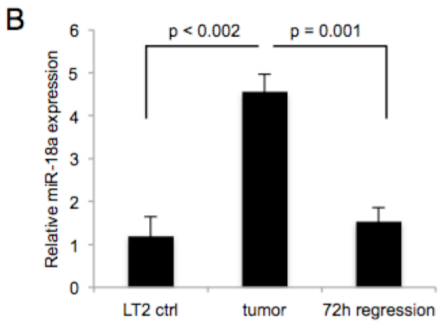
B
Relative miR-18a expression
p < 0.002
p = 0.001
LT2 ctrl
tumor
72h regression

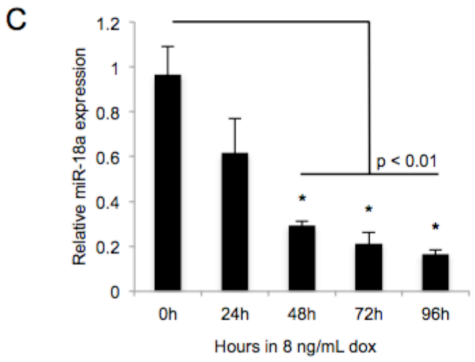
C
Relative miR-18a expression
p < 0.01
0h
24h
48h
72h
96h
Hours in 8 ng/mL dox

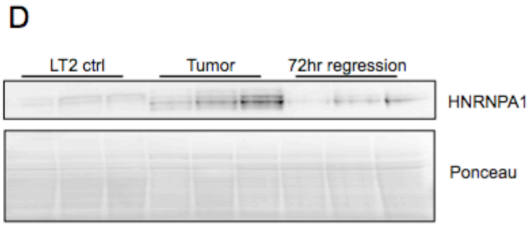
D
LT2 ctrl
Tumor
72hr regression
HNRNPA1
Ponceau

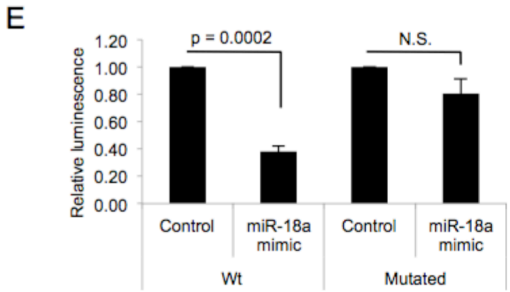
E
Relative luminescence
p = 0.0002
N.S.
Control
miR-18a mimic
Control
miR-18a mimic
Wt
Mutated

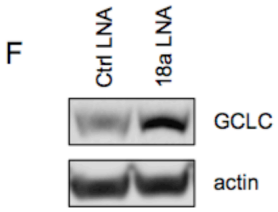
F
Ctrl LNA
18a LNA
GCLC
actin

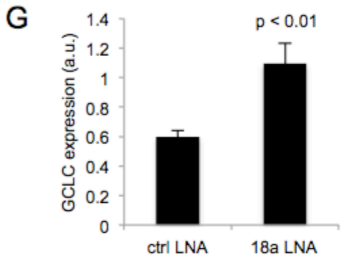
G
GCLC expression (a.u.)
p < 0.01
ctrl LNA
18a LNA

Figure 19, **miR-18a is elevated in LT2-MYC tumors and targets *GCLC* transcript.** A, Fold expression changes of miRNAs predicted to target *GCLC* by Targetscan analysis, in LT2-MYC tumors as compared to non-tumor controls (Data represented as mean ± SEM; p<1e-06). MiRNA array data previously described (Lim et al., 2014). B, qPCR analysis of miR-18a expression in LT2-MYC tumors, control liver tissues, and tumors regressed for 3 days (n=4 each; data represented as mean ± SEM; $p < 0.002$). C, qPCR analysis of miR-18a expression in cultured liver tumor cells indicates MYC-dependent expression (n=3 separate experiments; data represented as mean ± SEM; $p < 0.01$). D, Western blot analysis of HNRNPA1 in LT2-MYC tumors, control livers, and tumors regressed for 72 hours (n=3 each). E, Luciferase reporter expression in cultured liver tumor cells treated with a miR-18a mimic or control (n=3 separate experiments; data represented as mean ± SEM; $p = 0.0002$). F, Representative Western blot analysis of GCLC protein expression following treatment of cultured liver tumor cells with locked nucleic acid (LNA) inhibitors of miR-18a. G, Summary of change in GCLC protein expression following LNA treatment (n=2 separate experiments; data represented as mean ± SEM; $p < 0.01$).

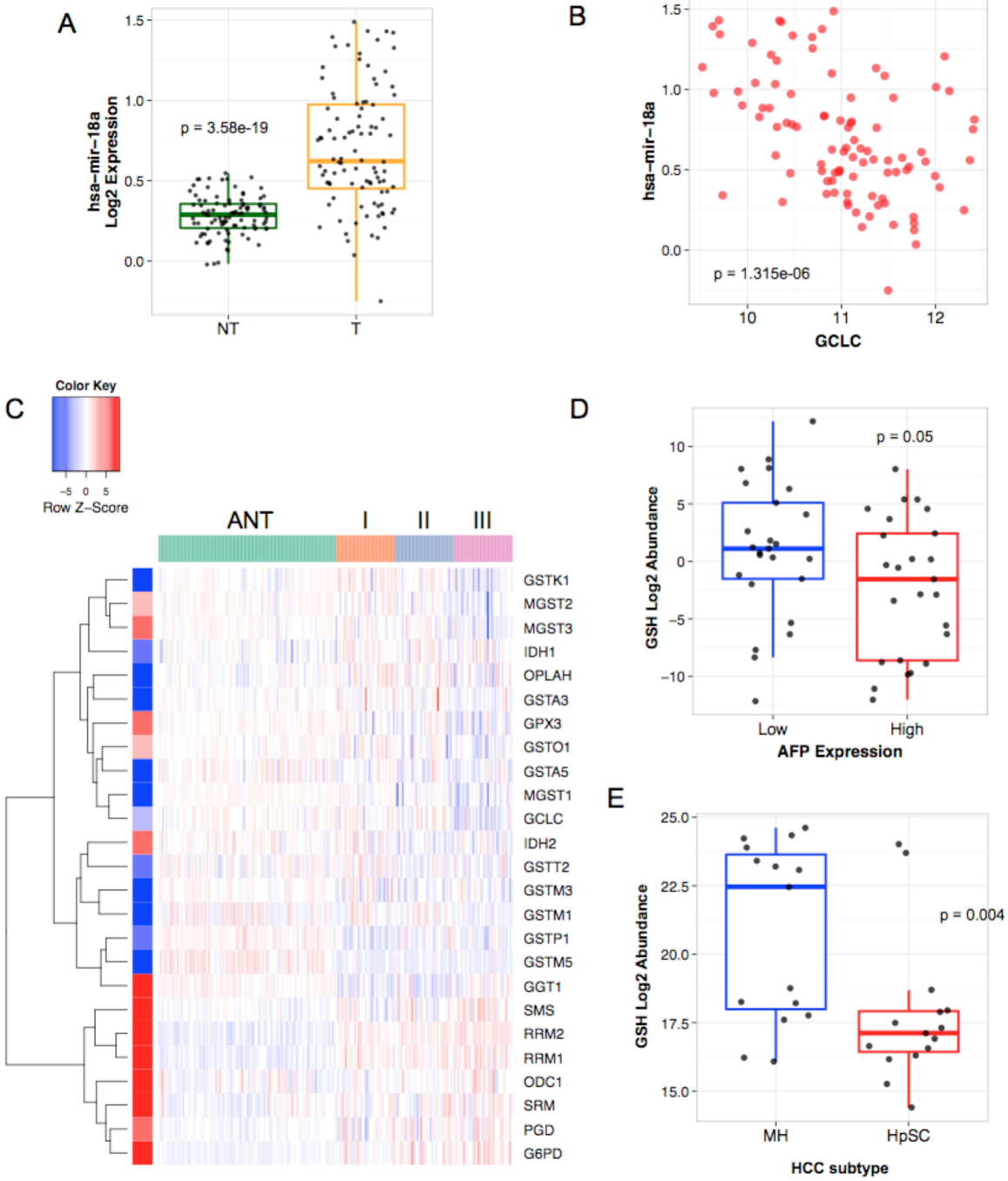
A
hsa−mir−18a Log2 Expression
p = 3.58e-19
NT
T
B
hsa−mir−18a
p = 1.315e-06
GCLC
C
Color Key
Row Z−Score
ANT
I
II
III
GSTK1
MGST2
MGST3
IDH1
OPLAH
GSTA3
GPX3
GSTO1
GSTA5
MGST1
GCLC
IDH2
GSTT2
GSTM3
GSTM1
GSTP1
GSTM5
GGT1
SMS
RRM2
RRM1
ODC1
SRM
PGD
G6PD
D
GSH Log2 Abundance
p = 0.05
Low
High
AFP Expression
E
GSH Log2 Abundance
p = 0.004
MH
HpSC
HCC subtype

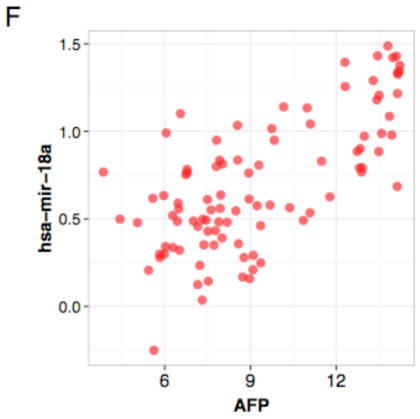

Figure 20, miR-18a is elevated in human HCC and correlates with altered glutathione pathway transcript expression. A, miR-18a expression in human HCC versus adjacent non-tumor tissue (n=96 each; p = 3.58E-19). B, *GCLC* mRNA expression inversely correlates with miR-18a expression in human HCC (n=96; Rp = -0.47; p=1.315e-06). C, Human HCCs with high miR-18a expression exhibit a glutathione pathway gene expression pattern similar to LT2-MYC tumors. ANT, adjacent non-tumor. Roman numerals represent ranked tertiles of increasing miR-18a expression. Colored bar on left indicates relative gene expression in LT2-MYC tumors versus control livers for reference. D, Tumor GSH abundance is lower in HCC patients with high serum AFP status (n = 25 per group; Mann-Whitney U test, p=0.05). E, Tumor GSH abundance is lower in hepatic stem-cell-like human HCC subtype than in mature hepatocyte-like HCC subtype (n=15 per group; Mann-Whitney U test, p=0.004). F, Pearson correlation of miR-18a and *AFP* mRNA in human HCC (n = 96; Rp=0.70; p=2.665e-15). Data previously described (Burchard et al., 2010).

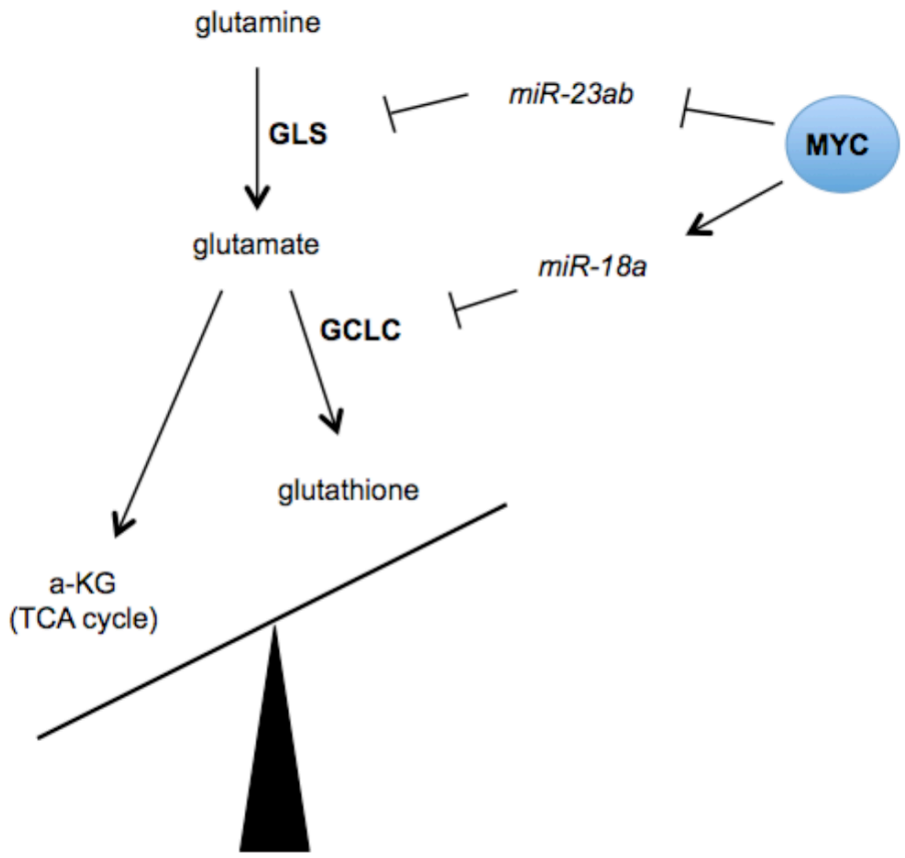

Figure 21, Summary of MYC-dependent regulation of glutamine and glutathione metabolism in MYC-driven murine liver tumors. MYC inhibits miR-23a/b, leading to elevated expression of glutaminase (GLS) and increased conversion of glutamine to glutamate (Gao et al., 2009). MYC activates miR-18a expression, which inhibits GCLC expression and leads to diminished glutathione biosynthesis. Glutamate is preferentially used in central carbon metabolism pathways such as the TCA cycle.

miRNA	conserved sites				poorly conserved sites				Total Context score
	Total	8mer	7mer-m8	7mer-1A	Total	8mer	7mer-m8	7mer-1A	
miR-18ab/4735-3p	1	1	0	0	0	0	0	0	-0.36
miR-101/101ab	1	0	0	1	1	0	1	0	-0.32
miR-190/190ab	0	0	0	0	1	0	1	0	-0.26
miR-193/193b/193a-3p	0	0	0	0	1	0	1	0	-0.25
miR-15abc/16/16abc/195/322/424/497/1907	0	0	0	0	1	0	1	0	-0.23
miR-30abcdef/30abe-5p/384-5p	1	0	1	0	0	0	0	0	-0.19
miR-216b/216b-5p	0	0	0	0	2	0	1	1	-0.18
miR-148ab-3p/152	0	0	0	0	1	0	0	1	-0.16
miR-133abc	1	0	0	1	0	0	0	0	-0.16
miR-24/24ab/24-3p	0	0	0	0	1	0	0	1	-0.15
miR-135ab/135a-5p	1	0	1	0	0	0	0	0	-0.15
miR-196abc	0	0	0	0	1	0	1	0	-0.15
miR-26ab/1297/4465	0	0	0	0	2	0	0	2	-0.13
miR-122/122a/1352	0	0	0	0	1	0	0	1	-0.13
miR-1ab/206/613	1	0	0	1	0	0	0	0	-0.12
miR-25/32/92abc/363/363-3p/367	0	0	0	0	1	0	0	1	-0.1
miR-144	1	0	0	1	0	0	0	0	-0.1
miR-137/137ab	0	0	0	0	1	0	0	1	-0.08
miR-216a	0	0	0	0	1	0	0	1	-0.04

TargetScanHuman, v6.2

Table 2, Summary of TargetScanHuman (v6.2) predictions of GCLC 3' UTR-binding miRNAs. miR-18ab exhibited the lowest Total Context Score, indicating that it had the highest predicted efficacy of GCLC 3' UTR targeting.

Chapter 4

MYC-DRIVEN LIVER TUMORS UPREGULATE COMPENSATORY ANTIOXIDANT PATHWAYS AND ARE SENSITIVE TO EXOGENOUS OXIDATIVE STRESS

4.1 INTRODUCTION

Oxidative stress in cancer cells is a hotly debated topic. It is generally agreed that elevated oxidative stress can contribute to tumorigenesis by aiding oxidative DNA damage. However, whether established tumors have elevated ROS is unknown. Some research suggests that tumors may upregulate antioxidant pathways in response to elevated oxidative stress; however, at the same time it has been suggested that tumors exhibit a more reducing environment that aids cellular biosynthesis and proliferation. Certainly, little is know about the state of antioxidant systems and redox homeostasis in tumor cells *in situ*.

Our finding in Chapter 1 that glutathione, a major cellular antioxidant, is depleted in MYC-driven liver tumors was very intriguing. We hypothesized that these tumors subsequently exhibited elevated oxidative stress due to a lack of antioxidant capacity. We thus set out to determine if the MYC-driven liver tumors had signs of an activated oxidative stress response. Our findings highlight the metabolic flexibility that tumor cells can possess.

4.2 RESULTS

Glutathione is a major cellular antioxidant (Sies, 1999). Because we observed that total glutathione is markedly depleted in MYC-driven liver tumors (**Figure 5 & Figure 11**), we sought to determine whether these tumors subsequently exhibit markers of elevated oxidative stress. We first asked whether transcriptional targets of the canonical ROS response gene NRF2 (Gorrini et al., 2013a) are elevated in MYC-driven liver tumors compared to naïve non-tumor tissue. Surprisingly, we found that the expression of most NRF2-regulated transcripts was lower in LT2-MYC tissues than in non-tumor control tissues (**Figure 22**). Of the four transcripts that are elevated in tumors versus controls, three are involved in the regeneration of the canonical antioxidants NADPH (*G6pdx*, *Pgd*) and GSH (*Gsr*), while *Txn1* encodes the thioredoxin antioxidant protein (Gorrini et al., 2013a).

Because three of four NRF2 response genes elevated in MYC-driven tumors are specific to antioxidant regeneration, we asked whether there might be a wholesale upregulation of such genes in tumors in order to compensate for loss of the total glutathione pool. We find that the majority of transcripts of 11 genes involved in regeneration of the major antioxidant systems NADPH, GSH, and Vitamin C/ascorbate are markedly elevated in LT2-MYC tumors relative to non-tumor controls. In addition, thioredoxins (either Txn1 or Txn2) are upregulated in a mutually exclusive manner in LT2-MYC tumors relative to non-tumor controls (**Figure 23**). We confirmed elevated protein expression of several of these genes, including GSR, G6PD, PKM2 and PGD in tumor versus control tissues (**Figure 24**).

Given the marked depletion of glutathione and simultaneous up-regulation of antioxidant regeneration enzymes, we sought to determine if net oxidative stress was altered in primary tumors. We examined isoprostane abundance, a clinical marker of tissue oxidative stress that specifically detects lipid peroxidation (Han et al., 2008), between tumor and adjacent non-tumor tissues. We observed no significant difference in the levels of isoprostanes (compare saline treated in **Figure 25**), indicating that despite markedly depleted total glutathione, MYC-driven tumors do not have increased baseline oxidative stress. Taken together, these data suggest that MYC-driven liver tumors upregulate antioxidant regeneration programs to compensate for their depleted glutathione pool.

Although MYC-driven liver tumors do not have elevated ROS at baseline (**Figure 25**), we sought to determine whether they have an impaired response to exogenous oxidative stress because of their markedly diminished glutathione pool. We treated tumor-bearing LT2-MYC mice with a potent ROS inducer, diquat, which can be reduced to an autoxidisable free radical *in vivo* and causes damaging redox cycling in affected tissues (Fussell et al., 2011; Han et al., 2008), and collected tissues 24 hours post treatment. Interestingly, we find that isoprostanes are elevated similarly in tumor and adjacent non-tumor tissues following diquat treatment (**Figure 25**), suggesting comparable antioxidant capacity in the tissues. Despite similar ROS burden in the two tissues following diquat treatment, we observed tumor-specific depletion of the remaining glutathione pool (**Figure 26**) and upregulation of genes related to necrosis, steatosis, and oxidative stress and antioxidant response (**Figure 27**). Diquat treatment of tumor-bearing LT2-MYC mice increased the percent of steatosis (fat) in tumors from 6.8% to 31.1% ($p = 0.01$), without significantly changing the amount of steatosis in adjacent non-tumor liver tissue (**Figure 28**). Steatosis, or lipid droplet accumulation, has been linked to generalized hepatic stress previously (Lee et al., 2013). Similarly, diquat-treated LT2-MYC mice showed an increase

in TUNEL staining in tumors (18.8% TUNEL-positive cells) compared to saline-treated tumors (13.9% TUNEL-positive cells) ($p = 0.003$) that was not observed in adjacent non-tumor tissue in response to diquat treatment (**Figure 29**). In summary, our data suggest that although MYC-driven liver tumors compensate for the loss of glutathione by upregulating antioxidant regeneration systems, they exhibit elevated sensitivity to exogenous oxidative stress.

4.3 DISCUSSION

In Chapter 2, we determined that the cellular antioxidant glutathione is depleted in a mouse model of MYC-driven liver tumors. Since glutathione is a major scavenger of ROS, we hypothesized that MYC-driven liver tumors exhibit elevated baseline ROS and are more sensitive to exogenous oxidative stress than corresponding non-tumor liver tissue. In this chapter, we find that MYC-driven liver tumors compensate for loss of glutathione by upregulating multiple alternative antioxidant regeneration pathways. Others have shown that tumor cells are able to survive loss of certain antioxidants by upregulating compensatory antioxidant systems such as thioredoxin (Arnér and Holmgren, 2006) or NRF2 (Shibata et al., 2008; Singh et al., 2010). However, despite sufficient antioxidant capacity at baseline, we show that MYC-driven liver tumors exhibit elevated sensitivity to exogenous ROS, as indicated by tumor-specific elevation of stress markers, steatosis, and a cell death marker following diquat treatment. Thus, although tumor cells may be able to compensate for loss of antioxidant systems at baseline, they may still exhibit sensitivity to exogenous oxidative stress. The therapeutic potential of modulating oxidative stress in tumors is an area of active investigation. Accordingly, many preclinical and approved anticancer treatments modulate ROS directly or indirectly (Gorrini et al., 2013a). The utility of these or other compounds for targeting MYC-driven

cancers remains to be determined.

4.4 FIGURES AND TABLES

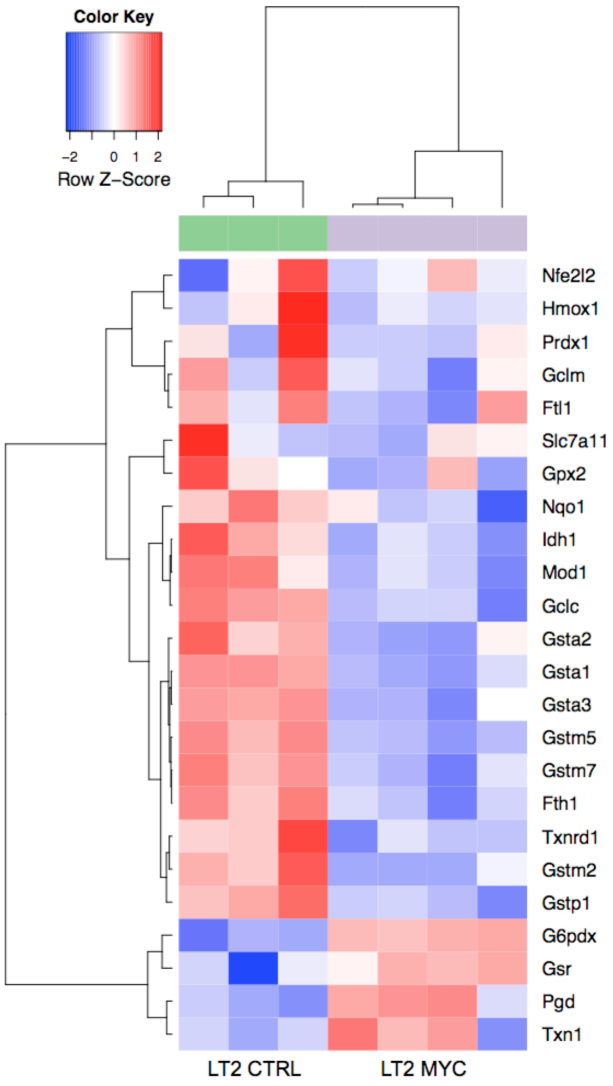

Figure 22, Most NRF2 targets are not transcriptionally upregulated in LT2-MYC tumors.

Heatmap depicting unsupervised hierarchical clustering of NRF2 target gene expression in LT2-MYC tumor tissues as compared to LT2 control tissues (n=3-4 each).

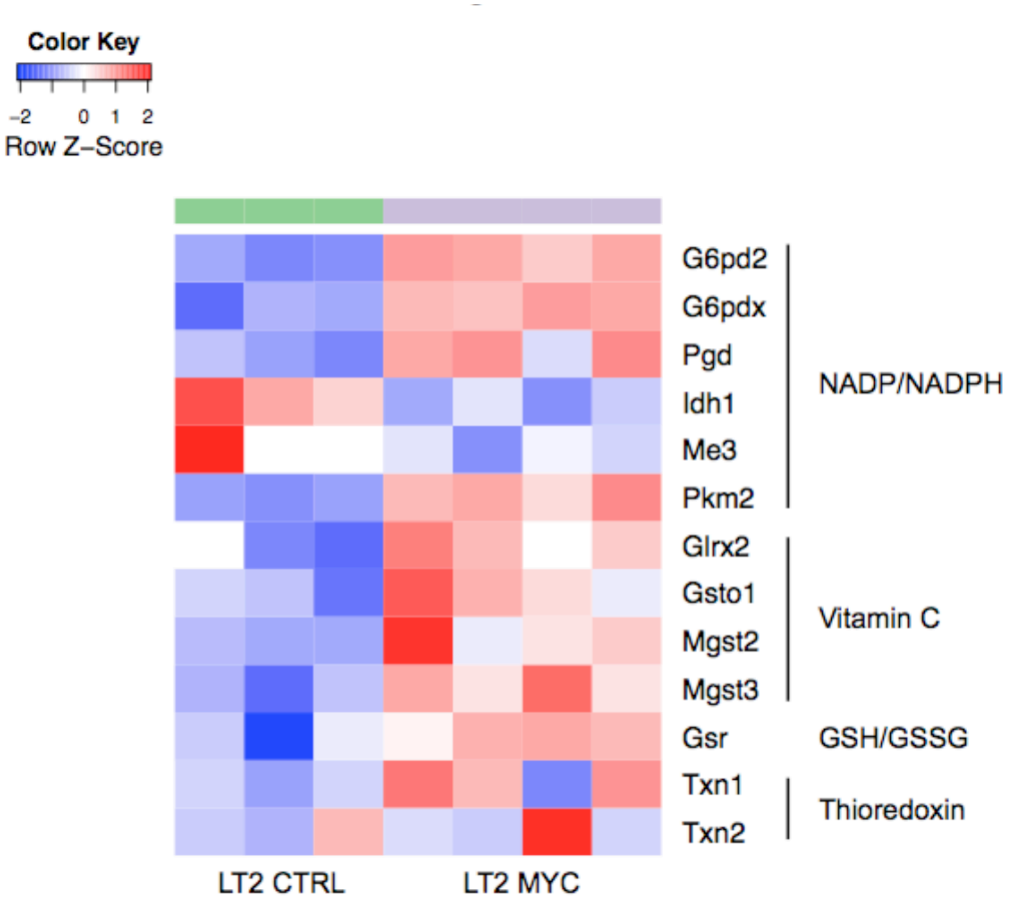

Figure 23, Antioxidant regeneration systems are upregulated transcriptionally in LT2-MYC tumors. Heatmap depicting mRNA expression of genes involved in antioxidant regeneration in LT2-MYC tumor tissues as compared to LT2 control tissues (n=3-4 each).

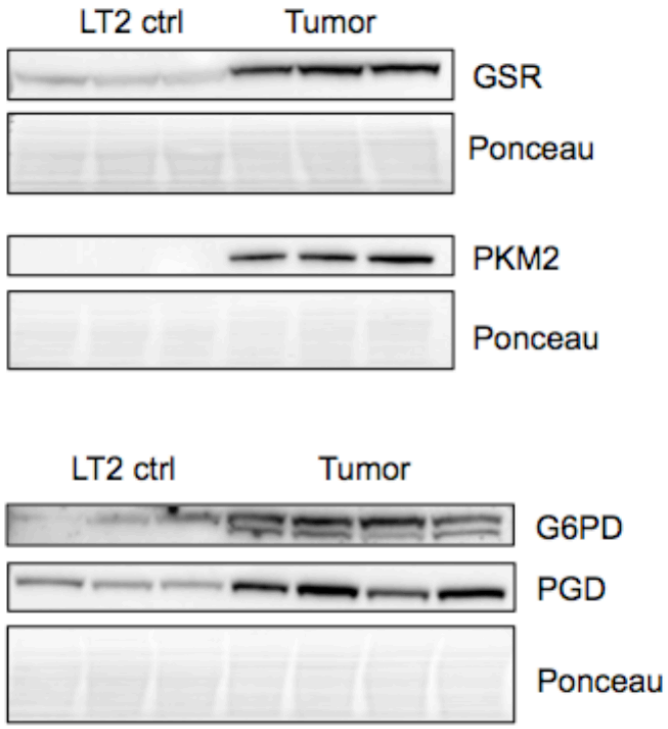

Figure 24, **Several antioxidant-regenerating proteins are elevated in MYC-driven liver tumors**. Western blot analysis of GSR, PKM2, G6PD, and PGD in LT2 control versus LT2-MYC tumor tissues (n=3-4 each).

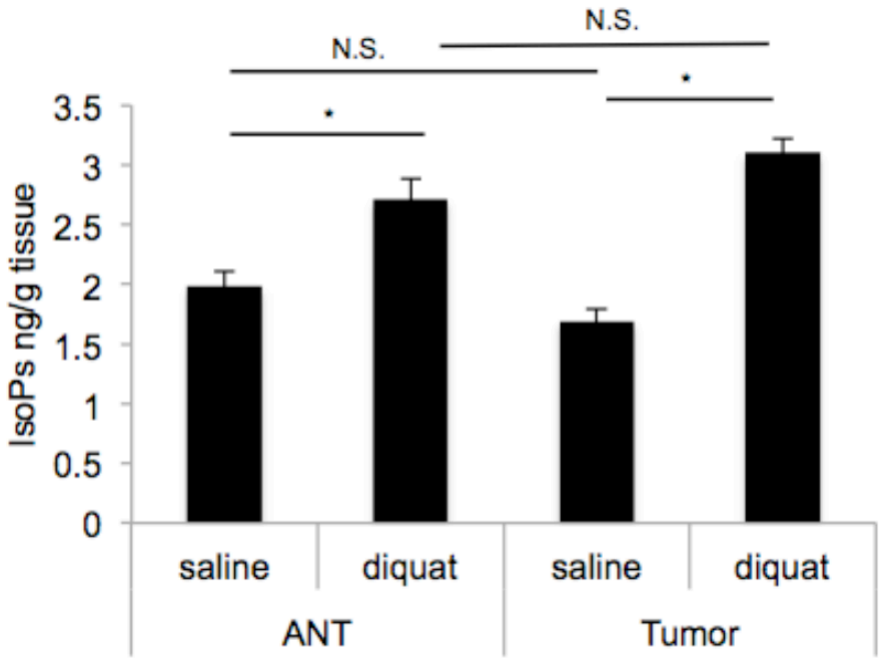

Figure 25, Tissue ROS assessed by lipid peroxidation analysis in MYC-driven liver tumors. Isoprostane levels (ng/g tissue) in adjacent non-tumor (ANT) or tumor tissues treated with saline or 50 mg/kg diquat, 24h (n=4-5/group; data represented as mean ± SEM; $p < 0.01$).

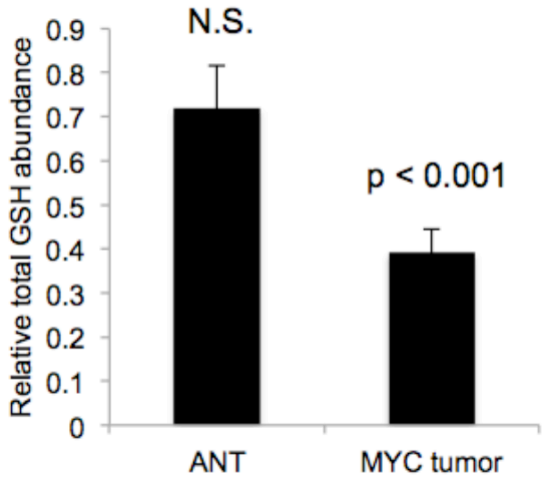

Figure 26, Glutathione is depleted in MYC-driven liver tumors following diquat treatment. Total glutathione abundance (nMol/mg tissue) relative to respective saline-treated tissue in tumor and adjacent NT tissues treated with 50mg/kg diquat, 24h (n=4 or 7 each; data represented as mean ± SEM; $p < 0.001$).

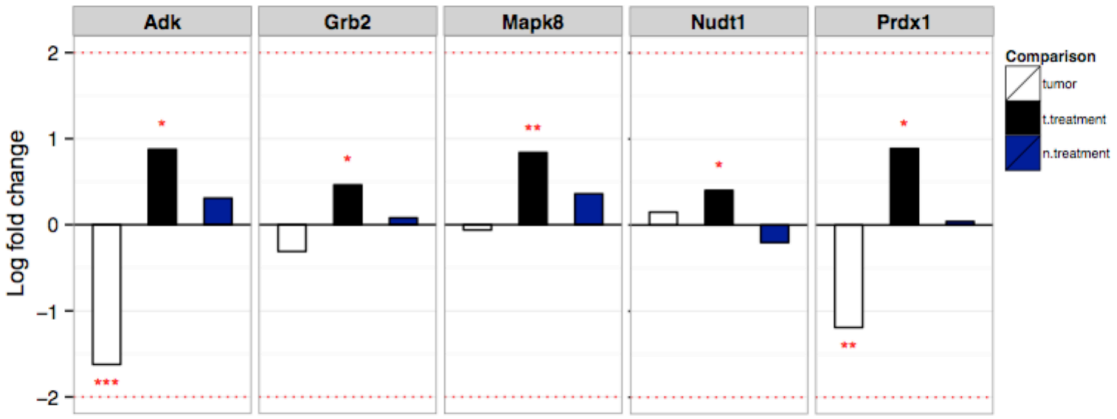

Figure 27, **Tumor-specific activation of hepatotoxicity response genes following diquat treatment**. mRNA expression log fold change of genes related to hepatotoxicity (specifically steatosis, necrosis, oxidative stress and antioxidant response) in tumor and adjacent non-tumor in response to 50mg/kg diquat, 24h (n=4/group; $p < 0.05$).

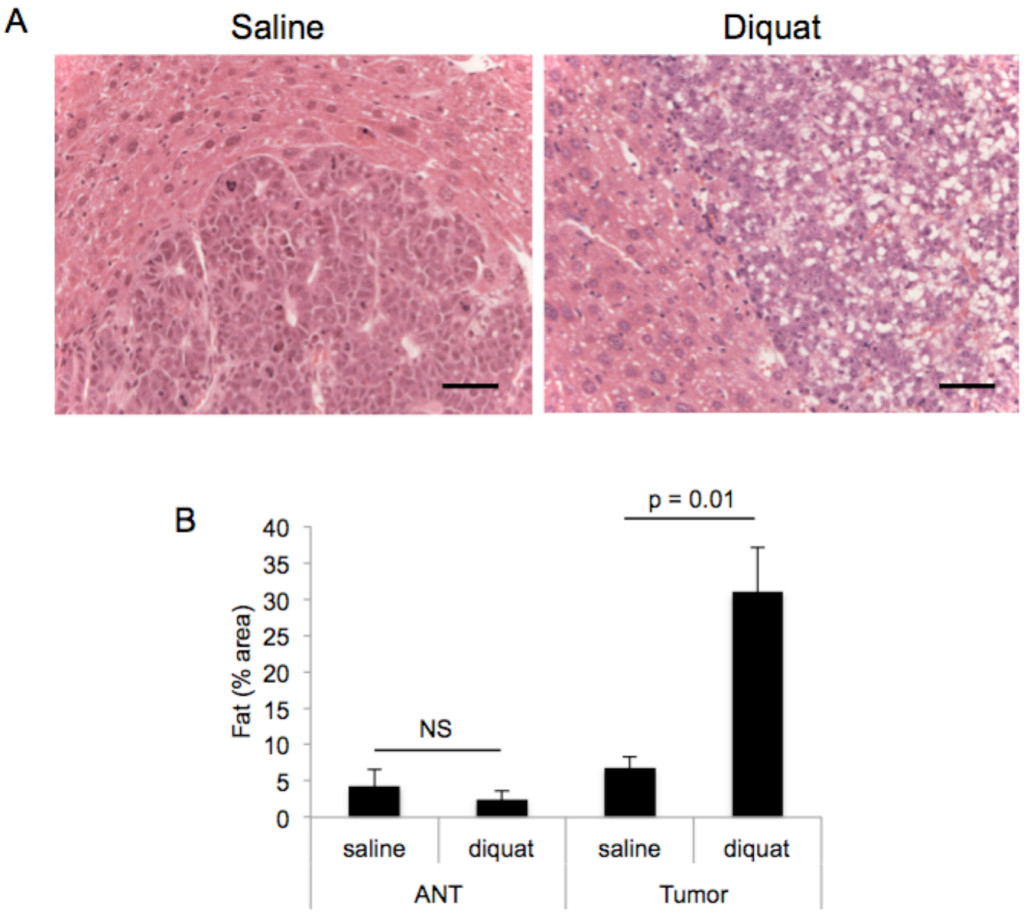

Figure 28, **Tumor-specific fat accumulation observed following diquat treatment**. A, Representative histology of H&E sections from LT2-MYC tumor-bearing mice treated with saline or 50 mg/kg diquat, 24h. Scale is 50um. B, Percent area of fat accumulation in adjacent non-tumor and tumor tissue treated with saline or 50 mg/kg diquat, 24h (adjacent NT n=4, p=n.s.; tumor n=7, p=0.03; t test; data represented as mean ± SEM).

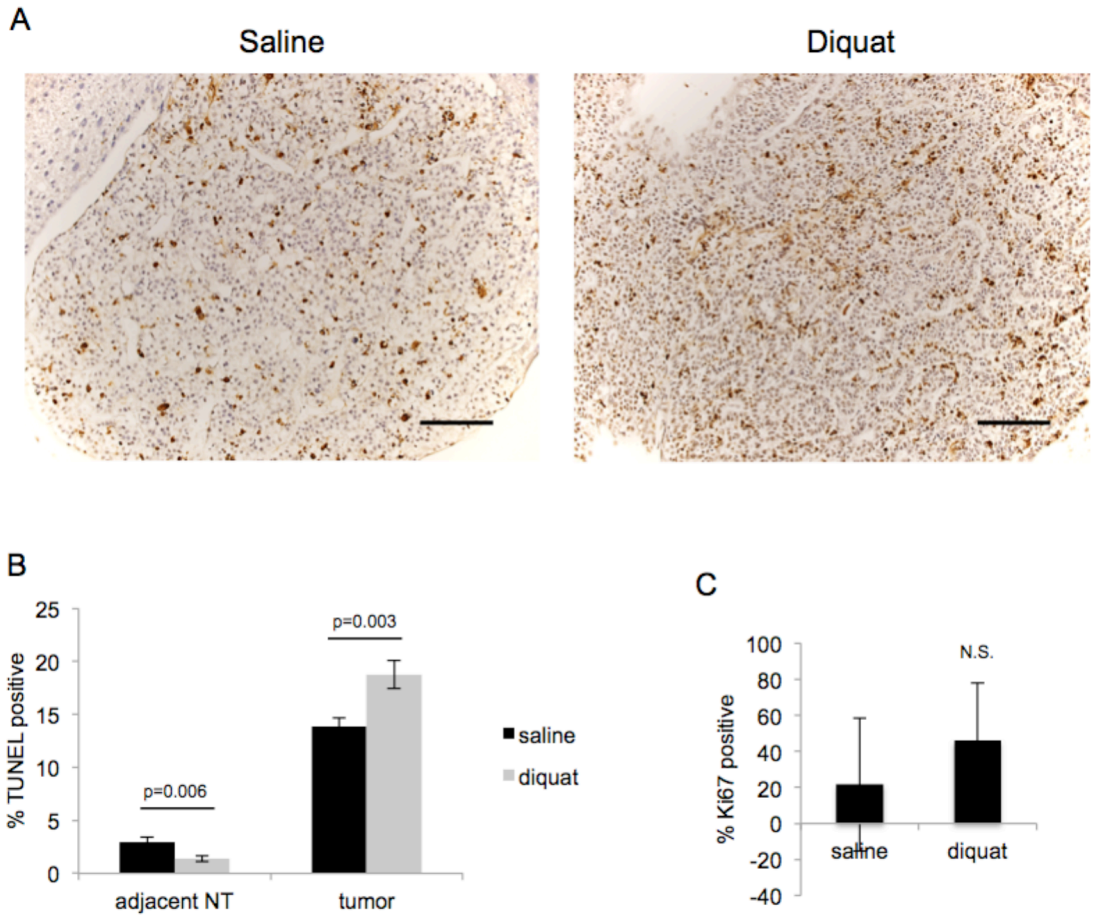

Figure 29, **Cell death is elevated and proliferation is unchanged in MYC-driven tumors treated with diquat**. A, Representative histology of TUNEL (cell death marker) staining of tumor sections from LT2-MYC tumor-bearing mice treated with saline or 50 mg/kg diquat, 24h. Scale bar is 100um. B, Percent total TUNEL-positive cells detected by immunohistochemistry in tumor and ANT treated with saline or 50 mg/kg diquat, 24h (n=3-5 mice per condition, 10 fields/mouse; data represented as mean ± SEM; $p < 0.01$). C, Percent total Ki67-positive (proliferation marker) cells detected by immunohistochemistry in tumor treated with saline or 50 mg/kg diquat, 24h (n=2 saline; n=6 diquat; data represented as mean ± SEM; N.S.).

CONCLUSIONS AND FUTURE DIRECTIONS

Altered metabolism is a bona fide hallmark of cancer. However, the importance of many metabolic pathways to cancer cell survival and their regulation by oncogenes remains largely unknown. In Chapter 2 of this work, we used an unbiased, integrated approach to elucidate novel metabolic pathways deregulated by the transcription factor proto-oncogene MYC *in vivo*. We identified six metabolic pathways that are significantly altered at both the metabolite and transcript level in MYC-driven liver cancer. At least two of these pathways, serine metabolism and ABC transporters, have been described in connection with MYC signaling previously (Nikiforov et al., 2002; Porro et al., 2011), while to our knowledge the remaining pathways have yet to be associated with MYC activation in primary tumors. The most striking pathway alteration we identified in our integrated approach is suppressed glutathione biosynthesis. We show that both the reduced and oxidized forms of glutathione (GSH and GSSG, respectively) are depleted and glutamine-derived carbons are preferentially shunted away from glutathione synthesis and toward central carbon metabolism in MYC-driven liver tumors as compared to non-tumor liver tissue.

In Chapter 3, we found that expression of the rate-limiting enzyme of glutathione synthesis, GCLC (Wu et al., 2004), is diminished in MYC-driven liver tumors and is MYC-dependent. We identified a novel regulatory axis whereby the MYC-induced miRNA, miR-18a (Dews et al., 2006; He et al., 2005), targets GCLC and leads to glutathione depletion (**Figure 21**). We found that miR-18a expression is elevated and strongly correlates with altered glutathione pathway gene expression in human HCC (Burchard et al., 2010). We found that HCC patients with high serum and tissue AFP, a marker of

aggressive, poorly differentiated disease, exhibit lower GSH abundance in their tumor tissues than patients with low AFP. Accordingly, we observe concomitant expression of MYC and AFP protein in MYC-driven murine liver tumors (**Figure 3**). Thus, high tumor miR-18a expression and/or high serum or tumor AFP levels may indicate tumor glutathione synthesis suppression due to MYC activation in human HCC.

Glutathione is a major cellular antioxidant. Thus, in Chapter 4, we tested the hypothesis that MYC-driven liver tumors with depleted glutathione have higher tissue ROS at baseline and are more sensitive to exogenous oxidative stress. We find that MYC-driven liver tumors do not exhibit activation of a canonical antioxidant response pathway at baseline and in fact upregulate multiple alternative antioxidant regeneration pathways. Further, MYC-driven liver tumors do not exhibit elevated tissue ROS at baseline. However, despite sufficient antioxidant capacity, MYC-driven liver tumors exhibit elevated sensitivity to exogenous ROS, as indicated by tumor-specific lipid droplet accumulation and elevation of a cell death marker following treatment with a potent oxidative stress inducer. Thus, although MYC-driven liver tumors compensate for loss of glutathione, they are still sensitive to exogenous oxidative stress.

In conclusion, this work provides a novel example of metabolic reprogramming by MYC. We show that MYC regulates glutamate utilization by attenuating glutathione production via miR-18a, leading to preferential shunting of glutamine-derived carbons toward proliferative metabolism in tumors. Further, we show a vulnerability of MYC-driven tumors to exogenous oxidative stress. Moving forward, it will be important to explore whether inhibition of miR-18a or modulation of oxidative

stress present viable therapeutic strategies for MYC-driven cancers. Certainly, manipulating miRNAs *in vivo* has been shown to attenuate MYC-driven liver tumor growth in previous studies (Kota et al., 2009; Lim et al., 2014). Thus, it is likely that inhibition of miR-18a during tumor growth or maintenance may reverse or diminish the metabolic phenotype described in this thesis (**Figure 21**) and may inhibit tumor cell survival or proliferation. The clinical applications of miRNA agonists or inhibitors are being actively explored (Jackstadt and Hermeking, 2015). Additionally, the manipulation of tissue redox state has been proposed as a therapeutic strategy for tumors (Gorrini et al., 2013a). Several oxidative stress-inducing compounds are in preclinical trials; thus, it will be interesting to explore the utility of these compounds in the context of MYC-driven cancers as well.

Finally, the relevance of the five additional metabolic pathways identified in our integrated analysis (glycine, serine, and threonine metabolism; aminoacyl-tRNA biosynthesis; cysteine and methionine metabolism; ABC transporters; mineral absorption) to MYC-driven tumor growth and maintenance are worthwhile to explore further. Understanding the biological significance and regulation of these pathways will not only provide a greater understanding of MYC's role in metabolic reprogramming, it may also reveal novel therapeutic targets. In summary, investigating MYC's role as a master regulator of tumor cell metabolism will likely reveal promising targets that can be exploited therapeutically in the future.

MATERIALS AND METHODS

Ethics Statement

All animal work was approved by the institutional animal research committee (University of California, San Francisco IACUC). Animals were handled in accordance with good animal practices as defined by national and local animal welfare bodies.

LT2-MYC tumor generation

Tet-o-MYC/LAP-tTA (LT2-MYC) double-transgenic mice have been described (Shachaf et al., 2004). Mice were maintained on doxycycline (200 mg/kg doxy chow) to suppress oncogene expression until at least 8 weeks of age. Doxycycline was then removed to allow induction of transgene expression and tumor formation. Mice were monitored weekly for tumor development by inspection and palpating the abdomen. Mice were sacrificed as per ethical guidelines. Average time to tumor detection was 8-10 weeks.

mRNA Microarray

Total RNA from four samples per genotype (LT2 Control, LT2/MYC) was extracted as per manufacturer's instructions (mirVana^{TM} mirna isolation kit, Ambion). RNA quality was assessed using a Pico Chip on an Agilent 2100 Bioanalyzer (Agilent Technologies). Four samples per genotype were

selected for Agilent stock mouse 44K (014868) array analysis. Sample preparation, labeling, and array hybridizations were performed according to standard protocols from UCSF Shared Microarray Core Facilities and Agilent Technologies (http://www.arrays.ucsf.edu; http://www.agilent.com). RNA was amplified and labeled with Cy3-CTP using the Agilent low RNA input fluorescent linear amplification kits following the manufacturers protocol (Agilent). Labeled cRNA was assessed using Nandrop ND-100 (Nanodrop Technologies, Inc.). Cy3 labeled target was hybridized to Agilent whole mouse genome 4x44K Ink-jet arrays (Agilent). Hybridization samples were randomized on the 4 x 44K format to correct any batch bias. Hybridizations were performed for 14 hrs, according to the manufacturers protocol (Agilent). Arrays were scanned using the Agilent microarray scanner (Agilent) and raw signal intensities were extracted with Feature Extraction v9.5 software (Agilent). Primary normalization and data extraction were performed by the Microarray Core Facility. Briefly, single channel data were normalized using quantile normalization method. No background subtraction was performed, and the median feature pixel intensity was used as the raw signal before normalization.

Metabolomics

Mass spectrometry analysis was performed to obtain global biochemical profiles of control liver tissue and LT2-MYC liver tumor tissue (Metabolon, Inc., Durham, NC). Flash frozen tissue samples from seven mice were provided for each group. Samples were extracted and prepared for analysis using Metabolon's standard solvent extraction method. The extracted samples were split into equal parts for analysis on the GC/MS and LC/MS/MS platforms. Technical replicate samples were created from sample homogenates. The mView product specification includes all detectable compounds of known identity (named biochemicals). The present dataset from Metabolon comprises a total of 334 named

biochemicals. Initial statistical analysis was carried out by Metabolon. Briefly, following log transformation and imputation with minimum observed values for each compound, Welch's two-sample t-test was used to identify biochemicals that differed significantly between control liver tissue and tumor tissue.

For U-^{13}C-glutamine flux analyses, the labeled metabolite (Cambridge Isotope Labs) was administered as described previously (Yuneva et al., 2012) to MYC tumor-bearing mice established through hydrodynamic transfection (**Supplemental Figure 2A**) (Tward et al., 2005). Fifteen minutes after the final dose, the mice were sacrificed and liver tumor and adjacent non-tumor tissues were collected, flash frozen and analyzed using a slight modification of previously described procedures (Benjamin et al., 2014). Briefly, 100mg of frozen tissue were extracted in 300 ml of 40:40:20 acetonitrile:methanol:water with 1 nM final concentration of d_3-N^{15} serine (Cambridge Isotope Labs). Manual disruption of tissue was performed via TissueLyser using a 5 mm stainless steel bead for 30 s (Qiagen). Metabolite-containing supernatant was separated from insoluble tissue debris by refrigerated centrifugation at 15,000 rpm for 10min. An aliquot of the supernatant was then injected into an Agilent 6460 QQQ LC-MS/MS for targeted single-reaction monitoring (SRM)-based quantitation of metabolites. For separation of polar metabolites a Luna 5mm NH_2 column (Phenomenex, 50mm x 4.6mm) was used for normal-phase chromatography. The mobile phase was as follows: Buffer A, acetonitrile; Buffer B, 95:5 water/acetonitrile with either 0.1% formic acid or 0.2% ammonium hydroxide plus 50 mM ammonium acetate for positive and negative ionization mode, respectively. The flow rate for each run started at 0.2 mL/min for 5min, followed by a gradient starting at 0% B and increasing linearly to 100% B over the course of 45 min with a flow rate of 0.7 mL/min, followed by an isocratic gradient of 100% B for 17 min at 0.7 mL/min before equilibrating for 8 min at 0% B with

a flow rate of 0.7 mL/min. MS analysis was performed with an electrospray ionization (ESI) source on an Agilent 6430 QQQ LC−MS/MS. The capillary voltage was set to 3.0 kV, and the fragmentor voltage was set to 100 V. The drying gas temperature was 350 °C, the drying gas flow rate was 10 L/min, and the nebulizer pressure was 35 psi. Representative metabolites were quantified by integrating the area under the curve for the SRM of the transition from precursor to product ions at associated collision energies and normalized to internal standards and external standard curves. Expected expressions of MYC and GCLC were confirmed in samples taken from the same tumors (Supplemental Figure 2B).

Microarray and metabolomics statistical analyses

Method for processing raw data into normalized expression values: Differential gene expression and metabolite abundance between LT2-MYC tumors and LT2 control tissue was performed using the *Limma* R package (Smyth, 2005). Genes or metabolites that were significantly different between these groups at a false discovery rate of 0.05 were extracted for downstream analyses. Pathway enrichment within this set of genes or metabolites was quantified using the Fisher's Exact Test based on annotations from the Kyoto Encyclopedia of Genes and Genomes (KEGG) (Tanabe and Kanehisa, 2012). Significantly enriched pathways were identified at a p-value cutoff of 0.05.

Human orthologs of dys-regulated glutathione pathway genes in mice were identified using homology group definitions compiled and published by the Mouse Genome Database Group (Blake et al., 2014).

Heatmaps and clustering analyses were performed using the *gplots* and *cluster* R packages respectively.

Raw metabolite abundance values were obtained for the tumor samples from Huang *et al* (Huang et al., 2013). Missing values were imputed with the minimum abundance across all samples for the respective metabolites. The resulting metabolite levels were then normalized to those from matched distal non-tumor samples from the same patients, and log-transformed. The tumor samples were dichotomized based on AFP expression using a cut-point at the 50th percentile mark and statistical significance of the differences in metabolite abundance between the groups was determined using a Mann-Whitney U test.

Glutathione assay

The GSH-Glo Glutathione Assay kit (Promega) was used as per the manufacturer's instructions. Briefly, flash frozen tissue samples were homogenized in ice-cold PBS containing 2mM EDTA (1mL PBS/EDTA per 10mg tissue) using a Dounce homogenizer. The extracts were centrifuged at 4C (10,000 RPM, 10mins) and the supernatant was collected and used immediately for the assay at a dilution of 1:10 in PBS/EDTA. Luminescence was read on a Tecan Safire II plate reader.

Protein preparation and Western blot analysis

Cultured cells or flash-frozen tissues were homogenized in ice-cold radioimmunoprecipitation assay (RIPA) buffer (50 mM Tris, 150 mM NaCl, 0.5% sodium-deoxycholate, 1% NP-40, 0.1% SDS, 2 mM EDTA [pH 7.5]) containing COMPLETE protease inhibitor cocktail (Roche) and phosphatase inhibitors (Santa Cruz Biotechnology). Protein concentrations were determined by performing DC

Protein Assay (Bio-Rad) using BSA as standard. Samples were run in 4-12% Bis-Tris SDS-PAGE gels (Invitrogen) in a Bolt apparatus with 1x MOPS buffer (Invitrogen). Blotting was performed on an iBlot apparatus (Invitrogen). Antibodies were purchased and used as indicated by the manufacturer (MYC, Abcam; GCLC, Santa Cruz; GLUD1, Abcam; GPT1, Santa Cruz; GOT2, Proteintech; GOT1, Sigma; GPT2, Sigma; AFP, Thermo Scientific; GSR, Thermo Scientific; PKM2, Cell Signaling; G6PD, GeneTex; PGD, Sigma)

Murine liver tumor cell lines

The LT2M cell line was isolated and established from an LT2-MYC mouse liver tumor by Dr. Andrei Goga. After establishing this line, it was grown and expanded further in RPMI 1640 media supplemented with 10% fetal bovine serum. To make the immortalized LT2MR cell line used in the luciferase experiments, LT2M cells were engineered to stably express RAS by retroviral infection with pMSCV-HRAS V12 virus. The EC4 conditional line was a gift of D. Felsher. Similar lines were described previously (Cao et al., 2011). EC4 cells were grown in high glucose DMEM supplemented with 10% fetal bovine serum and 1X each of glutamine, non-essential amino acids, and sodium pyruvate.

Real-time Quantitative PCR

Total RNA from liver samples or cultured cells was extracted using mirVana^{TM} mirna isolation kit (Ambion) and DNAse treated with Turbo DNA-free Dnase Treatment kit (Ambion) as per manufacturer's protocol. cDNA was synthesized from one microgram of DNAse-treated total RNA

using iScript™ cDNA synthesis Kit (Bio-rad). Real-time PCR was performed using TaqMan probes (Applied Biosystems) for *Gclc* (Mm00802655_m1) and *mir-18a* (Mm04238185_s1); *Gapdh* (Mm99999915_g1) and *sno*RNA*202* (Cat #4427975) genes served as endogenous controls, respectively. Samples were run in triplicate on a Real-Time Thermal Cycler (Bio-Rad Laboratories), and variation was calculated using the ΔΔCT method with respective endogenous controls. Significance of differences in gene expression was determined by performing a students ttest on the replicate 2^(- Delta Ct) values for each gene in control and experimental groups and p values less than 0.05 were considered significant.

For *Adk*, *Grb2*, *Mapk8*, *Nudt1*, and *Prdx1*, we used a 384-well real time PCR-based array (RT2 Profiler PCR Array Mouse Molecular Toxicology PathwayFinder 384HT (SAB, PAMM-3401Z)), according to manufacturer's directions. cDNA was prepared from 400ng of total RNA using RT2 First Strand Kit (SAB) and arrays were run a Roche LightCycler 480II. RT2 Profiler PCR Array data was analyzed in ***R*** (version 3.1.0) (R Core Team, 2014) using the ***HTqPCR*** package (Dvinge and Bertone, 2009). Raw Ct values of 0 or those greater than 40 were first adjusted to 40, based on SABioscience's recommendations. Subsequent normalization was performed using the *delta-Ct* method. Specifically, the arithmetic mean of the Ct values of the house-keeping genes within each sample were subtracted from all raw values within the corresponding sample. Differential expression analyses between the Diquat- and saline- treated tumor and adjacent non-tumor samples were performed using the *Limma* (Smyth, 2005) wrapper within the package. p-values were adjusted for multiple testing using the Benjamini-Hochberg method for false discovery rate (Benjamini and Hochberg, 1995). Log fold change, or the negative ddCt (delta-delta- Ct), of the genes of interest for the respective comparisons were illustrated using the ***ggplot2*** package (Wickham, 2009).

Luciferase assays

A 467 bp fragment of the GCLC 3'UTR containing the putative miR-18a binding site was PCR amplified from genomic DNA of LT2MR cells. The following primers were used to amplify the GCLC 3' UTR fragment: GCLC3'UTR-Short_For: caccGGCATTCCAGAGTTTCAAATGT and GCLC3'UTR-Short_Rev: CAGCCTGTCAATCTGCTCCT. To make the mutated binding site construct, four bases of the putative miR-18a binding site on GCLC 3' UTR were mutated using site-directed mutagenesis, as per manufacturer's instructions (QuikChange Lightning Site-Directed Mutagenesis Kit, Agilent). The following primers were designed: Forward: TGCCCTCCGTGGGTGAGGT**T**A**G**C**AG**ACCTGTGATATTTC. Reverse: GAAATATCACAGGTCTGCTACCTCACCCACGGAGGGCA. (The miR-18a seed sequence is underlined and the mutated bases are in a bold font). The PCR products (GCLC 3'UTR WT and mutant) were then cloned by Topo cloning into pMSCV-Luciferase reporter vectors.

LT2MR cells were plated in each well of a 12-well plate (75,000 cells/well). Co-transfection of the pMSCV-Luciferase reporter vector containing the GCLC 3' UTR (WT or mutant) (1ug/well), a Renilla-Luciferase (Renilla-Luc) reporter construct (100ng/well) and either mir-18a mimic (50nM) or control mimic (50nM) was carried out. Dharmafect Duo (Dharmacon) was used as a transfection reagent. The Dual luciferase reporter assay system (Promega) was used as per product instructions. 250ul of Passive Lysis buffer (Promega) was added to each well of the 12-well plate, 48h post transfection. The plate was covered with aluminium foil and placed in -20 C overnight. Luciferase assays were performed on a luminometer. Firefly luciferase activity was normalized to Renilla relative luminescence units (RLUs) for each sample.

Locked-nucleic acid (LNA) experiments

LT2M cells were plated in each well of a 6-well dish, 75,000 cells/well. Cells were transfected with 50nM of either control or 18a LNA (Exiqon) using RNAiMax transfection reagent (Invitrogen) as per manufacturer's instruction. Cells were trypsinized and pelleted 48hrs post-transfection. Pellets were lysed and protein extracts made for subsequent Western Blot analysis.

Analysis of tissue isoprostanes

Tissue lipid peroxidation was measured by assessing F2-isoprostanes as described previously (Han et al., 2008). Briefly, flash-frozen mouse liver samples (~150 mg) were homogenized, and whole lipid was extracted with chloroform-heptane. The levels of F2-isoprostanes from liver (esterified) were determined with gas chromatography-mass spectrometry (GC-MS). F2-isoprostane measurement and analysis was performed by Wenbo Qi in the laboratory of Holly Van Remmen at the University of Texas Health Science Center at San Antonio as a core service.

Histological analyses of murine liver tumor samples

Mouse livers were fixed in 4% paraformaldehyde in PBS at 4°C for 24 hours, then switched to 70% ethanol. Paraffin-embedded blocks and hematoxylin-and-eosin-stained slides were prepared at the Gladstone Histology and Light Microscopy Core Facility. TUNEL assay was performed using the ApopTag Peroxidase In Situ Apoptosis Detection Kit (EMD Millipore/Calbiochem) following the manufacturer's protocol. Immunohistochemistry for Ki-67 was performed using pre-diluted Ki-67

antibody (Thermo Scientific; Catalog Number RM-9106-R7) following xylene deparaffinization, rehydration, heat-induced epitope retrieval with 10mM sodium citrate buffer (0.05% Tween, pH 6.0), quenching of endogenous peroxidase activity by hydrogen peroxide incubation, and blocking in 5% normal goat serum in PBS. Goat anti-rabbit IgG-Biotin secondary antibody was used (Santa Cruz; Catalog Number sc-2040). Samples were detected with VECTASTAIN Elite ABC Reagent (Vector Labs) and Vector DAB substrate kit (Vector Labs) and counterstained with hematoxylin. To quantify tissue fat abundance and cell proliferation, slides were blinded and a pathologist (K.J.E.) assessed the approximate total tissue area containing fat droplets or counted the number of Ki-67-positive cells in 10-30 high-power fields for each mouse, respectively. To quantify cell death, slides were blinded and B.N.A. counted the number of TUNEL-positive cells in 10 high-power fields for each mouse, respectively.

REFERENCES

Abe, W., Nasu, K., Nakada, C., Kawano, Y., Moriyama, M., and Narahara, H. (2013). miR-196b targets c-myc and Bcl-2 expression, inhibits proliferation and induces apoptosis in endometriotic stromal cells. Hum. Reprod. *28*, 750–761.

Alexander, A., Cai, S.-L., Kim, J., Nanez, A., Sahin, M., MacLean, K.H., Inoki, K., Guan, K.-L., Shen, J., Person, M.D., et al. (2010). ATM signals to TSC2 in the cytoplasm to regulate mTORC1 in response to ROS. Proc. Natl. Acad. Sci. U. S. A. *107*, 4153–4158.

Ambros, V. (1989). A hierarchy of regulatory genes controls a larva-to-adult developmental switch in C. elegans. Cell *57*, 49–57.

Amelio, I., Cutruzzolá, F., Antonov, A., Agostini, M., and Melino, G. (2014). Serine and glycine metabolism in cancer. Trends Biochem. Sci. *39*, 191–198.

Anastasiou, D., Poulogiannis, G., Asara, J.M., Boxer, M.B., Jiang, J., Shen, M., Bellinger, G., Sasaki, A.T., Locasale, J.W., Auld, D.S., et al. (2011). Inhibition of Pyruvate Kinase M2 by Reactive Oxygen Species Contributes to Antioxidant Responses. Science (80-.). *334*, 1278–1283.

Arabi, A., Wu, S., Ridderstråle, K., Bierhoff, H., Shiue, C., Fatyol, K., Fahlén, S., Hydbring, P., Söderberg, O., Grummt, I., et al. (2005). c-Myc associates with ribosomal DNA and activates RNA polymerase I transcription. Nat. Cell Biol. *7*, 303–310.

Arnér, E.S.J., and Holmgren, A. (2006). The thioredoxin system in cancer. Semin. Cancer Biol. *16*, 420–426.

Arrate, M.P., Vincent, T., Odvody, J., Kar, R., Jones, S.N., and Eischen, C.M. (2010). MicroRNA biogenesis is required for Myc-induced b-cell lymphoma development and survival. Cancer Res. *70*, 6083–6092.

Bae, I., Fan, S., Meng, Q., Jeong, K.R., Hee, J.K., Hyo, J.K., Xu, J., Goldberg, I.D., Jaiswal, A.K., and Rosen, E.M. (2004). BRCA1 induces antioxidant gene expression and resistance to oxidative stress. Cancer Res. *64*, 7893–7909.

Balsano, C., Avantaggiati, M.L., Natoli, G., De Marzio, E., Will, H., Perricaudet, M., and Levrero, M. (1991). Full-length and truncated versions of the hepatitis B virus (HBV) X protein (pX) transactivate the cmyc protooncogene at the transcriptional level. Biochem. Biophys. Res. Commun. *176*, 985–992.

Bartel, D.P. (2004). MicroRNAs: Genomics, Biogenesis, Mechanism, and Function. Cell *116*, 281–297.

Barzilai, A., Rotman, G., and Shiloh, Y. (2002). ATM deficiency and oxidative stress: A new dimension of defective response to DNA damage. DNA Repair (Amst). *1*, 3–25.

Behm-Ansmant, I., Rehwinkel, J., Doerks, T., Stark, A., Bork, P., and Izaurralde, E. (2006). mRNA degradation by miRNAs and GW182 requires both CCR4:NOT deadenylase and DCP1:DCP2 decapping complexes. Genes Dev. *20*, 1885–1898.

Ben-Porath, I., Thomson, M.W., Carey, V.J., Ge, R., Bell, G.W., Regev, A., and Weinberg, R.A. (2008). An embryonic stem cell-like gene expression signature in poorly differentiated aggressive human tumors. Nat. Genet. *40*, 499–507.

Benassi, B., Fanciulli, M., Fiorentino, F., Porrello, A., Chiorino, G., Loda, M., Zupi, G., and Biroccio, A. (2006). c-Myc phosphorylation is required for cellular response to oxidative stress. Mol. Cell *21*, 509–519.

De Benedetti, A., and Graff, J.R. (2004). eIF-4E expression and its role in malignancies and metastases. Oncogene *23*, 3189–3199.

Benjamin, D.I., Louie, S.M., Mulvihill, M.M., Kohnz, R.A., Li, D.S., Chan, L.G., Sorrentino, A., Bandyopadhyay, S., Cozzo, A., Ohiri, A., et al. (2014). Inositol phosphate recycling regulates glycolytic and lipid metabolism that drives cancer aggressiveness. ACS Chem. Biol. *9*, 1340–1350.

Benjamini, Y., and Hochberg, Y. (1995). Controlling the False Discovery Rate: A Practical and Powerful Approach to Multiple Testing. J. R. Stat. Soc. Ser. B *57*, 289–300.

Blake, J.A., Bult, C.J., Eppig, J.T., Kadin, J.A., and Richardson, J.E. (2014). The Mouse Genome Database: Integration of and access to knowledge about the laboratory mouse. Nucleic Acids Res. *42*.

Budhu, A., Roessler, S., Zhao, X., Yu, Z., Forgues, M., Ji, J., Karoly, E., Qin, L.X., Ye, Q.H., Jia, H.L., et al. (2013). Integrated metabolite and gene expression profiles identify lipid biomarkers associated with progression of hepatocellular carcinoma and patient outcomes. Gastroenterology *144*.

Bui, T. V., and Mendell, J.T. (2010). Myc: Maestro of MicroRNAs. Genes Cancer *1*, 568–575.

Burchard, J., Zhang, C., Liu, A.M., Poon, R.T.P., Lee, N.P.Y., Wong, K.-F., Sham, P.C., Lam, B.Y., Ferguson, M.D., Tokiwa, G., et al. (2010). microRNA-122 as a regulator of mitochondrial metabolic gene network in hepatocellular carcinoma. Mol. Syst. Biol. *6*, 402.

Cai, X., Hagedorn, C.H., and Cullen, B.R. (2004). Human microRNAs are processed from capped, polyadenylated transcripts that can also function as mRNAs. RNA *10*, 1957–1966.

Cao, Z., Fan-Minogue, H., Bellovin, D.I., Yevtodiyenko, A., Arzeno, J., Yang, Q., Gambhir, S.S., and Felsher, D.W. (2011). MYC phosphorylation, activation, and tumorigenic potential in hepatocellular carcinoma are regulated by HMG-CoA reductase. Cancer Res. *71*, 2286–2297.

Cascoń, A., and Robledo, M. (2012). MAX and MYC: A heritable breakup. Cancer Res. *72*, 3119–3124.

Challagundla, K.B., Sun, X.-X., Zhang, X., Devine, T., Zhang, Q., Sears, R.C., and Dai, M.-S. (2011). Ribosomal Protein L11 Recruits miR-24/miRISC To Repress c-Myc Expression in Response to Ribosomal Stress. Mol. Cell. Biol. *31*, 4007–4021.

Chan, K.L., Guan, X.Y., and Ng, I.O.L. (2004). High-throughput tissue microarray analysis of c-myc activation in chronic liver diseases and hepatocellular carcinoma. Hum. Pathol. *35*, 1324–1331.

Chandriani, S., Frengen, E., Cowling, V.H., Pendergrass, S.A., Perou, C.M., Whitfield, M.L., and Cole, M.D. (2009). A core MYC gene expression signature is prominent in basal-like breast cancer but only partially overlaps the core serum response. PLoS One *4*.

Chang, T.-C., Yu, D., Lee, Y.-S., Wentzel, E.A., Arking, D.E., West, K.M., Dang, C. V, Thomas-Tikhonenko, A., and Mendell, J.T. (2008). Widespread microRNA repression by Myc contributes to tumorigenesis. Nat. Genet. *40*, 43–50.

Chang, T.-C., Zeitels, L.R., Hwang, H.-W., Chivukula, R.R., Wentzel, E.A., Dews, M., Jung, J., Gao, P., Dang, C. V, Beer, M.A., et al. (2009). Lin-28B transactivation is necessary for Myc-mediated let-7 repression and proliferation. Proc. Natl. Acad. Sci. U. S. A. *106*, 3384–3389.

Chang, T.C., Wentzel, E.A., Kent, O.A., Ramachandran, K., Mullendore, M., Lee, K.H., Feldmann, G., Yamakuchi, M., Ferlito, M., Lowenstein, C.J., et al. (2007). Transactivation of miR-34a by p53 Broadly Influences Gene Expression and Promotes Apoptosis. Mol. Cell *26*, 745–752.

Christoffersen, N.R., Shalgi, R., Frankel, L.B., Leucci, E., Lees, M., Klausen, M., Pilpel, Y., Nielsen, F.C., Oren, M., and Lund, A.H. (2010). p53-independent upregulation of miR-34a during oncogene-induced senescence represses MYC. Cell Death Differ. *17*, 236–245.

Cimmino, A., Calin, G.A., Fabbri, M., Iorio, M. V, Ferracin, M., Shimizu, M., Wojcik, S.E., Aqeilan, R.I., Zupo, S., Dono, M., et al. (2005). miR-15 and miR-16 induce apoptosis by targeting BCL2. Proc. Natl. Acad. Sci. U. S. A. *102*, 13944–13949.

Clapham, D.E. (2007). Calcium Signaling. Cell *131*, 1047–1058.

Clements, C.M., McNally, R.S., Conti, B.J., Mak, T.W., and Ting, J.P.-Y. (2006). DJ-1, a cancer- and Parkinson's disease-associated protein, stabilizes the antioxidant transcriptional master regulator Nrf2. Proc. Natl. Acad. Sci. U. S. A. *103*, 15091–15096.

Conacci-Sorrell, M., McFerrin, L., and Eisenman, R.N. (2014). An overview of MYC and its interactome. Cold Spring Harb. Perspect. Med. *4*.

Conklin, K.A. (2004). Chemotherapy-associated oxidative stress: impact on chemotherapeutic effectiveness. Integr. Cancer Ther. *3*, 294–300.

Conkrite, K., Sundby, M., Mukai, S., Michael Thomson, J., Mu, D., Hammond, S.M., and MacPherson, D. (2011). Mir-17~92 cooperates with RB pathway mutations to promote retinoblastoma. Genes Dev. *25*, 1734–1745.

Dang, C. V. (2012). MYC on the path to cancer. Cell *149*, 22–35.

Dang, C. V. (2013). MYC, metabolism, cell growth, and tumorigenesis. Cold Spring Harb. Perspect. Biol. *5*.

David, C.J., Chen, M., Assanah, M., Canoll, P., and Manley, J.L. (2010). HnRNP proteins controlled by c-Myc deregulate pyruvate kinase mRNA splicing in cancer. Nature *463*, 364–368.

Davis, A.C., Wims, M., Spotts, G.D., Hann, S.R., and Bradley, A. (1993). A null c-myc mutation causes lethality before 10.5 days of gestation in homozygotes and reduced fertility in heterozygous female mice. Genes Dev. *7*, 671–682.

DeBerardinis, R.J., Mancuso, A., Daikhin, E., Nissim, I., Yudkoff, M., Wehrli, S., and Thompson, C.B. (2007). Beyond aerobic glycolysis: transformed cells can engage in glutamine metabolism that exceeds the requirement for protein and nucleotide synthesis. Proc. Natl. Acad. Sci. U. S. A. *104*, 19345–19350.

DeBerardinis, R.J., Lum, J.J., Hatzivassiliou, G., and Thompson, C.B. (2008). The Biology of Cancer: Metabolic Reprogramming Fuels Cell Growth and Proliferation. Cell Metab. *7*, 11–20.

DeNicola, G.M., Karreth, F.A., Humpton, T.J., Gopinathan, A., Wei, C., Frese, K., Mangal, D., Yu, K.H., Yeo, C.J., Calhoun, E.S., et al. (2011). Oncogene-induced Nrf2 transcription promotes ROS detoxification and tumorigenesis. Nature *475*, 106–109.

Dews, M., Homayouni, A., Yu, D., Murphy, D., Sevignani, C., Wentzel, E., Furth, E.E., Lee, W.M., Enders, G.H., Mendell, J.T., et al. (2006). Augmentation of tumor angiogenesis by a Myc-activated microRNA cluster. Nat. Genet. *38*, 1060–1065.

Diehn, M., Cho, R.W., Lobo, N.A., Kalisky, T., Dorie, M.J., Kulp, A.N., Qian, D., Lam, J.S., Ailles, L.E., Wong, M., et al. (2009). Association of reactive oxygen species levels and radioresistance in cancer stem cells. Nature *458*, 780–783.

Dvinge, H., and Bertone, P. (2009). HTqPCR: high-throughput analysis and visualization of quantitative real-time PCR data in R. Bioinformatics *25*, 3325–3326.

Fabbri, M., Bottoni, A., Shimizu, M., Spizzo, R., Nicoloso, M.S., Rossi, S., Barbarotto, E., Cimmino, A., Adair, B., Wojcik, S.E., et al. (2011). Association of a microRNA/TP53 feedback circuitry with pathogenesis and outcome of B-cell chronic lymphocytic leukemia. JAMA *305*, 59–67.

Feng, M., Li, Z., Aau, M., Wong, C.H., Yang, X., and Yu, Q. (2011). Myc/miR-378/TOB2/cyclin D1 functional module regulates oncogenic transformation. Oncogene *30*, 2242–2251.

Finkel, T. (2012). Signal transduction by mitochondrial oxidants. J. Biol. Chem. *287*, 4434–4440.

Fletcher, J.I., Haber, M., Henderson, M.J., and Norris, M.D. (2010). ABC transporters in cancer: more than just drug efflux pumps. Nat. Rev. Cancer *10*, 147–156.

Forbes, J.R., and Gros, P. (2003). Iron, manganese, and cobalt transport by Nramp1 (Slc11a1) and Nramp2 (Slc11a2) expressed at the plasma membrane. Blood *102*, 1884–1892.

Friedman, R.C., Farh, K.K.H., Burge, C.B., and Bartel, D.P. (2009). Most mammalian mRNAs are conserved targets of microRNAs. Genome Res. *19*, 92–105.

Fussell, K.C., Udasin, R.G., Gray, J.P., Mishin, V., Smith, P.J.S., Heck, D.E., and Laskin, J.D. (2011). Redox cycling and increased oxygen utilization contribute to diquat-induced oxidative stress and cytotoxicity in Chinese hamster ovary cells overexpressing NADPH-cytochrome P450 reductase. Free Radic. Biol. Med. *50*, 874–882.

Gao, P., Tchernyshyov, I., Chang, T.-C., Lee, Y.-S., Kita, K., Ochi, T., Zeller, K.I., De Marzo, A.M., Van Eyk, J.E., Mendell, J.T., et al. (2009). c-Myc suppression of miR-23a/b enhances mitochondrial glutaminase expression and glutamine metabolism. Nature *458*, 762–765.

Gorrini, C., Harris, I.S., and Mak, T.W. (2013a). Modulation of oxidative stress as an anticancer strategy. Nat. Rev. Drug Discov. *12*, 931–947.

Gorrini, C., Baniasadi, P.S., Harris, I.S., Silvester, J., Inoue, S., Snow, B., Joshi, P. a, Wakeham, A., Molyneux, S.D., Martin, B., et al. (2013b). BRCA1 interacts with Nrf2 to regulate antioxidant signaling and cell survival. J. Exp. Med. *210*, 1529–1544.

Grandori, C., Gomez-Roman, N., Felton-Edkins, Z.A., Ngouenet, C., Galloway, D.A., Eisenman, R.N., and White, R.J. (2005). c-Myc binds to human ribosomal DNA and stimulates transcription of rRNA genes by RNA polymerase I. Nat. Cell Biol. *7*, 311–318.

Gregory, R.I., Chendrimada, T.P., and Shiekhattar, R. (2006). MicroRNA biogenesis: isolation and characterization of the microprocessor complex. Methods Mol. Biol. *342*, 33–47.

Grimson, A., Farh, K.K.H., Johnston, W.K., Garrett-Engele, P., Lim, L.P., and Bartel, D.P. (2007). MicroRNA Targeting Specificity in Mammals: Determinants beyond Seed Pairing. Mol. Cell *27*, 91–105.

Grishok, A., Pasquinelli, A.E., Conte, D., Li, N., Parrish, S., Ha, I., Baillie, D.L., Fire, A., Ruvkun, G., and Mello, C.C. (2001). Genes and mechanisms related to RNA interference regulate expression of the small temporal RNAs that control C. elegans developmental timing. Cell *106*, 23–34.

Guil, S., and Cáceres, J.F. (2007). The multifunctional RNA-binding protein hnRNP A1 is required for processing of miR-18a. Nat. Struct. Mol. Biol. *14*, 591–596.

Hammond, S.M., Boettcher, S., Caudy, A.A., Kobayashi, R., and Hannon, G.J. (2001). Argonaute2, a link between genetic and biochemical analyses of RNAi. Science *293*, 1146–1150.

Han, E.-S., Muller, F.L., Pérez, V.I., Qi, W., Liang, H., Xi, L., Fu, C., Doyle, E., Hickey, M., Cornell, J., et al. (2008). The in vivo gene expression signature of oxidative stress. Physiol. Genomics *34*, 112–126.

Han, H., Sun, D., Li, W., Shen, H., Zhu, Y., Li, C., Chen, Y., Lu, L., Li, W., Zhang, J., et al. (2013). A c-Myc-MicroRNA functional feedback loop affects hepatocarcinogenesis. Hepatology *57*, 2378–2389.

Hanahan, D., and Weinberg, R.A. (2011). Hallmarks of cancer: The next generation. Cell *144*, 646–674.

Handy, D.E., and Loscalzo, J. (2012). Redox Regulation of Mitochondrial Function. Antioxid. Redox Signal. *16*, 1323–1367.

Hayes, J.D., and McMahon, M. (2009). NRF2 and KEAP1 mutations: permanent activation of an adaptive response in cancer. Trends Biochem. Sci. *34*, 176–188.

He, L., and Hannon, G.J. (2004). MicroRNAs: small RNAs with a big role in gene regulation. Nat. Rev. Genet. *5*, 522–531.

He, L., Thomson, J.M., Hemann, M.T., Hernando-Monge, E., Mu, D., Goodson, S., Powers, S., Cordon-Cardo, C., Lowe, S.W., Hannon, G.J., et al. (2005). A microRNA polycistron as a potential human oncogene. Nature *435*, 828–833.

Heiden Vander, M.G., Lunt, S.Y., Dayton, T.L., Fiske, B.P., Israelsen, W.J., Mattaini, K.R., Vokes, N.I., Stephanopoulos, G., Cantley, L.C., Metallo, C.M., et al. (2011). Metabolic pathway alterations that support: Cell Proliferation. Cold Spring Harb. Symp. Quant. Biol. *76*, 325–334.

Horiuchi, D., Anderton, B., and Goga, A. (2014). Taking on Challenging Targets: Making MYC Druggable. Am. Soc. Clin. Oncol. Educ. Book *34*, e497–e502.

Huang, Q., Tan, Y., Yin, P., Ye, G., Gao, P., Lu, X., Wang, H., and Xu, G. (2013). Metabolic characterization of hepatocellular carcinoma using nontargeted tissue metabolomics. Cancer Res. *73*, 4992–5002.

Ishimoto, T., Nagano, O., Yae, T., Tamada, M., Motohara, T., Oshima, H., Oshima, M., Ikeda, T., Asaba, R., Yagi, H., et al. (2011). CD44 Variant Regulates Redox Status in Cancer Cells by Stabilizing the xCT Subunit of System xc- and Thereby Promotes Tumor Growth. Cancer Cell *19*, 387–400.

Ito, K., Hirao, A., Arai, F., Matsuoka, S., Takubo, K., Hamaguchi, I., Nomiyama, K., Hosokawa, K., Sakurada, K., Nakagata, N., et al. (2004). Regulation of oxidative stress by ATM is required for self-renewal of haematopoietic stem cells. Nature *431*, 997–1002.

Jackstadt, R., and Hermeking, H. (2015). MicroRNAs as regulators and mediators of c-MYC function. Biochim. Biophys. Acta - Gene Regul. Mech.

Jain, M., Nilsson, R., Sharma, S., Madhusudhan, N., Kitami, T., Souza, A.L., Kafri, R., Kirschner, M.W., Clish, C.B., and Mootha, V.K. (2012). Metabolite profiling identifies a key role for glycine in rapid cancer cell proliferation. Science *336*, 1040–1044.

Janssen-Heininger, Y.M.W., Mossman, B.T., Heintz, N.H., Forman, H.J., Kalyanaraman, B., Finkel, T., Stamler, J.S., Rhee, S.G., and van der Vliet, A. (2008). Redox-based regulation of signal transduction: Principles, pitfalls, and promises. Free Radic. Biol. Med. *45*, 1–17.

Jemal, A., Siegel, R., Ward, E., Hao, Y., Xu, J., and Thun, M.J. (2009). Cancer Statistics. CA. Cancer J. Clin. *59*, 225–249.

Jin, B., and Robertson, K.D. (2013). DNA methyltransferases, DNA damage repair, and cancer. Adv. Exp. Med. Biol. *754*, 3–29.

Jones, R.G., and Thompson, C.B. (2009). Tumor suppressors and cell metabolism: A recipe for cancer growth. Genes Dev. *23*, 537–548.

Kaler, S.G. (2014). Translational research investigations on ATP7A: An important human copper ATPase. Ann. N. Y. Acad. Sci. *1314*, 64–68.

Kaposi-Novak, P., Libbrecht, L., Woo, H.G., Lee, Y.H., Sears, N.C., Conner, E.A., Factor, V.M., Roskams, T., and Thorgeirsson, S.S. (2009). Central role of c-Myc during malignant conversion in human hepatocarcinogenesis. Cancer Res. *69*, 2775–2782.

Karube, Y., Tanaka, H., Osada, H., Tomida, S., Tatematsu, Y., Yanagisawa, K., Yatabe, Y., Takamizawa, J., Miyoshi, S., Mitsudomi, T., et al. (2005). Reduced expression of Dicer associated with poor prognosis in lung cancer patients. Cancer Sci. *96*, 111–115.

Kawate, S., Fukusato, T., Ohwada, S., Watanuki, A., and Morishita, Y. (1999). Amplification of c-myc in hepatocellular carcinoma: Correlation with clinicopathologic features, proliferative activity and p53 overexpression. Oncology *57*, 157–163.

Kim, V.N. (2005). MicroRNA biogenesis: coordinated cropping and dicing. Nat. Rev. Mol. Cell Biol. *6*, 376–385.

Kim, S., Li, Q., Dang, C. V, and Lee, L.A. (2000). Induction of ribosomal genes and hepatocyte hypertrophy by adenovirus-mediated expression of c-Myc in vivo. Proc. Natl. Acad. Sci. U. S. A. *97*, 11198–11202.

Kim, S., You, S., and Hwang, D. (2011). Aminoacyl-tRNA synthetases and tumorigenesis: more than housekeeping. Nat. Rev. Cancer *11*, 813–813.

Kim, Y.R., Oh, J.E., Kim, M.S., Kang, M.R., Park, S.W., Han, J.Y., Eom, H.S., Yoo, N.J., and Lee, S.H. (2010). Oncogenic NRF2 mutations in squamous cell carcinomas of oesophagus and skin. J. Pathol. *220*, 446–451.

Kota, J., Chivukula, R.R., O'Donnell, K.A., Wentzel, E.A., Montgomery, C.L., Hwang, H.W., Chang, T.C., Vivekanandan, P., Torbenson, M., Clark, K.R., et al. (2009). Therapeutic microRNA Delivery Suppresses Tumorigenesis in a Murine Liver Cancer Model. Cell *137*, 1005–1017.

Krol, J., Loedige, I., and Filipowicz, W. (2010). The widespread regulation of microRNA biogenesis, function and decay. Nat. Rev. Genet. *11*, 597–610.

Kumar, M.S., Pester, R.E., Chen, C.Y., Lane, K., Chin, C., Lu, J., Kirsch, D.G., Golub, T.R., and Jacks, T. (2009). Dicer1 functions as a haploinsufficient tumor suppressor. Genes Dev. *23*, 2700–2704.

Kumar, P., Luo, Y., Tudela, C., Alexander, J.M., and Mendelson, C.R. (2013). The c-Myc-regulated microRNA-17~92 (miR-17~92) and miR-106a~363 clusters target hCYP19A1 and hGCM1 to inhibit human trophoblast differentiation. Mol. Cell. Biol. *33*, 1782–1796.

Lal, A., Navarro, F., Maher, C.A., Maliszewski, L.E., Yan, N., O'Day, E., Chowdhury, D., Dykxhoorn, D.M., Tsai, P., Hofmann, O., et al. (2009). miR-24 Inhibits Cell Proliferation by Targeting E2F2, MYC, and Other Cell-Cycle Genes via Binding to "Seedless" 3???UTR MicroRNA Recognition Elements. Mol. Cell *35*, 610–625.

Le, A., Cooper, C.R., Gouw, A.M., Dinavahi, R., Maitra, A., Deck, L.M., Royer, R.E., Vander Jagt, D.L., Semenza, G.L., and Dang, C. V (2010). Inhibition of lactate dehydrogenase A induces oxidative stress and inhibits tumor progression. Proc. Natl. Acad. Sci. U. S. A. *107*, 2037–2042.

Le, A., Lane, A.N., Hamaker, M., Bose, S., Gouw, A., Barbi, J., Tsukamoto, T., Rojas, C.J., Slusher, B.S., Zhang, H., et al. (2012). Glucose-independent glutamine metabolism via TCA cycling for proliferation and survival in b cells. Cell Metab. *15*, 110–121.

Lee, R.C., Feinbaum, R.L., and Ambros, V. (1993). The C. elegans heterochronic gene lin-4 encodes small RNAs with antisense complementarity to lin-14. Cell *75*, 843–854.

Lee, S.J., Zhang, J., Choi, A.M.K., and Kim, H.P. (2013). Mitochondrial dysfunction induces formation of lipid droplets as a generalized response to stress. Oxid. Med. Cell. Longev.

Lee, Y., Kim, M., Han, J., Yeom, K.-H., Lee, S., Baek, S.H., and Kim, V.N. (2004). MicroRNA genes are transcribed by RNA polymerase II. EMBO J. *23*, 4051–4060.

Leslie, N.R., Bennett, D., Lindsay, Y.E., Stewart, H., Gray, A., and Downes, C.P. (2003). Redox regulation of PI 3-kinase signalling via inactivation of PTEN. EMBO J. *22*, 5501–5510.

Levy, S., and Forman, H.J. (2010). c-Myc is a Nrf2-interacting protein that negatively regulates phase II genes through their electrophile responsive elements. IUBMB Life *62*, 237–246.

Lewis, B.P., Burge, C.B., and Bartel, D.P. (2005). Conserved seed pairing, often flanked by adenosines, indicates that thousands of human genes are microRNA targets. Cell *120*, 15–20.

Li, B., and Simon, M.C. (2013). Molecular pathways: Targeting MYC-induced metabolic reprogramming and oncogenic stress in cancer. Clin. Cancer Res. *19*, 5835–5841.

Li, B., Gordon, G.M., Du, C.H., Xu, J., and Du, W. (2010). Specific Killing of Rb Mutant Cancer Cells by Inactivating TSC2. Cancer Cell *17*, 469–480.

Li, F., Wang, Y., Zeller, K.I., Potter, J.J., Wonsey, D.R., O'Donnell, K.A., Kim, J.-W., Yustein, J.T., Lee, L.A., and Dang, C. V (2005). Myc stimulates nuclearly encoded mitochondrial genes and mitochondrial biogenesis. Mol. Cell. Biol. *25*, 6225–6234.

Li, L., Guo, Z., Wang, J., Mao, Y., and Gao, Q. (2012). Serum miR-18a: A potential marker for hepatitis B virus-related hepatocellular carcinoma screening. Dig. Dis. Sci. *57*, 2910–2916.

Lim, L., Balakrishnan, A., Huskey, N., Jones, K.D., Jodari, M., Ng, R., Song, G., Riordan, J., Anderton, B., Cheung, S.T., et al. (2014). MicroRNA-494 within an oncogenic microRNA megacluster regulates G1/S transition in liver tumorigenesis through suppression of mutated in colorectal cancer. Hepatology.

Lin, C.P., Liu, C.R., Lee, C.N., Chan, T.S., and Liu, H.E. (2010). Targeting c-Myc as a novel approach for hepatocellular carcinoma. World J. Hepatol. *2*, 16–20.

Lin, C.Y., Lovén, J., Rahl, P.B., Paranal, R.M., Burge, C.B., Bradner, J.E., Lee, T.I., and Young, R.A. (2012). Transcriptional amplification in tumor cells with elevated c-Myc. Cell *151*, 56–67.

Liu, L., Ulbrich, J., Müller, J., Wüstefeld, T., Aeberhard, L., Kress, T.R., Muthalagu, N., Rycak, L., Rudalska, R., Moll, R., et al. (2012a). Deregulated MYC expression induces dependence upon AMPK-related kinase 5. Nature *483*, 608–612.

Liu, Q., Fu, H., Sun, F., Zhang, H., Tie, Y., Zhu, J., Xing, R., Sun, Z., and Zheng, X. (2008). miR-16 family induces cell cycle arrest by regulating multiple cell cycle genes. Nucleic Acids Res. *36*, 5391–5404.

Liu, W., Le, A., Hancock, C., Lane, A.N., Dang, C. V., Fan, T.W.-M., and Phang, J.M. (2012b). Reprogramming of proline and glutamine metabolism contributes to the proliferative and metabolic responses regulated by oncogenic transcription factor c-MYC. Proc. Natl. Acad. Sci. *109*, 8983–8988.

Liu, W.H., Yeh, S.H., Lu, C.C., Yu, S.L., Chen, H.Y., Lin, C.Y., Chen, D.S., and Chen, P.J. (2009). MicroRNA-18a Prevents Estrogen Receptor-?? Expression, Promoting Proliferation of Hepatocellular Carcinoma Cells. Gastroenterology *136*, 683–693.

Locasale, J.W., Grassian, A.R., Melman, T., Lyssiotis, C.A., Mattaini, K.R., Bass, A.J., Heffron, G., Metallo, C.M., Muranen, T., Sharfi, H., et al. (2011). Phosphoglycerate dehydrogenase diverts glycolytic flux and contributes to oncogenesis. Nat. Genet. *43*, 869–874.

Loenen, W.A.M. (2006). S-adenosylmethionine: jack of all trades and master of everything? Biochem. Soc. Trans. *34*, 330–333.

Lu, S.C. (2013). Glutathione synthesis. Biochim. Biophys. Acta *1830*, 3143–3153.

Lund, E., and Dahlberg, J.E. (2006). Substrate selectivity of exportin 5 and Dicer in the biogenesis of microRNAs. In Cold Spring Harbor Symposia on Quantitative Biology, pp. 59–66.

Ma, L., Young, J., Prabhala, H., Pan, E., Mestdagh, P., Muth, D., Teruya-Feldstein, J., Reinhardt, F., Onder, T.T., Valastyan, S., et al. (2010). miR-9, a MYC/MYCN-activated microRNA, regulates E-cadherin and cancer metastasis. Nat. Cell Biol. *12*, 247–256.

Maggi, L.B., Kuchenruether, M., Dadey, D.Y.A., Schwope, R.M., Grisendi, S., Townsend, R.R., Pandolfi, P.P., and Weber, J.D. (2008). Nucleophosmin serves as a rate-limiting nuclear export chaperone for the Mammalian ribosome. Mol. Cell. Biol. *28*, 7050–7065.

Martindale, J.L., and Holbrook, N.J. (2002). Cellular response to oxidative stress: Signaling for suicide and survival. J. Cell. Physiol. *192*, 1–15.

Meister, A. (1991). Glutathione deficiency produced by inhibition of its synthesis, and its reversal; applications in research and therapy. Pharmacol. Ther. *51*, 155–194.

Menssen, A., Hydbring, P., Kapelle, K., Vervoorts, J., Diebold, J., Luscher, B., Larsson, L.-G., and Hermeking, H. (2012). The c-MYC oncoprotein, the NAMPT enzyme, the SIRT1-inhibitor DBC1, and the SIRT1 deacetylase form a positive feedback loop. Proc. Natl. Acad. Sci. *109*, E187–E196.

Meyer, N., and Penn, L.Z. (2008). Reflecting on 25 years with MYC. Nat. Rev. Cancer *8*, 976–990.

Miao, L.J., Huang, S.F., Sun, Z.T., Gao, Z.Y., Zhang, R.X., Liu, Y., and Wang, J. (2013). MiR-449c targets c-Myc and inhibits NSCLC cell progression. FEBS Lett. *587*, 1359–1365.

Mitsuishi, Y., Taguchi, K., Kawatani, Y., Shibata, T., Nukiwa, T., Aburatani, H., Yamamoto, M., and Motohashi, H. (2012). Nrf2 Redirects Glucose and Glutamine into Anabolic Pathways in Metabolic Reprogramming. Cancer Cell *22*, 66–79.

Mott, J.L., Kurita, S., Cazanave, S.C., Bronk, S.F., Werneburg, N.W., and Fernandez-Zapico, M.E. (2010). Transcriptional suppression of mir-29b-1/mir-29a promoter by c-Myc, hedgehog, and NF-kappaB. J. Cell. Biochem. *110*, 1155–1164.

Mourelatos, Z., Dostie, J., Paushkin, S., Sharma, A., Charroux, B., Abel, L., Rappsilber, J., Mann, M., and Dreyfuss, G. (2002). miRNPs: A novel class of ribonucleoproteins containing numerous microRNAs. Genes Dev. *16*, 720–728.

Mu, P., Han, Y.C., Betel, D., Yao, E., Squatrito, M., Ogrodowski, P., De Stanchina, E., D'Andrea, A., Sander, C., and Ventura, A. (2009). Genetic dissection of the miR-17-92 cluster of microRNAs in Myc-induced B-cell lymphomas. Genes Dev. *23*, 2806–2811.

Naka, K., Hoshii, T., Muraguchi, T., Tadokoro, Y., Ooshio, T., Kondo, Y., Nakao, S., Motoyama, N., and Hirao, A. (2010). TGF-beta-FOXO signalling maintains leukaemia-initiating cells in chronic myeloid leukaemia. Nature *463*, 676–680.

Nie, Z., Hu, G., Wei, G., Cui, K., Yamane, A., Resch, W., Wang, R., Green, D.R., Tessarollo, L., Casellas, R., et al. (2012). c-Myc Is a Universal Amplifier of Expressed Genes in Lymphocytes and Embryonic Stem Cells. Cell *151*, 68–79.

Nikiforov, M.A., Chandriani, S., O'Connell, B., Petrenko, O., Kotenko, I., Beavis, A., Sedivy, J.M., and Cole, M.D. (2002). A functional screen for Myc-responsive genes reveals serine hydroxymethyltransferase, a major source of the one-carbon unit for cell metabolism. Mol. Cell. Biol. *22*, 5793–5800.

Noor, E., Eden, E., Milo, R., and Alon, U. (2010). Central Carbon Metabolism as a Minimal Biochemical Walk between Precursors for Biomass and Energy. Mol. Cell *39*, 809–820.

O'Donnell, K.A., Wentzel, E.A., Zeller, K.I., Dang, C. V, and Mendell, J.T. (2005). c-Myc-regulated microRNAs modulate E2F1 expression. Nature *435*, 839–843.

Ohgami, R.S., Campagna, D.R., McDonald, A., and Fleming, M.D. (2006). The Steap proteins are metalloreductases. Blood *108*, 1388–1394.

Orban, T.I., and Izaurralde, E. (2005). Decay of mRNAs targeted by RISC requires XRN1, the Ski complex, and the exosome. RNA *11*, 459–469.

Osthus, R.C., Shim, H., Kim, S., Li, Q., Reddy, R., Mukherjee, M., Xu, Y., Wonsey, D., Lee, L.A., and Dang, C. V (2000). Deregulation of glucose transporter 1 and glycolytic gene expression by c-Myc. J. Biol. Chem. *275*, 21797–21800.

Parker, R., and Sheth, U. (2007). P Bodies and the Control of mRNA Translation and Degradation. Mol. Cell *25*, 635–646.

Pasquinelli, A.E., Reinhart, B.J., Slack, F., Martindale, M.Q., Kuroda, M.I., Maller, B., Hayward, D.C., Ball, E.E., Degnan, B., Müller, P., et al. (2000). Conservation of the sequence and temporal expression of let-7 heterochronic regulatory RNA. Nature *408*, 86–89.

Pedica, F., Ruzzenente, A., Bagante, F., Capelli, P., Cataldo, I., Pedron, S., Iacono, C., Chilosi, M., Scarpa, A., Brunelli, M., et al. (2013). A Re-Emerging Marker for Prognosis in Hepatocellular Carcinoma: The Add-Value of FISHing c-myc Gene for Early Relapse. PLoS One *8*.

Peng, S.Y., Lai, P.L., and Hsu, H.C. (1993). Amplification of the c-myc gene in human hepatocellular carcinoma: biologic significance. J.Formos.Med.Assoc. *92*, 866–870.

Porro, A., Iraci, N., Soverini, S., Diolaiti, D., Gherardi, S., Terragna, C., Durante, S., Valli, E., Kalebic, T., Bernardoni, R., et al. (2011). c-MYC Oncoprotein Dictates Transcriptional Profiles of ATP-Binding Cassette Transporter Genes in Chronic Myelogenous Leukemia CD34+ Hematopoietic Progenitor Cells. Mol. Cancer Res. *9*, 1054–1066.

Possemato, R., Marks, K.M., Shaul, Y.D., Pacold, M.E., Kim, D., Birsoy, K., Sethumadhavan, S., Woo, H.-K., Jang, H.G., Jha, A.K., et al. (2011). Functional genomics reveal that the serine synthesis pathway is essential in breast cancer. Nature *476*, 346–350.

R Core Team (2014). R: A language and environment for statistical computing. R Found. Stat. Comput. Vienna, Austria URL http://www.R – project.org/.

Ranjan, P., Anathy, V., Burch, P.M., Weirather, K., Lambeth, J.D., and Heintz, N.H. (2006). Redox-dependent expression of cyclin D1 and cell proliferation by Nox1 in mouse lung epithelial cells. Antioxid Redox Signal *8*, 1447–1459.

Raver-Shapira, N., Marciano, E., Meiri, E., Spector, Y., Rosenfeld, N., Moskovits, N., Bentwich, Z., and Oren, M. (2007). Transcriptional Activation of miR-34a Contributes to p53-Mediated Apoptosis. Mol. Cell *26*, 731–743.

Reinhart, B.J., Slack, F.J., Basson, M., Pasquinelli, A.E., Bettinger, J.C., Rougvie, A.E., Horvitz, H.R., and Ruvkun, G. (2000). The 21-nucleotide let-7 RNA regulates developmental timing in Caenorhabditis elegans. Nature *403*, 901–906.

Rhee, S.G. (2006). H2O2, a necessary evil for cell signaling. Science *312*, 1882–1883.

Van Riggelen, J., Yetil, A., and Felsher, D.W. (2010). MYC as a regulator of ribosome biogenesis and protein synthesis. Nat. Rev. Cancer *10*, 301–309.

Ritter, C.A., Jedlitschky, G., Meyer zu Schwabedissen, H., Grube, M., Köck, K., and Kroemer, H.K. (2005). Cellular export of drugs and signaling molecules by the ATP-binding cassette transporters MRP4 (ABCC4) and MRP5 (ABCC5). Drug Metab. Rev. *37*, 253–278.

Sachdeva, M., Zhu, S., Wu, F., Wu, H., Walia, V., Kumar, S., Elble, R., Watabe, K., and Mo, Y.-Y. (2009). p53 represses c-Myc through induction of the tumor suppressor miR-145. Proc. Natl. Acad. Sci. U. S. A. *106*, 3207–3212.

Saha, T., Rih, J.K., and Rosen, E.M. (2009). BRCA1 down-regulates cellular levels of reactive oxygen species. FEBS Lett. *583*, 1535–1543.

Sampson, V.B., Rong, N.H., Han, J., Yang, Q., Aris, V., Soteropoulos, P., Petrelli, N.J., Dunn, S.P., and Krueger, L.J. (2007). MicroRNA let-7a down-regulates MYC and reverts MYC-induced growth in Burkitt lymphoma cells. Cancer Res. *67*, 9762–9770.

Sander, S., Bullinger, L., Klapproth, K., Fiedler, K., Kestler, H.A., Barth, T.F.E., Möller, P., Stilgenbauer, S., Pollack, J.R., and Wirth, T. (2008). MYC stimulates EZH2 expression by repression of its negative regulator miR-26a. Blood *112*, 4202–4212.

Sandhu, S.K., Fassan, M., Volinia, S., Lovat, F., Balatti, V., Pekarsky, Y., and Croce, C.M. (2013). B-cell malignancies in microRNA Eμ-miR-17~92 transgenic mice. Proc. Natl. Acad. Sci. U. S. A. *110*, 18208–18213.

Sanyal, A.J., Yoon, S.K., and Lencioni, R. (2010). The etiology of hepatocellular carcinoma and consequences for treatment. Oncologist *15 Suppl 4*, 14–22.

Schlaeger, C., Longerich, T., Schiller, C., Bewerunge, P., Mehrabi, A., Toedt, G., Kleeff, J., Ehemann, V., Eils, R., Lichter, P., et al. (2008). Etiology-dependent molecular mechanisms in human hepatocarcinogenesis. Hepatology *47*, 511–520.

Schmitz, G., Langmann, T., and Heimerl, S. (2001). Role of ABCG1 and other ABCG family members in lipid metabolism. J. Lipid Res. *42*, 1513–1520.

Schwaller, B. (2010). Ca2+ buffers. In Handbook of Cell Signaling, 2/e, pp. 955–962.

Sena, L.A., and Chandel, N.S. (2012). Physiological roles of mitochondrial reactive oxygen species. Mol. Cell *48*, 158–166.

Shachaf, C.M., Kopelman, A.M., Arvanitis, C., Karlsson, A., Beer, S., Mandl, S., Bachmann, M.H., Borowsky, A.D., Ruebner, B., Cardiff, R.D., et al. (2004). MYC inactivation uncovers pluripotent differentiation and tumour dormancy in hepatocellular cancer. Nature *431*, 1112–1117.

Shibata, T., Ohta, T., Tong, K.I., Kokubu, A., Odogawa, R., Tsuta, K., Asamura, H., Yamamoto, M., and Hirohashi, S. (2008). Cancer related mutations in NRF2 impair its recognition by Keap1-Cul3 E3 ligase and promote malignancy. Proc. Natl. Acad. Sci. U. S. A. *105*, 13568–13573.

Shim, H., Chun, Y.S., Lewis, B.C., and Dang, C. V (1998). A unique glucose-dependent apoptotic pathway induced by c-Myc. Proc. Natl. Acad. Sci. U. S. A. *95*, 1511–1516.

Shiue, C.-N., Berkson, R.G., and Wright, A.P.H. (2009). c-Myc induces changes in higher order rDNA structure on stimulation of quiescent cells. Oncogene *28*, 1833–1842.

Siemens, H., Jackstadt, R., Hünten, S., Kaller, M., Menssen, A., Götz, U., and Hermeking, H. (2011). miR-34 and SNAIL form a double-negative feedback loop to regulate epithelial-mesenchymal transitions. Cell Cycle *10*, 4256–4271.

Siemens, H., Jackstadt, R., Kaller, M., and Hermeking, H. (2013). Repression of c-Kit by p53 is mediated by miR-34 and is associated with reduced chemoresistance, migration and stemness. Oncotarget *4*, 1399–1415.

Sies, H. (1999). Glutathione and its role in cellular functions. Free Radic. Biol. Med. *27*, 916–921.

Singh, A., Bodas, M., Wakabayashi, N., Bunz, F., and Biswal, S. (2010). Gain of Nrf2 function in non-small-cell lung cancer cells confers radioresistance. Antioxid. Redox Signal. *13*, 1627–1637.

Smyth, G. (2005). limma: Linear Models for Microarray Data. In Bioinformatics and Computational Biology Solutions Using R and Bioconductor, pp. 397–420.

Son, J., Lyssiotis, C. a, Ying, H., Wang, X., Hua, S., Ligorio, M., Perera, R.M., Ferrone, C.R., Mullarky, E., Shyh-Chang, N., et al. (2013). Glutamine supports pancreatic cancer growth through a KRAS-regulated metabolic pathway. Nature *496*, 101–105.

Song, S.J., Poliseno, L., Song, M.S., Ala, U., Webster, K., Ng, C., Beringer, G., Brikbak, N.J., Yuan, X., Cantley, L.C., et al. (2013). MicroRNA-antagonism regulates breast cancer stemness and metastasis via TET-family-dependent chromatin remodeling. Cell *154*.

Sotillo, E., Laver, T., Mellert, H., Schelter, J.M., Cleary, M.A., McMahon, S., and Thomas-Tikhonenko, A. (2011). Myc overexpression brings out unexpected antiapoptotic effects of miR-34a. Oncogene *30*, 2587–2594.

Suzuki, H.I., Yamagata, K., Sugimoto, K., Iwamoto, T., Kato, S., and Miyazono, K. (2009). Modulation of microRNA processing by p53. Nature *460*, 529–533.

Sykes, S.M., Lane, S.W., Bullinger, L., Kalaitzidis, D., Yusuf, R., Saez, B., Ferraro, F., Mercier, F., Singh, H., Brumme, K.M., et al. (2011). AKT/FOXO signaling enforces reversible differentiation blockade in myeloid leukemias. Cell *146*, 697–708.

Takahashi, E., Hori, T., O'Connell, P., Leppert, M., and White, R. (1991). Mapping of the MYC gene to band 8q24.12----q24.13 by R-banding and distal to fra(8)(q24.11), FRA8E, by fluorescence in situ hybridization. Cytogenet. Cell Genet. *57*, 109–111.

Tanabe, M., and Kanehisa, M. (2012). Using the KEGG database resource. Curr. Protoc. Bioinforma.

Tanzer, A., and Stadler, P.F. (2004). Molecular evolution of a microRNA cluster. J. Mol. Biol. *339*, 327–335.

Tarasov, V., Jung, P., Verdoodt, B., Lodygin, D., Epanchintsev, A., Menssen, A., Meister, G., and Hermeking, H. (2007). Differential regulation of microRNAs by p53 revealed by massively parallel sequencing: miR-34a is a p53 target that induces apoptosis and G 1-arrest. Cell Cycle *6*, 1586–1593.

Tenbaum, S.P., Ordóñez-Morán, P., Puig, I., Chicote, I., Arqués, O., Landolfi, S., Fernández, Y., Herance, J.R., Gispert, J.D., Mendizabal, L., et al. (2012). β-catenin confers resistance to PI3K and AKT inhibitors and subverts FOXO3a to promote metastasis in colon cancer. Nat. Med. *18*, 892–901.

Terradillos, O., Billet, O., Renard, C.A., Levy, R., Molina, T., Briand, P., and Buendia, M.A. (1997). The hepatitis B virus X gene potentiates c-myc-induced liver oncogenesis in transgenic mice. Oncogene *14*, 395–404.

Townsend, D.M., Tew, K.D., and Tapiero, H. (2004). Sulfur containing amino acids and human disease. Biomed. Pharmacother. *58*, 47–55.

Tward, A.D., Jones, K.D., Yant, S., Kay, M.A., Wang, R., and Bishop, J.M. (2005). Genomic progression in mouse models for liver tumors. In Cold Spring Harbor Symposia on Quantitative Biology, pp. 217–224.

Uribesalgo, I., Buschbeck, M., Gutiérrez, A., Teichmann, S., Demajo, S., Kuebler, B., Nomdedéu, J.F., Martín-Caballero, J., Roma, G., Benitah, S.A., et al. (2011). E-box-independent regulation of transcription and differentiation by MYC. Nat. Cell Biol. *13*, 1443–1449.

Uziel, T., Karginov, F. V, Xie, S., Parker, J.S., Wang, Y.-D., Gajjar, A., He, L., Ellison, D., Gilbertson, R.J., Hannon, G., et al. (2009). The miR-17~92 cluster collaborates with the Sonic Hedgehog pathway in medulloblastoma. Proc. Natl. Acad. Sci. U. S. A. *106*, 2812–2817.

Vazquez, A., Markert, E.K., and Oltvai, Z.N. (2011). Serine biosynthesis with one carbon catabolism and the glycine cleavage system represents a novel pathway for ATP generation. PLoS One *6*.

Volinia, S., Calin, G.A., Liu, C.-G., Ambs, S., Cimmino, A., Petrocca, F., Visone, R., Iorio, M., Roldo, C., Ferracin, M., et al. (2006). A microRNA expression signature of human solid tumors defines cancer gene targets. Proc. Natl. Acad. Sci. U. S. A. *103*, 2257–2261.

Wang, X., Zhao, X., Gao, P., and Wu, M. (2013). c-Myc modulates microRNA processing via the transcriptional regulation of Drosha. Sci. Rep. *3*, 1942.

Wickham, H. (2009). ggplot2.

Winter, J., Jung, S., Keller, S., Gregory, R.I., and Diederichs, S. (2009). Many roads to maturity: microRNA biogenesis pathways and their regulation. Nat. Cell Biol. *11*, 228–234.

Wise, D.R., DeBerardinis, R.J., Mancuso, A., Sayed, N., Zhang, X.-Y., Pfeiffer, H.K., Nissim, I., Daikhin, E., Yudkoff, M., McMahon, S.B., et al. (2008). Myc regulates a transcriptional program that stimulates mitochondrial glutaminolysis and leads to glutamine addiction. Proc. Natl. Acad. Sci. U. S. A. *105*, 18782–18787.

Wu, C.H., Sahoo, D., Arvanitis, C., Bradon, N., Dill, D.L., and Felsher, D.W. (2008). Combined analysis of murine and human microarrays and ChIP analysis reveals genes associated with the ability of MYC to maintain tumorigenesis. PLoS Genet. *4*.

Wu, G., Fang, Y.-Z., Yang, S., Lupton, J.R., and Turner, N.D. (2004). Glutathione metabolism and its implications for health. J. Nutr. *134*, 489–492.

Yamamura, S., Saini, S., Majid, S., Hirata, H., Ueno, K., Chang, I., Tanaka, Y., Gupta, A., and Dahiya, R. (2012a). Microrna-34a suppresses malignant transformation by targeting c-myc transcriptional complexes in human renal cell carcinoma. Carcinogenesis *33*, 294–300.

Yamamura, S., Saini, S., Majid, S., Hirata, H., Ueno, K., Deng, G., and Dahiya, R. (2012b). Microrna-34a modulates c-Myc transcriptional complexes to suppress malignancy in human prostate cancer cells. PLoS One *7*.

Yamashita, T., Forgues, M., Wang, W., Kim, J.W., Ye, Q., Jia, H., Budhu, A., Zanetti, K.A., Chen, Y., Qin, L.-X., et al. (2008). EpCAM and alpha-fetoprotein expression defines novel prognostic subtypes of hepatocellular carcinoma. Cancer Res. *68*, 1451–1461.

Yang, J.D., and Roberts, L.R. (2010). Hepatocellular carcinoma: A global view. Nat. Rev. Gastroenterol. Hepatol. *7*, 448–458.

Yong, S.L., and Dutta, A. (2007). The tumor suppressor microRNA let-7 represses the HMGA2 oncogene. Genes Dev. *21*, 1025–1030.

Yoshida, T., Goto, S., Kawakatsu, M., Urata, Y., and Li, T. (2012). Mitochondrial dysfunction, a probable cause of persistent oxidative stress after exposure to ionizing radiation. Free Radic. Res. *46*, 147–153.

Yu, Z., Willmarth, N.E., Zhou, J., Katiyar, S., Wang, M., Liu, Y., McCue, P.A., Quong, A.A., Lisanti, M.P., and Pestell, R.G. (2010). microRNA 17/20 inhibits cellular invasion and tumor metastasis in breast cancer by heterotypic signaling. Proc. Natl. Acad. Sci. U. S. A. *107*, 8231–8236.

Yuneva, M., Zamboni, N., Oefner, P., Sachidanandam, R., and Lazebnik, Y. (2007). Deficiency in glutamine but not glucose induces MYC-dependent apoptosis in human cells. J. Cell Biol. *178*, 93–105.

Yuneva, M.O., Fan, T.W.M., Allen, T.D., Higashi, R.M., Ferraris, D. V., Tsukamoto, T., Matés, J.M., Alonso, F.J., Wang, C., Seo, Y., et al. (2012). The metabolic profile of tumors depends on both the responsible genetic lesion and tissue type. Cell Metab. *15*, 157–170.

Zeller, K.I., Haggerty, T.J., Barrett, J.F., Guo, Q., Wonsey, D.R., and Dang, C. V. (2001). Characterization of Nucleophosmin (B23) as a Myc Target by Scanning Chromatin Immunoprecipitation. J. Biol. Chem. *276*, 48285–48291.

Zhang, X., Chen, X., Lin, J., Lwin, T., Wright, G., Moscinski, L.C., Dalton, W.S., Seto, E., Wright, K., Sotomayor, E., et al. (2012a). Myc represses miR-15a/miR-16-1 expression through recruitment of HDAC3 in mantle cell and other non-Hodgkin B-cell lymphomas. Oncogene *31*, 3002–3008.

Zhang, X., Zhao, X., Fiskus, W., Lin, J., Lwin, T., Rao, R., Zhang, Y., Chan, J.C., Fu, K., Marquez, V.E., et al. (2012b). Coordinated Silencing of MYC-Mediated miR-29 by HDAC3 and EZH2 as a Therapeutic Target of Histone Modification in Aggressive B-Cell Lymphomas. Cancer Cell *22*, 506–523.

Zhen, Y., Liu, Z., Yang, H., Yu, X., Wu, Q., Hua, S., Long, X., Jiang, Q., Song, Y., Cheng, C., et al. (2013). Tumor suppressor PDCD4 modulates miR-184-mediated direct suppression of C-MYC and BCL2 blocking cell growth and survival in nasopharyngeal carcinoma. Cell Death Dis. *4*, e872.

Zhu, D.-X., Fan, L., Lu, R.-N., Fang, C., Shen, W.-Y., Zou, Z.-J., Wang, Y.-H., Zhu, H.-Y., Miao, K.-R., Liu, P., et al. (2012). Downregulated Dicer expression predicts poor prognosis in chronic lymphocytic leukemia. Cancer Sci. *103*, 875–881.

Zhuang, G., Wu, X., Jiang, Z., Kasman, I., Yao, J., Guan, Y., Oeh, J., Modrusan, Z., Bais, C., Sampath, D., et al. (2012). Tumour-secreted miR-9 promotes endothelial cell migration and angiogenesis by activating the JAK-STAT pathway. EMBO J. *31*, 3513–3523.

Publishing Agreement

It is the policy of the University to encourage the distribution of all theses, dissertations, and manuscripts. Copies of all UCSF theses, dissertations, and manuscripts will be routed to the library via the Graduate Division. The library will make all theses, dissertations, and manuscripts accessible to the public and will preserve these to the best of their abilities, in perpetuity.

Please sign the following statement:

I hereby grant permission to the Graduate Division of the University of California, San Francisco to release copies of my thesis, dissertation, or manuscript to the Campus Library to provide access and preservation, in whole or in part, in perpetuity.

Brittany N. Anderton
Author Signature

8/17/15
Date